UNIVERSIDADE DE LISBOA
FACULDADE DE CIÊNCIAS
DEPARTAMENTO DE FÍSICA

Testar os acoplamentos da energia escura

Vitor Manuel da Fonseca

Mestrado em Física

Especialização em Astrofísica e Cosmologia

Dissertação orientada por:
Doutor Nelson Nunes
e Doutor Tiago Barreiro

2020

"Le temps a deux visages, se dit Khayyam, il a deux dimensions, la longueur est au rythme du soleil, l'épaisseur au rythme des passions."

Amin Maalouf (Samarcande).

Acknowledgments

I am immensely grateful to Nelson Nunes and Tiago Barreiro who granted me the eminent honor of supervising my dissertation. I warmly thank Nelson for opening my mind to cosmology through his course on General Relativity. I am profoundly indebted by Tiago's wise and enlightening guidance, especially when I needed a hand to unlock deadlocks. I want to pay tribute to Ismael Tereno and Antonio Silva who have been inspiring teachers. I largely owe them the presentation style of key topics throughout the dissertation. It has been a comforting pleasure to exchange views with Bruno and Elsa respectively on Russian literature and CLASS code. I have also been extraordinary lucky with the outstanding support offered by Brice who lent me computational power in London. I deeply apologize for Spinel mutating into a noisy helicopter in his living room. My daughter Joana deserves a special mention for sharing with me the common fate of being a student under pandemic lockdown. I shall be forever grateful to Alix who owns my loving heart.

Resumo

A nossa dissertação tem como objectivo explorar possíveis extensões do modelo padrão ΛCDM[1] generalizando a constante cosmológica com quintessência, ou seja, um campo escalar ϕ cuja equação de estado $w = p/\rho$ varia com o tempo. Em vez de tentar elucidar a própria natureza da energia escura, adoptamos uma abordagem fenomenológica para construir diferentes modelos sob a forma de uma parametrização simples de um campo escalar, que também pode estar acoplado à matéria escura. A ambição é propor alternativas viáveis ao modelo padrão, limitando o número de parâmetros adicionais ao mínimo estritamente necessário porque modelos mais complexos não podem normalmente ser constrangidos por observações devido às degenerescências que aumentam com o número de parâmetros. O nosso trabalho esforça-se por cobrir as etapas clássicas da construção e testes de modelos em cosmologia. Começamos com a procura de parametrizações adequadas das quais possamos extrair expressões analíticas. Elas permitem-nos estudar teoricamente o desempenho assimptótico dos modelos, tanto em termos da evolução cosmológica de fundo como da evolução das perturbações. Modificamos um código de Einstein-Boltzmann existente para confirmar numericamente a viabilidade dos cenários e calcular quantidades observáveis, tais como distâncias de luminosidade e espectros de potência. Os resultados numéricos permitem-nos avaliar a sensibilidade dos observáveis previstos aos graus de liberdade adicionais. Finalmente, realizamos análises com Markov Chain Monte Carlo para estimar o valor dos parâmetros e constranger os modelos considerados com observações astronómicas. Alem de recorrer a trabalhos anteriores, particularmente os que estudam sistemas dinâmicos em cosmologia, procedemos oportunisticamente à revisão de conceitos-chave ao longo da dissertação sempre que necessário para interpretar características cosmológicas. Acreditamos que esta abordagem prática é pedagogicamente inestimável na medida em que permite aprender e apresentar esta área complexa através de um estudo concreto e abrangente. Esperamos que a dissertação também ofereça de forma convincente modelos promissores cuja originalidade reside principalmente na simplicidade da parametrização, embora capaz de cobrir uma vasta gama de evoluções com apenas um parâmetro adicional.

O nosso objectivo no Capítulo 1 é introduzir o modelo padrão ΛCDM que especula nomeadamente a existência de uma constante cosmológica que acelera a expansão do Universo. É a referência contra a qual iremos testar os modelos dinâmicos de energia escura considerados neste trabalho. O modelo padrão é construído sobre os fundamentos teóricos da cosmologia moderna que descrevemos no Apêndice A por conveniência. Adicionalmente, vamos ver brevemente como a equação de estado da energia escura pode ser parametrizada como o meio mais simples de lidar com o problema da constante cosmológica.

No Capítulo 2, como alternativa à habitual parametrização da equação de estado, examinamos em pormenor uma parametrização linear de quintessência sob a forma de uma dependência logarítmica

[1] Λ Cold Dark Matter

do factor de escala: $\phi = \lambda \ln a$. Após a apresentação da quintessência como um campo escalar responsável pela energia escura, vamos construir fenomenologicamente um modelo parametrizado a que chamámos λCDM para estender o modelo padrão com apenas um único parâmetro λ. Veremos que prevê soluções de escala que aliviam o problema de ajuste das condições iniciais, ao mesmo tempo que permite a aceleração cósmica tardia. A fim de avaliarmos o comportamento do nosso modelo λCDM no universo perturbado, também prestamos atenção à evolução das flutuações da matéria. Comparamos a parametrização do campo escalar com o modelo ΛCDM no que diz respeito à dinâmica das perturbações da matéria escura.

Agora que estamos confiantes que a nossa parametrização λCDM é um modelo teoricamente credível de energia escura dinâmica, queremos no Capítulo 3 estimar os valores mais adequados dos parâmetros que asseguram que o modelo satisfaz os conjuntos de dados observacionais. Avaliamos em primeiro lugar a sensibilidade das quantidades observáveis previstas pelo modelo ao parâmetro relevante λ. Descreveremos em termos gerais o código Einstein-Boltzmann chamado CLASS que modificámos para adaptar o potencial do campo escalar parametrizado. Apresentamos também os diferentes conjuntos de dados de observações cosmológicas e astrofísicas que escolhemos. Finalmente, discutimos os resultados das análises das cadeias de Markov Monte Carlo que realizamos com o pacote de inferências Bayesianas chamado MontePython. Descobrimos que a parametrização reproduz notavelmente bem as observações e é ao mesmo tempo indistinguível de uma constante cosmológica, que não pode ser descartada.

No Capítulo 4, queremos testar acoplamentos de energia escura com matéria escura, considerando um acoplamento constante β que parametriza a interacção entre a matéria escura fria e o campo de quintessência. Em primeiro lugar, construímos o nosso modelo $\lambda\beta$CDM para avaliar os efeitos do acoplamento sobre a evolução teórica de fundo do universo. Tratamos também da evolução das perturbações para identificar o impacto do acoplamento sobre os observáveis previstos. Para este efeito, modificámos novamente o código do CLASS para adaptar o módulo das perturbações. Terminamos com uma análise Bayiesana para estimar e constringir os parâmetros do modelo acoplado.

O nosso último Capítulo 5 encerra a dissertação oferecendo considerações finais, bem como perspectivas de desenvolvimento futuro do nosso trabalho. Dizem especialmente respeito à necessidade de completar a análise estatística e de explorar acoplamentos suplementares, por exemplo com matéria escura mista e o sector electromagnético. Este último seria útil para ajudar a constranger λ and β com a variação da estrutura fina constante α.

Palavras-chave: Energia Escura, Quintessência Acoplada, Cosmologia Observacional

Abstract

Our dissertation aims to examine possible extensions of the standard ΛCDM[2] model by generalizing the cosmological constant with quintessence, i.e. a scalar field ϕ whose equation of state $w = p/\rho$ varies as time goes on. Rather than trying to elucidate the very nature of dark energy, we adopt a phenomenological approach to construct different models in the form of a simple parametrisation of a scalar field, that could also be coupled to dark matter. The ambition is to propose viable alternatives to the standard model, limiting the number of additional parameters to the strict minimum as more complex models cannot usually be constrained by observations because of the degeneracies that increase with the number of parameters. Our work endeavours to cover the classical steps of model building and testing in cosmology. We begin with seeking suitable parametrisations from which we can extract analytic expressions. They enable us to theoretically study the asymptotic performance of the models in terms of both background and perturbations evolution. We modify an existing Einstein-Boltzmann code to numerically confirm the viability of the scenarios and compute related observable quantities such as luminosity distances and power spectra. The numerical results allow us to assess the sensitivity of the predicted observables to the extra degrees of freedom. We finally carry-out Markov Chain Monte Carlo analyses to estimate the parameters values and constrain the models considered with astronomical observations. While relying on previous works, particularly those studying dynamical systems in cosmology, we review key concepts across the dissertation whenever required to interpret cosmological features. We believe that this hands-on approach is pedagogically invaluable in that it permits learning and presenting this complex domain by doing a concrete and comprehensive study. We hope the dissertation is also convincingly offering promising models whose originality mainly lies in the simplicity of the parametrisation which is though able to cover a wide range of evolutions with only one additional parameter.

We aim in Chapter 1 to introduce the standard ΛCDM model that notably speculates the existence of a cosmological constant accelerating the expansion of the Universe. It is the benchmark against which we will be testing the dynamical dark energy models considered in this work. The standard model is built on the theoretical foundations of modern cosmology that we describe in Appendix A for convenience. Additionally, we are briefly reviewing how the equation of state of dark energy can be parametrised as the simplest means to address the cosmological constant problem.

In Chapter 2, as an alternative to the usual parametrisation of the equation of state, we examine in detail a linear parametrisation of quintessence in the form of a logarithmic dependence on the scale factor: $\phi = \lambda \ln a$. Following the presentation of quintessence as a scalar field responsible for dark energy, we will be phenomenologically constructing a parametrised model we called λCDM to extend the standard one with just one single parameter λ. We will see that it provides for scaling solutions in

[2] Λ Cold Dark Matter

the universe background that alleviate the problem of the initial conditions fine-tuning, while at the same time allows for the late-time cosmic acceleration. In order to appreciate the behaviour of our λCDM model in the perturbed universe, we also pay regard to the evolution of matter fluctuations. We will be describing the linear perturbation theory in the synchronous gauge, and later apply it to compare the scalar field parametrisation with the ΛCDM model as regards the dynamical evolution of the cold dark matter perturbations.

Now that we are confident our scalar field λCDM parametrisation is a theoretically credible model of dynamical dark energy, we want in Chapter 3 to estimate the best-fit values of the parameters that ensure the model satisfies observational datasets. We first assess the sensitivity of observable quantities predicted by the model to the relevant parameter λ. We will broadly describe the Einstein-Boltzmann code called CLASS that we have modified to accommodate the analytic expression of the self-interacting potential of the parametrised scalar field. We will also be presenting the different datasets of cosmological and astrophysical observations we have chosen as probe of either background or perturbation evolution. We will finally be discussing the results of the Markov Chain Monte Carlo analyses we are carrying out with the Bayesian inference package called MontePython. We figure out that the parametrisation reproduces remarkably well the observations and is at the same time indistinguishable from a cosmological constant, which cannot be discarded.

In Chapter 4, we are testing dark energy couplings with dark matter by considering a constant coupling strength β that parametrises the interaction between cold dark matter and the quintessence field. First of all, we will be building our model $\lambda\beta$CDM to assess the effects of the coupling on the theoretical background evolution of the universe. We will also be addressing the evolution of the cosmological perturbations to identify the impact of the coupling on the corresponding predicted observables. To this end, we have again modified the CLASS code to notably adapt the perturbations module to the coupling. We will finish with a MCMC analysis to estimate and constrain the parameters of the model we are considering.

Our last Chapter 5 wraps up the dissertation by offering concluding remarks, as well as prospects for future development of our work. They especially concern the necessity to complement the statistical analysis and to explore supplementary couplings, for instance with mixed dark matter and the electromagnetic sector. The latter would be useful to help constrain λ and β with the variation of the fine structure constant α.

Keywords: Dark Energy, Coupled Quintessence, Observational Cosmology

Contents

List of Tables

List of Figures

Chapter 1

Standard cosmology challenges

The dominant paradigm in modern cosmology is currently formalised in the ΛCDM model. It successfully describes the Universe in expansion that began with a hot Big Bang at the origin of time. Even though the standard model fits well the available astrophysical observations, it faces serious challenges on the determination of the Universe composition which is shrouded in mystery. It is built on the underlying postulate that the Universe comprises two elusive ingredients accounting for no less than ninety five percent of its content. 'Dark matter', which necessarily complements the tiny part of ordinary matter we are made of, is itself a minute fraction of the overall mass-energy that governs the whole expansion. 'Dark energy', as a hypothetical and overwhelming ethereal extra essence of unknown nature and negative pressure, is needed to explain the paradoxical acceleration of the universe.

1.1 ΛCDM model in brief

According to the Raychaudhuri equation[1], the known content of the universe should slow the expansion because the acceleration of the scale factor, $\ddot{a}$, is negative for both radiation and matter. This is however in total contradiction with astrophysical observations. The acceleration of the expansion was discovered by two independent teams who found in 1998 that remote supernovae of type Ia (SNIa) were fainter than expected in a universe dominated by matter [1, 2]. This pivotal discovery suggests the existence of an unknown component dubbed dark energy, provided that both General Relativity and the cosmological principle still hold [3, 4]. In order for the universe to accelerate, the Raychaudhuri equation imposes that dark energy must have a negative pressure ($\rho + 3p < 0 \Leftrightarrow p < -\rho/3 < 0$). The cosmological constant has logically been evoked as a candidate for dark energy exponentially accelerating the universe[2],

$$\rho_\Lambda = \Lambda \quad \Rightarrow \quad a \propto e^{\sqrt{\Lambda/3}\, t}. \tag{1.1}$$

[1] The basics of cosmology are summarized in Appendix A for convenience.

[2] The cosmological constant pressure is negative according to the continuity equation (A.21), $\dot{\rho}_\Lambda = \dot{\Lambda} = 0 \Rightarrow p_\Lambda = -\Lambda$

Taking account of the relation between the density parameters[3] Ω_i (A.22), the evolution of the universe background can be described in terms of five cosmological parameters only: Ω_{k_0}, Ω_{r_0}, Ω_{m_0}, Ω_{Λ_0} and H_0 (or h). In order to extrapolate the past and future evolution of the universe background, it would then be sufficient to measure the values of the present density of radiation, matter, curvature and Λ, as well as H_0, and apply the Friedmann equation,

$$H^2(a) = H_0^2 \left(\frac{\Omega_{r_0}}{a^4} + \frac{\Omega_{m_0}}{a^3} + \frac{\Omega_{k_0}}{a^2} + \Omega_{\Lambda_0} \right). \tag{1.2}$$

Observational cosmology precisely aims to measure the value of these cosmological parameters. In fact, spatial curvature and radiation are negligible. The universe is nearly flat as it was found that $\Omega_{k_0} = 0.001 \pm 0.002$ at 68% confidence level [5]. The density of radiation is a nearly fixed quantity as it relates to today's Cosmic Microwave Background (CMB) temperature $T_\gamma \sim 2.726K$. It is thus a very well constrained parameter of the model. The energy density of electromagnetic radiation is dominated by the photons of the CMB. According to the Stefan-Boltzmann law, $\Omega_{\gamma_0} = 2.47 \times 10^{-5} h^{-2}$. Other relativistic species additionally contribute to the radiation density, particularly the neutrino background. Assuming the existence of three families of massless neutrinos, one obtains,

$$\Omega_{r_0} = \left[1 + 3 \times \frac{7}{8} \times \left(\frac{4}{11} \right)^{4/3} \right] \Omega_{\gamma_0} \simeq 4.1 \times 10^{-5} h^{-2}. \tag{1.3}$$

Given that radiation and curvature are negligible, Eq. (A.23) reads $\Omega_\Lambda = 1 - \Omega_m = 1 - (\Omega_c + \Omega_b)$. Hence, the free parameters describing the background evolution of the ΛCDM universe are limited to Ω_{c_0}, Ω_{b_0} and h. Alternatively, one can use absolute densities $\omega_i = \Omega_i h^2$ instead of the density parameters. According to the most recent Planck results [5], approximatively 68% of the universe content is made of the cosmological constant, 27% of cold dark matter and 5% of baryons. By rewinding the scale factor back, Eq. (1.2) shows that the universe was dominated by radiation at early times, and later by matter, before entering into the present dark energy era. The time at equality between radiation and matter ($a_{\rm eq}$) and the transition between matter and the cosmological constant (a_Λ) are background quantities that can be estimated with the density parameters.

The model foresees a hot Big Bang corresponding to the initial singularity when $a \to 0$. Since the temperature varies with the scale factor as $T \propto a^{-1}$, the universe was not only denser but also hotter in the past. Big Bang nucleosynthesis took place 3 minutes after the Big Bang, and was followed by an opaque plasma epoch when radiation domination ended. The Universe later became transparent with the decoupling of the primordial photons that compose the CMB. Moreover, the ΛCDM model is complemented by the existence of a period of inflation at the very early time when the universe was dominated by quantum vacuum, supposedly 10^{-34} s after the Big Bang [6]. It notably provides the

[3] k, r, m, Λ, c and b respectively stand for curvature, radiation, matter, cosmological constant, cold dark matter and baryon.

adiabatic initial conditions of the scalar perturbations in the standard model.

In spite of the necessity to speculate the existence of a dark sector accounting for no less than 95% of the universe content, as only 5% of the matter would be in the form of baryons predicted by the Standard Model of particles, the standard cosmology is very much in agreement with the observations. Nevertheless, while the cosmological constant identified with the energy of the vacuum exercising a negative pressure is a natural choice for identifying dark energy, it suffers from several shortcomings [7]. Because the cosmological constant is roughly speaking currently dominating the other components, Eq. (1.2) gives its order of magnitude: $\Lambda \sim H_0^2$. The corresponding energy density is $\Lambda \sim 10^{-47}\text{GeV}^4$. However, the vacuum energy density that can be estimated in quantum field theory is $\rho_{\text{vac}} \sim 10^{74}\text{GeV}^4$. Therefore, accounting the energy of vacuum for dark energy leads to an anomalous discrepancy of about 121 orders of magnitude [8]. Furthermore, there is another issue known as the coincidence problem [9, 10]. According to Eq. (A.26), the energy density of matter dilutes as a^{-3} while the energy density of the cosmological constant remains constant with the expansion by definition. The equality between matter and dark energy takes place at,

$$z_\Lambda = \left(\frac{\Omega_{\Lambda_0}}{\Omega_{m_0}}\right)^{1/3} - 1 \approx 0.3, \tag{1.4}$$

leaving unexplained the reason why it is happening so recently since this would necessitate initial conditions for the matter and dark energy densities intriguingly severe at the origin of time.

Rather than considering it constant, dynamical dark energy whose density varies with time would appropriately address the cosmic coincidence issue [11]. Even though the very nature of dark energy is unlikely to be unveiled, its time variation could logically ensure its observed abundance. The simplest and model independent approach is to phenomenologically parametrise the equation of state with redshift as reviewed in the next section.

1.2 Cosmological constant simplest alternative

The measurement of luminosity distances suggests that the expansion of the universe is currently accelerating. Assuming that non-relativistic matter, in the form of baryons and dark matter, contributes to the expansion with energy density ρ_m and no pressure, as well as dark energy with energy density ρ_{de} and unknown pressure p_{de}, the Raychaudhuri equation (A.19) gives the condition for the universe acceleration to be satisfied by the dark energy equation of state parameter,

$$-1 \leq w < -\frac{1}{3}\left(1 + \frac{\Omega_m}{\Omega_{\text{de}}}\right) < -\frac{1}{3}, \tag{1.5}$$

where $w = p_{\text{de}}/\rho_{\text{de}}$. $w > -1$ corresponds to a dark energy component that slowly dilutes. $w = -1$ corresponds to a constant dark energy component identical to the cosmological constant.

While we know that the dark energy equation of state must satisfy $w < -1/3$, there is no indication on whether it is varying with time. To potentially disqualify the cosmological constant, it is appropriate to parametrise the equation of state as a function of redshift z and confront it with astrophysical observations to estimate the values of the parameters. Based on a phenomenological approach, the simplest parametrisation is linear and comes from Taylor expanding the function $w(z)$ around $z = 0$ at first-order with only two free parameters w_0 and w_1 [12],

$$w(z) = w_0 + w_1 z. \tag{1.6}$$

Being at first order, linear parametrisations are thus valid in the local universe only and should be constrained with local observation datasets. The function $w(z)$ can be expanded to higher orders to extend its validity yet at the expense of additional parameters. The shortcoming of these Taylor expansions lies in the absence of ceiling for the value of the equation of state that continuously increases with redshift, unsuitably going beyond $+1$ for large z. Alternatively, the w parametrisation can also be a function of the scale factor [13, 14],

$$w(a) = w_0 + w_a(1 - a) = w_0 + w_a \frac{z}{1 + z}, \tag{1.7}$$

or number of e-folds $N = \ln a$ [15],

$$w(z) = w_0 - w_1 \log(1 + z). \tag{1.8}$$

A means to further extend the validity of the equation of state is to define a parametrisation stepwise in redshift $w(z_i) = w_i$ for every redshift bin z_i, or equivalently for every scale factor bin a_i [16]. It allows dark energy to be differently parametrised during the successive universe domination by radiation and matter,

$$w(a) = F_1 f_r(a) + F_2 f_m(a) + F_3, \tag{1.9}$$

where the functions f_i take the following form,

$$f_i(a) = \left[1 + \exp\left(-\frac{a - a_i}{\Delta_i}\right)\right]^{-1}, \qquad i = r, m. \tag{1.10}$$

(a_r, a_m) are the values of the scale factor at the times of transition and (Δ_r,Δ_m) the duration of transitions. F_1, F_2 and F_3 are constants that are set by imposing the values of the equation of state at radiation domination, at matter domination and today. Stepwise parametrisation requires no less than seven parameters. Instead, it is possible, with a reduced number of parameters, to parametrise a scalar field called quintessence that would be responsible for a dynamical dark energy component both in the early universe and at the present time. This is the subject of the next chapter.

Chapter 2

λCDM quintessence model

Given the unknown nature of dark energy, it is natural to look into known physics to at least attempt to describe its possible dynamics. Promising candidates are scalar fields because they already exist in particle physics models. Although the Standard Model Higgs field is the only one detected so far in Nature, it has been raising expectations on the existence of other fields [17]. Moreover, the current acceleration can be compared to the inflationary period thought to be possibly sourced by a scalar field in the primordial universe [18]. Yet even in the eventuality that they are not really responsible for the acceleration of the Universe, the properties of the true model of dark energy may be described by a scalar field [19].

2.1 Quintessence general description

Quintessence denotes a self-interacting scalar field weakly coupled to ordinary matter through gravity, and playing the role of dark energy responsible for the accelerated expansion [20, 21]. It varies with time and thus carries kinetic energy. Also, a potential energy density $V(\phi)$, that should be specified to completely define the model, is associated with each value of the field. Quintessence can therefore be characterized by a Lagrangian density that sums a canonical (or standard) kinetic energy term to the potential energy one,

$$\mathcal{L}_\phi = -\frac{1}{2} g^{\mu\nu} \partial_\mu \phi \partial_\nu \phi - V(\phi). \tag{2.1}$$

Similarly to Eq. (A.11), the action of the cosmological model that includes quintessence along with an usual matter source reads,

$$S = \int d^4x \sqrt{-g} \left[\frac{1}{2\kappa^2} R + \mathcal{L}_\phi \right] + S_M, \tag{2.2}$$

where S_M is the matter action that depends on the metric $g_{\mu\nu}$ and all types of matter fields (radiation and

non-relativistic matter), but not on the quintessence field,

$$S_M = \int \mathcal{L}_M \sqrt{-g}\, d^4x. \tag{2.3}$$

Similarly to Eq. (A.12), the field's contribution to the energy momentum is defined by the following stress-energy tensor,

$$T_{\mu\nu} = \frac{-2}{\sqrt{-g}} \frac{\delta(\sqrt{-g}\mathcal{L}_\phi)}{\delta g^{\mu\nu}} = \partial_\mu\phi\partial_\nu\phi - g_{\mu\nu}\left[\frac{1}{2}\partial^\alpha\phi\partial_\alpha\phi + V(\phi)\right]. \tag{2.4}$$

Assuming that quintessence is spatially homogeneous, in accordance with the cosmological principle (e.g. it is a function of time only), the tensor is that of a perfect fluid, as in Eq. (A.15), with the following energy density and pressure,

$$\rho_\phi = -\frac{1}{2}\partial^\mu\phi\partial_\mu\phi + V(\phi) = \frac{1}{2}\dot{\phi}^2 + V(\phi), \tag{2.5}$$

$$p_\phi = -\frac{1}{2}\partial^\mu\phi\partial_\mu\phi - V(\phi) = \frac{1}{2}\dot{\phi}^2 - V(\phi). \tag{2.6}$$

The scalar field energy density is the sum of the kinetic energy density $\frac{1}{2}\dot{\phi}^2$ and the potential energy density $V(\phi)$, whereas the pressure is the difference between the two. It follows that,

$$\dot{\phi}^2 = \rho_\phi + p_\phi = \rho_\phi\left(1 + w_\phi\right), \tag{2.7}$$

where w_ϕ is the quintessence equation of state,

$$w_\phi = \frac{p_\phi}{\rho_\phi} = \frac{\frac{1}{2}\dot{\phi}^2 - V(\phi)}{\frac{1}{2}\dot{\phi}^2 + V(\phi)} = 1 - \frac{2V(\phi)}{\rho_\phi}. \tag{2.8}$$

w_ϕ can vary between the cosmological constant limit -1 when the scalar field is dominated by the potential energy $V(\phi)$, and $+1$ when it is the kinetic energy $\dot{\phi}^2$ that dominates.

By considering the flat FLRW metric (A.2) for the homogeneous and isotropic universe, the action (2.2) implies the following Friedmann equations,

$$H^2 = \frac{\kappa^2}{3}\left[\frac{\dot{\phi}^2}{2} + V(\phi) + \rho_M\right], \tag{2.9}$$

$$\dot{H} = -\frac{\kappa^2}{2}\left[\dot{\phi}^2 + \left(1 + w_M\right)\rho_M\right]. \tag{2.10}$$

The equation of motion of the scalar field, called Klein-Gordon equation, can be derived by the variation of the action (2.2),

$$\ddot{\phi} + 3H\dot{\phi} + V_{,\phi} = 0, \tag{2.11}$$

where the subscript ϕ stands for the derivative with respect to the scalar field. The potential plays the role of a force acting on the scalar field through the term $V_{,\phi}$ while the term $H\dot{\phi}$ represents the friction added by the expansion of the universe. The Klein-Gordon equation also derives from the quintessence continuity equation when the scalar field is separately conserved,

$$\dot{\rho}_\phi + 3H\left(\rho_\phi + p_\phi\right) = \dot{\rho}_\phi + 3H\dot{\phi}^2 = 0. \tag{2.12}$$

Using Eq. (2.7) and the dark energy density parameter Ω_ϕ defined like in Eq. (A.22), the quintessence equation of state is expressed by,

$$w_\phi = -1 + \frac{(\kappa\dot{\phi})^2}{3H^2\Omega_\phi}. \tag{2.13}$$

Finally, one can define an effective equation of state $w_{\text{eff}} = p_{\text{total}}/\rho_{\text{total}}$ for the whole cosmological fluid. Neglecting radiation in a flat universe, it reads,

$$w_{\text{eff}} = \frac{p_\phi}{\rho_\phi + \rho_m} = \frac{p_\phi/\rho_\phi}{1 + \Omega_m/\Omega_\phi} = w_\phi\Omega_\phi. \tag{2.14}$$

2.2 Scalar field parametrisation

Rather than parametrising the dark energy equation of state as usual, it is the scalar field evolution itself that we want to parametrise in the present work. We have seen in the previous section that quintessence is defined by both the kinetic and potential terms. Usually in the literature, the analytic form of the potential $V(\phi)$ is arbitrarily and explicitly assumed a priori, along with the requirement that the field is slow-rolling for producing cosmic acceleration, e.g. in Ref. [22–28]. The latter assumption implies a flat potential that commonly satisfies $\dot{\phi}^2 \ll V(\phi)$ in order to provide for a negative pressure of the cosmological fluid when the scalar field dominates the matter content of the Universe. Moreover, to produce a sustainable acceleration, the quintessence field is further assumed to satisfy $|\ddot{\phi}| \ll |3H\dot{\phi}|$.

Instead, here, we do not postulate any potential shape from the outset, nor any prior slow-rolling conditions applying to the scalar field. We analytically derive the expression of the potential on the basis of suitable scalar field parametrisations, with the intention to phenomenologically build and constrain quintessence models as alternatives to the standard ΛCDM.

2.2.1 How to look for suitable parametrisations

Our starting point is the most general form the scalar field energy density can take, neglecting radiation in a flat universe also composed of pressureless matter [29]. It considers the number of e-folds $N = \ln a$ as the time variable,

$$\phi = \phi\,(N) \quad \Rightarrow \quad \dot{\phi} = H\phi', \tag{2.15}$$

where a prime denotes differentiation with respect to the number of e-folds, and ϕ is to be understood for convenience as the dimensionless field $\phi \to \hat{\phi} = \kappa\phi$. The latter convention is in line with the structure of the equations in the Boltzmann code CLASS[1] that we are using to numerically compute the observational outputs of the cosmological models. In that code, the scalar field is given in units of the reduced Planck mass $M_p = \sqrt{\hbar c/8\pi G} = \kappa^{-1} = 2.435 \times 10^{18}$ GeV, and the prefactor $8\pi G/3$ in the Friedmann equation is conventionally absorbed in the units of density. In this context, we work in natural units where $\kappa = \hbar = c = 1$, for the rest of the document. Using the number of e-folds, the conservation of the scalar field (2.12) reads,

$$\rho'_\phi = -3H^2\phi'^2, \tag{2.16}$$

with,

$$3H^2 = \rho_{m_0}\left(a^{-3} + \frac{\rho_\phi}{\rho_{m_0}}\right), \tag{2.17}$$

where ρ_{m_0} is today's energy density of non-relativistic matter. By combining the two last equations, one finds the following differential equation satisfied by the scalar field energy density [29],

$$\frac{\rho'_\phi}{\rho_{m_0}} = -\phi'^2\left(a^{-3} + \frac{\rho_\phi}{\rho_{m_0}}\right), \tag{2.18}$$

whose general solution, expressed in terms of quadratures with respect to ϕ'^2, is our starting point,

$$\frac{\rho_\phi}{\rho_{m_0}} = e^{-\int_0^N dN\phi'^2} \times \left[\frac{\Omega_{\phi_0}}{\Omega_{m_0}} - \int_0^N dN\phi'^2 e^{-3N+\int_0^N dN\phi'^2}\right]. \tag{2.19}$$

The question is whether there exists parametrisations of the scalar field that are suitable to derive analytic expressions of the energy density ρ_ϕ from Eq. (2.19), and consequently of the potential $V\,(\phi)$ itself. We present in what follows, two possibilities.

2.2.2 Exponential form: $\phi = \phi_0 e^{\epsilon N}$

Let us try a parametrisation with a single parameter ϵ of the form,

$$\phi = \phi_0 e^{\epsilon N} = \phi_0 a^\epsilon \quad \Rightarrow \quad \phi' = \epsilon\phi, \tag{2.20}$$

which is subject to time symmetry by making $\epsilon \to -\epsilon$. We therefore stick to positive values of the parameter, bearing in mind that the opposite sign interchanges the past and future cosmological evolution.

[1] Cosmic Linear Anisotropy Solving System

This parametrisation simplifies the analytic integrations in Eq. (2.19) thanks to a convenient change of variable from N to ϕ,

$$\int_0^N dN\phi'^{\,2} = \int_{\phi_0}^{\phi} dN\frac{d\phi}{dN}\phi' = \int_{\phi_0}^{\phi}\phi' d\phi = \epsilon\int_{\phi_0}^{\phi}\phi\, d\phi = \frac{\epsilon}{2}\left(\phi^2-\phi_0^2\right). \tag{2.21}$$

Therefore,

$$-3N+\int_0^N dN\phi'^{\,2} = \ln\left(\frac{\phi}{\phi_0}\right)^{-3/\epsilon} + \frac{\epsilon}{2}\left(\phi^2-\phi_0^2\right), \tag{2.22}$$

which means that,

$$e^{-3N+\int_0^N dN\phi'^{\,2}} = \left(\frac{\phi}{\phi_0}\right)^{-3/\epsilon} e^{\frac{\epsilon}{2}\left(\phi^2-\phi_0^2\right)}, \tag{2.23}$$

and consequently,

$$\int_0^N dN\phi'^{\,2} e^{-3N+\int_0^N dN\phi'^{\,2}} = \epsilon\phi_0^{3/\epsilon}e^{-\frac{\epsilon}{2}\phi_0^2}\int_{\phi_0}^{\phi}\phi^{1-3/\epsilon}e^{\frac{\epsilon}{2}\phi^2}d\phi. \tag{2.24}$$

By making another change of variable, $x=-\frac{\epsilon}{2}\phi^2$ and $s=1-\frac{3}{2\epsilon}$, we obtain,

$$\int_0^N dN\phi'^{\,2} e^{-3N+\int_0^N dN\phi'^{\,2}} = -x_0^{1-s}e^{x_0}\int_{x_0}^{x} x^{s-1}e^{-x}dx, \tag{2.25}$$

where we recognize the incomplete Gamma function $\Gamma(s,x)$,

$$\int x^{s-1}e^{-x}dx = -\Gamma\left(s,x\right). \tag{2.26}$$

Coming back to Eq. (2.19), we finally find an analytic expression for the scalar field energy density,

$$\rho_\phi\left(x\right) = \rho_{m_0}\, e^{x-x_0}\left\{\frac{\Omega_{\phi_0}}{\Omega_{m_0}} - x_0 e^{x_0}\left[\left(\frac{x}{x_0}\right)^s\frac{\Gamma\left(s,x\right)}{x^s} - \frac{\Gamma\left(s,x_0\right)}{x_0^s}\right]\right\}, \tag{2.27}$$

which is illustrated in Figure 2.1. The energy density of the scalar field is not negligible in the early universe. It dilutes with time, down until freezing in the late universe, mimicking a cosmological constant. It though resumes to dramatically dilute in the future.

With regards to the dark energy equation of state, we obtain from Eq. (2.13),

$$w_\phi = -1+\frac{\phi'^{\,2}}{3}\frac{\rho_m+\rho_\phi}{\rho_\phi} = -1+\frac{\epsilon^2}{3}\phi_0^2\, e^{2\epsilon N}\left(1+\frac{\rho_{m_0}}{\rho_\phi}e^{-3N}\right), \tag{2.28}$$

whose today's value is,

$$w_0 = -1+\frac{\epsilon^2\phi_0^2}{3\Omega_{\phi_0}}. \tag{2.29}$$

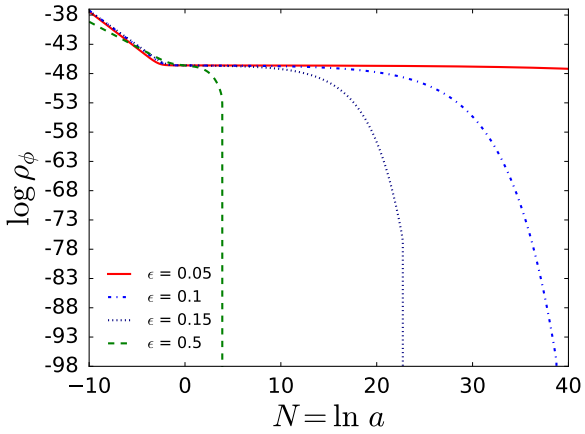

Figure 2.1: Energy density of the scalar field in the exponential parametrisation. The plot is based on the analytic expression (2.27) for $\Omega_{\phi_0} = 0.68$ and $\phi_0 = 1$.

When $\epsilon \to 0$, the cosmological constant is recovered, and the parameter ϵ should be small enough to match the observed value of $w_0 \sim -1$. Since the Universe is currently accelerating, today's effective equation of state of the whole cosmological fluid should satisfy $w_{\text{eff}} = \Omega_\phi w_\phi < -1/3$, entailing,

$$|\epsilon| < \frac{\sqrt{-1 + 3\Omega_{\phi_0}}}{|\phi_0|} \sim 1, \qquad \Omega_{\phi_0} > \frac{1}{3}. \tag{2.30}$$

Let us study the limits of w_ϕ. In the past, $N \to -\infty$, $\phi \to 0$ and $x \to 0$. The incomplete Gamma function simplifies into $\frac{\Gamma(s,x)}{x^s} \sim -\frac{1}{s}$, and the energy density becomes,

$$\rho_\phi(x) = \rho_{m_0}\, e^{x-x_0} \left\{ \frac{\Omega_{\phi_0}}{\Omega_{m_0}} + \frac{x_0 e^{x_0}}{s} \left[\left(\frac{x}{x_0} \right)^s - 1 \right] \right\}. \tag{2.31}$$

Provided that $\epsilon < 3/2$, implying that $s < 0$, we obtain,

$$\frac{\rho_\phi}{\rho_{m_0}} e^{3N} = \frac{\rho_\phi}{\rho_{m_0}} \left(\frac{x}{x_0} \right)^{3/2\epsilon} \sim \frac{x}{s}, \tag{2.32}$$

and therefore, when $N \to -\infty$ and $\epsilon < 3/2$, $w_\phi \to -\frac{2}{3}\epsilon$. In the future, $N \to +\infty$, $\phi \to +\infty$ and $x \to -\infty$. The incomplete Gamma function simplifies into $\Gamma(s,x) \sim x^{s-1}e^{-x}$, leading to the following approximated expression,

$$\frac{\rho_\phi}{\rho_{m_0}} = e^x \left(\frac{\Omega_{\phi_0}}{\Omega_{m_0}} e^{-x_0} - \frac{x_0}{s} \right) - \left(\frac{x}{x_0} \right)^{s-1}. \tag{2.33}$$

In the limit $N \to +\infty$ and $\epsilon < 3/2$, we obtain that $w_\phi + 1 \sim x^s e^x$, which implies $w_\phi \to -1$.

However, we notice the existence of a divergence at a time in the future that depends on the value of ϵ. The smaller ϵ the later it happens in Figure 2.2. The equation of state skyrockets beyond $w_\phi = +1$ once the pressure of the scalar field becomes larger than its decreasing density. The potential is obviously becoming negative too. We can reconstruct it using Eq. (2.5),

$$V(\phi) = \rho_\phi - \frac{1}{2}\dot{\phi}^2 = \rho_\phi - \frac{1}{2}H^2\phi'^2 = \rho_\phi - \frac{1}{2}H^2\epsilon^2\phi^2, \tag{2.34}$$

where H^2 is given in Eq. (2.17). Substituting Eq. (2.27) into the above equation, we obtain,

$$\frac{V(x)}{\rho_{m_0}} = e^{x-x_0}\left\{\frac{\Omega_{\phi_0}}{\Omega_{m_0}} - x_0 e^{x_0}\left[\left(\frac{x}{x_0}\right)^s \frac{\Gamma(s,x)}{x^s} - \frac{\Gamma(s,x_0)}{x_0^s}\right]\right\}\left(1+\frac{\epsilon x}{3}\right) + \frac{\epsilon x}{3}\left(\frac{x}{x_0}\right)^{s-1}. \tag{2.35}$$

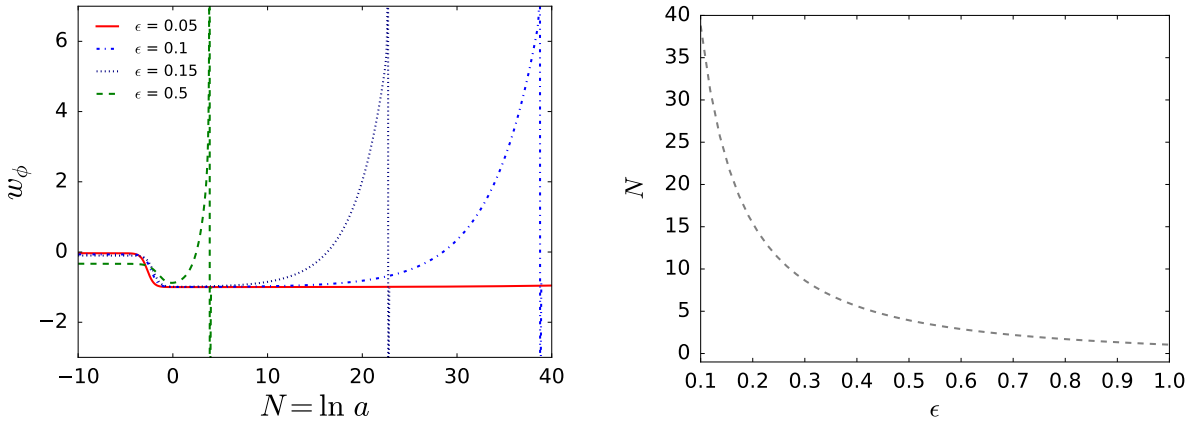

(a) Scalar field equation of state evolution

(b) Time of the divergence

Figure 2.2: Panel (a): Evolution of the quintessence equation of state with $\Omega_{\phi_0} = 0.68$ and $\phi_0 = 1$ today, based on the analytic expression (2.27). It diverges at a time determined by the value of ϵ. Panel (b): The divergence time is approximated by solving numerically the root of Eq. (2.33), e.g. $N \sim 3.90$ for $\epsilon = 0.5$.

The scalar field energy density even reaches negative values, ergo violating the weak energy condition. As the pressure in the scalar field remains positive, the equation of state suddenly changes sign and becomes negative again. When the scalar field energy density cancels with the energy density of matter, the Hubble rate H vanishes according to the Friedmann equation (2.17), as well as the scalar field kinetic energy, $\dot{\phi}^2 = H^2\phi'^2 = H^2\epsilon^2\phi^2 = 0$. Hence, at that time, $\rho_m = -\rho_\phi = p_\phi$ as shown in Figure 2.3, $w_\phi = -1$ and $\dot{\rho}_\phi = \dot{\rho}_m = \dot{a} = 0$ while $\ddot{a} \propto -3\rho_m < 0$. In the exponential parametrisation, the scale factor a grows up until a maximum and then decreases towards zero. In other words, the universe expands until a turn around point prior collapsing into a Big Crunch [30]. Although it could be worth further investigating this model, we decide to disregard the exponential parametrisation for the time being given that it reduces to the linear and simpler form presented in the next subsection.

2.2.3 Linear form: $\phi - \phi_0 = \lambda N$

We now examine the simplest parametrisation which takes the form of a linear function of N, with again a single parameter λ, already envisaged in Ref. [29],

$$\phi - \phi_0 = \lambda N, \qquad \phi' = \lambda, \qquad \phi'' = 0. \tag{2.36}$$

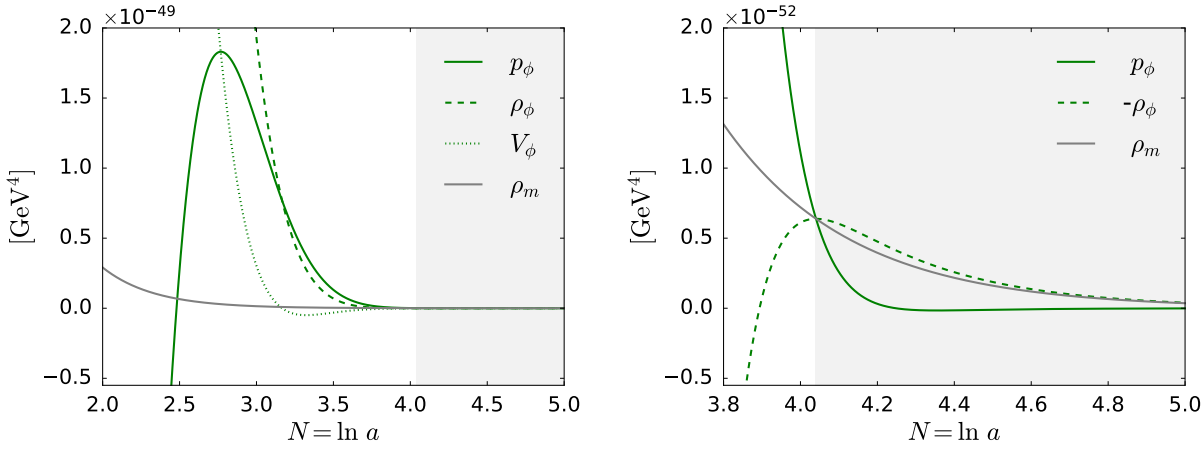

(a) Future evolution of the scalar field

(b) Zoom in the turn-around

Figure 2.3: Panel (a): The pressure in the scalar field becomes larger than its energy density around $N \sim 3.2$. The potential becomes negative at that time, allowing for $w_\phi > +1$. Panel (b): The scalar field energy density vanishes around $N \sim 3.9$ provoking the divergence of $w_\phi \to +\infty$. The three curves intersect at the turn around that takes place at $N \sim 4.04$ when $\dot{a} = 0$. The shaded area represents the excluded region as this universe begins to contract backwards towards a Big Crunch. In both panels, $\epsilon = 0.5$, $\Omega_{\phi_0} = 0.68$ and $\phi_0 = 1$.

This corresponds to a scalar field evolving logarithmically in time. It relates to the previous parametrisation in the limit that $\epsilon \ll 1$ for which $e^{\epsilon N} \sim \epsilon N + 1$. As there exists a symmetry with regards to the sign of λ by changing the sign of $\phi \to -\phi$, we decide to explore the linear parametrisation with $\lambda > 0$.

The analytic expression of the scalar field energy density is obtained by plugging Eq. (2.36) into Eq. (2.19),

$$\frac{\rho_\phi}{\rho_{m_o}} = \left(\frac{\Omega_{\phi_0}}{\Omega_{m_0}} + \frac{\lambda^2}{\lambda^2 - 3}\right) e^{-\lambda^2 N} - \left(\frac{\lambda^2}{\lambda^2 - 3}\right) e^{-3N}. \tag{2.37}$$

Unlike the exponential parametrisation, the energy density remains positive at all times provided,

$$|\lambda| < \sqrt{3\Omega_{\phi_0}}. \tag{2.38}$$

According to Eq. (2.17), the expansion of the universe is affected by the presence of the scalar field through the Hubble function that becomes,

$$H^2 = H_0^2 \left[\frac{3}{3 - \lambda^2}\Omega_{m_0} a^{-3} + \left(1 - \frac{3}{3 - \lambda^2}\Omega_{m_0}\right) a^{-\lambda^2}\right]. \tag{2.39}$$

Although the present parametrisation is also obtained following a linear approximation, it is not comparable with the linear parametrisation of the equation of state seen in Section 1.2. Its domain of validity is wider, not being limited to the local universe. Using Eq. (2.13), the equation of state becomes,

$$w_\phi = -1 + \frac{\lambda^2}{3}\left(1 + \frac{\rho_{m_0}}{\rho_\phi} e^{-3N}\right), \tag{2.40}$$

and today's value, $w_0 = -1 + \frac{\lambda^2}{3\Omega_{\phi_0}}$. Using Eq. (2.37), the equation of state can be analytically expressed as follows,

$$w_\phi = (\lambda^2 - 3)\left[3 - \frac{\lambda^2}{w_0}\frac{\Omega_{m_0}}{\Omega_{\phi_0}}\, e^{(\lambda^2-3)N}\right]^{-1}. \tag{2.41}$$

It is bound by the following limits: In the past, $w_\phi \to 0$, restricted to the matter dominated era, and in the future, $N \to +\infty \Rightarrow w_\phi \to -1 + \frac{\lambda^2}{3}$.

Finally, the analytic expression of the scalar field potential was reconstructed in Ref. [29] as well. According to Eq. (2.5), the scalar field potential can be found with,

$$V(\phi) = \rho_\phi - \frac{1}{2}\dot{\phi}^2 = \rho_\phi - \frac{1}{2}H^2\phi'^2 = \rho_\phi - \frac{1}{2}H^2\lambda^2, \tag{2.42}$$

where H^2 is given in Eq. (2.39). Substituting Eq. (2.37) into the above equation with $N = (\phi - \phi_0)/\lambda$, it was obtained the following potential of the self-interacting scalar field,

$$V(\phi) = Ae^{-\frac{3}{\lambda}\phi} + Be^{-\lambda\phi}, \tag{2.43}$$

where the mass scales are given by,

$$A = \frac{1}{2}\frac{\lambda^2}{3-\lambda^2}\rho_0\Omega_{m_0}e^{\frac{3}{\lambda}\phi_0}, \tag{2.44}$$

$$B = \frac{1}{2}\frac{\lambda^2-6}{3-\lambda^2}\rho_0\Omega_{\phi_0}w_0e^{\lambda\phi_0}. \tag{2.45}$$

with ρ_0 today's critical energy density. When $\lambda \to 0$, then the standard ΛCDM model is recovered. The background module of the existing Boltzmann code CLASS does not provide for this potential. We have to modify the code to implement Eq. (2.43), which is numerically plotted in Figure 2.4.

In the rest of the document, we call this model λCDM since the only difference with the standard one concerns the parametrised scalar field replacing the cosmological constant with the extra parameter λ. We will be statistically constraining it in Chapter 3 on the basis of cosmological and astrophysical observations. But first, in the next section, we use our modified version of CLASS to compute the cosmological background evolution of this model in order to confirm its viability and assess the expected parameter values range. The numerical results take also account of radiation and we assume Planck 2018 cosmological reference parameters in a spatially flat universe [5].

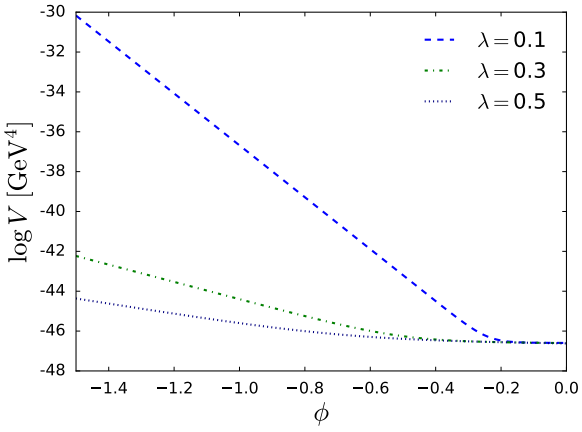

Figure 2.4: Potential energy in the linear parametrisation, computed with our modified CLASS code on the basis of Planck 2018 cosmological reference parameters [5]. The shallow part of the potential provides for the slow-rolling of the scalar field, enabling cosmic acceleration at late times. While the variation of ϕ is small over cosmic history, the potential varies by many orders of magnitude.

2.3 Background evolution: scaling regime and late-time acceleration

The particular appeal of the λCDM model lies in its apparent ability to address the cosmic coincidence problem by replacing the unnatural tuning of parameters with a dynamical behaviour. Exponential potentials of the type $V(\phi) \propto e^{-\frac{3}{\lambda}\phi}$ trigger exact scaling solutions that allow quintessence and matter fractional energy densities to be nowadays of the same order of magnitude, almost irrespectively of the initial conditions [31]. The scalar field energy density continuously scales with the total background energy density as the universe expands, be it dominated by radiation or matter. Therefore, it will necessarily approach the matter energy density as time goes by, as the ratios Ω_ϕ/Ω_r and Ω_ϕ/Ω_m are constant during the subsequent radiation and matter dominated epochs. These scaling solutions emerge from attractors of the dynamical system composed of the Klein-Gordon and Friedmann equations. As depicted in Figure 2.5, at the outset, deep in the radiation period, the equation of state parameter is frozen with $w_\phi = -1$ as the potential energy prevails over kinetic energy. Later, following an oscillatory transient period prior reaching the attractor, the scalar field equation of state is conform to the asymptotic trajectory in the phase space of the dynamical system: $w_\phi = 1/3$ during radiation domination and $w_\phi = 0$ during matter domination.

The attractor is stable whenever $(3/\lambda)^2 > 3(1 + w_\phi)$, i.e. $\lambda^2 < 9/4$ for radiation and $\lambda^2 < 3$ for matter. The corresponding fractional dark energy is fixed and determined by the parameter λ in the scaling regimes,

$$\Omega_\phi = \frac{\lambda^2}{3}(1 + w_\phi), \qquad w_{\text{eff}} = w_\phi. \tag{2.46}$$

However, since dark energy dilutes at the same rate as the dominant component of the universe, its

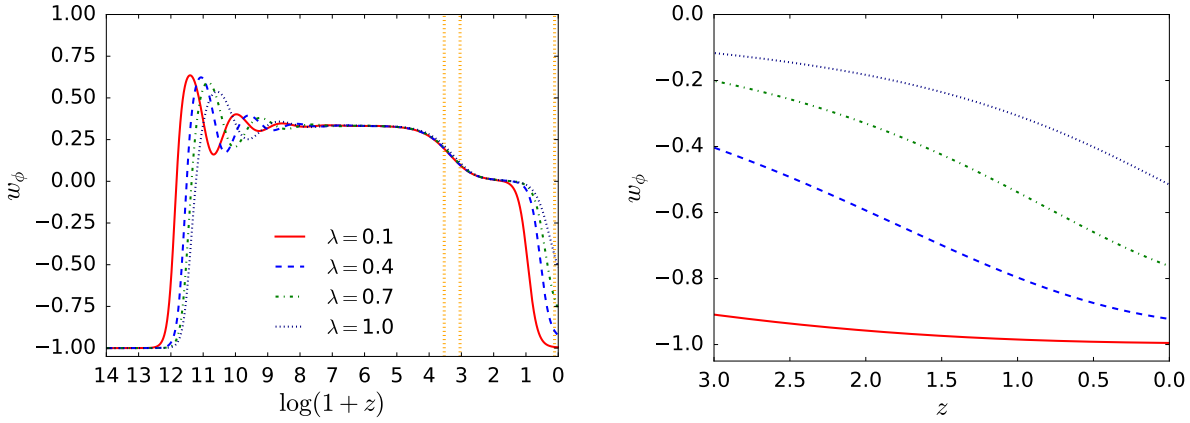

(a) Dark energy equation of state evolution

(b) Zoom in at lower redshift

Figure 2.5: Computed numerically for a selection of λ and vanishing $\dot{\phi}_i$ at initial time. Panel (a): The vertical dotted lines in orange respectively represent from left to right the times of matter-radiation equality, decoupling and matter-dark energy transition. Panel (b): The model allows for a large span of w_ϕ evolution determined by λ.

density is unable to catch up with that of matter. The exponential potential with this slope is too steep to prompt the attractor that permits late-time acceleration. In contrast, the existence of a second exponential shallow enough to slow-down the movement of the scalar field leads to an exit from the scaling regime towards the attractor consisting in a scalar field dominated universe at late times [32]. Despite that the late acceleration is unavoidable, the model offers a diversity of dark energy dynamics that only depend on the value of the parameter λ, as displayed in Figure 2.5.

In summary, with the potential $V(\phi) = Ae^{-\frac{3}{\lambda}\phi} + Be^{-\lambda\phi}$, the energy in the scalar field is provisionally captured in the scaling regime of the dominant component, driven by the first exponential term with the higher slope $e^{-\frac{3}{\lambda}\phi}$, for a large range of initial conditions. Once the second exponential term $e^{-\lambda\phi}$ takes the lead, the energy in the scalar field freezes and resembles a cosmological constant (see Figure 2.6). Given that matter continues to dilute as a^{-3}, the scalar field becomes dominant, naturally leading to the current repartition of energy densities. Eventually, in the end it entirely fills a near de Sitter universe dominated by the potential. At this future time, the equation of state is $w_\phi = -1 + \frac{\lambda^2}{3}$ with $w_\phi \to -1$ for small values of λ. Cosmic acceleration is realized whenever $w_\phi < -1/3$. Therefore, the slope of the exponentials must satisfy $|\lambda| < \sqrt{2}$. As we have evidence that the Universe is already accelerating, the current effective equation of state also satisfies $w_{\text{eff}} = w_0\Omega_{\phi_0} < -1/3$ according to Eq. (2.14). With Eq. (2.40), we find the following conditions,

$$|\lambda| < \sqrt{-1 + 3\Omega_{\phi_0}}, \qquad \Omega_{\phi_0} > \frac{1}{3}. \tag{2.47}$$

Moreover, there exists another theoretical bound on λ due to the existence of a ceiling for the early dark energy abundance (see Figure 2.6). The fractional energy density of quintessence Ω_ϕ at the Big Bang

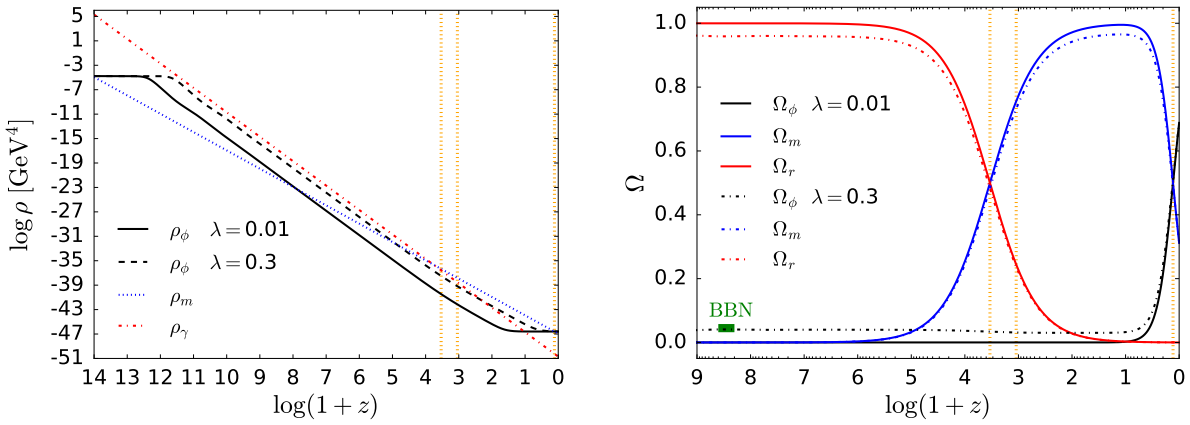

(a) Background evolution of the energy densities

(b) Background evolution of the fractional energy densities

Figure 2.6: Panel (a): The vertical dotted lines in orange represent from left to right the times of matter-radiation equality, at which the background energy density $\sim 10^{-37}\text{GeV}^4$, decoupling and matter-dark energy transition when $\rho_{\phi_0} \sim 10^{-47}\text{GeV}^4$. Panel (b): While early dark energy is not negligible, it is capped by a ceiling imposed by BBN, depicted by the horizontal green segment corresponding to the tighter bound in Eq. (2.48).

Nucleosynthesis (BBN) epoch around $z \sim 4 \times 10^8$, when the temperature of the Universe is about 1 MeV, is capped by $\Omega_\phi < 0.045$ at 2σ [33]. Otherwise, the production of primordial elements, particularly Hydrogen and Helium, is perturbed and contradicts the observation of their current abundance in the Universe. Since the radiation attractor is reached before primordial nucleosynthesis, we find the following ceiling by applying Eq. (2.46) with $w_\phi = 1/3$,

$$\Omega_\phi = \frac{4}{9}\lambda^2 < 0.045 \quad \Rightarrow \quad |\lambda| < \frac{3}{2}\sqrt{0.045} \sim 0.318. \tag{2.48}$$

The more conservative bounds $\Omega_\phi < 0.13 - 0.2$ also envisaged in [34] respectively relaxes the constraint to $|\lambda| \sim 0.54$ and $|\lambda| \sim 0.67$.

In the limit $\lambda \to 0$, the model is indistinguishable from ΛCDM and the early time dark energy abundance vanishes. The latter increases with increasing values of λ during radiation and matter domination. The abundance of radiation and matter decreases in the same proportion. Therefore, there is no change regarding the time of equality matter-radiation, which is given by,

$$\Omega_{m_0} a_{\text{eq}}^{-3} = \Omega_{r_0} a_{\text{eq}}^{-4} \quad \Longleftrightarrow \quad 1 + z_{\text{eq}} = \frac{\Omega_{m_0}}{\Omega_{r_0}} \approx 3450. \tag{2.49}$$

As far as the time of transition between matter and dark energy is concerned, the λCDM model has little influence for the values of λ compatible with BBN. Using Eq. (2.37), the time of that transition is given by,

$$e^{-3N_\phi} = \left(\frac{\Omega_{\phi_0}}{\Omega_{m_0}} + \frac{\lambda^2}{\lambda^2 - 3}\right) e^{-\lambda^2 N_\phi} - \left(\frac{\lambda^2}{\lambda^2 - 3}\right) e^{-3N_\phi}. \tag{2.50}$$

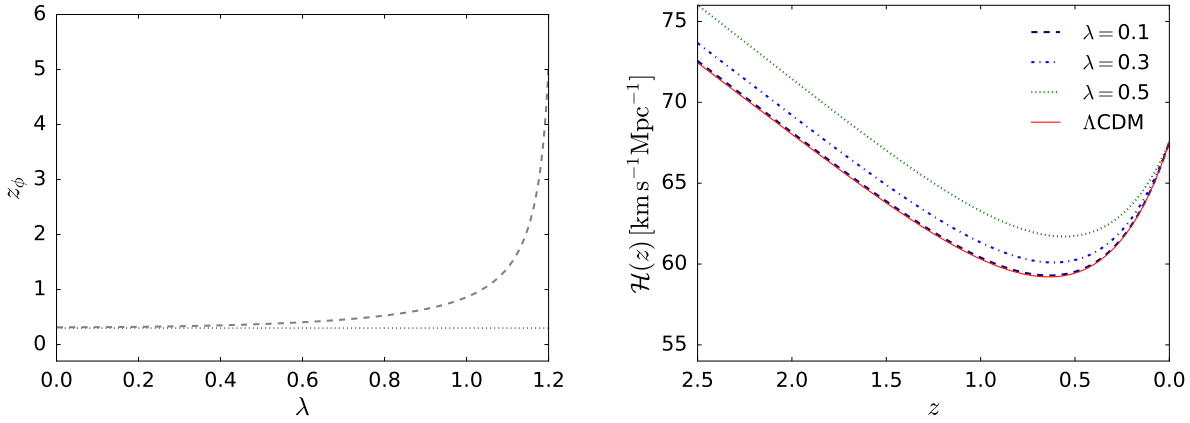

(a) Transition time between matter and dark energy

(b) Background evolution of the comoving Hubble parameter

Figure 2.7: Panel (a): The time of transition in λCDM (computed analytically) is close to that of the standard model: $z \sim 0.3$ (horizontal dotted line), except for higher values of λ. Panel (b): Comoving Hubble parameter as a function of redshift, computed with our modified CLASS code on the basis of Planck 2018 cosmological parameters results [5]. The minimum corresponds to the onset of acceleration at $z \sim 0.6$.

Putting the number of e-folds in evidence,

$$N_\phi = \frac{1}{\lambda^2 - 3}\left[\ln\left(\frac{\Omega_{\phi_0}}{\Omega_{m_0}} + \frac{\lambda^2}{\lambda^2 - 3}\right) - \ln\left(\frac{\lambda^2}{\lambda^2 - 3} + 1\right)\right], \tag{2.51}$$

we obtain the redshift at the transition $z_\phi = -1 + e^{-N_\phi}$,

$$z_\phi = -1 + \left[\frac{\lambda^2 - 3\Omega_{\phi_0}}{(2\lambda^2 - 3)\,\Omega_{m_0}}\right]^{\frac{1}{3-\lambda^2}}, \tag{2.52}$$

whose analytic plot in Figure 2.7 shows that it remains close to that in ΛCDM for the aforementioned acceptable values of λ.

The λCDM cosmological model appears to be viable in terms of the background evolution and is compatible with the current acceleration period as shown by the evolution of the conformal Hubble parameter plotted in Figure 2.7. In this respect, the parametrisation of the scalar field appears to be a realistic alternative to the standard model in reproducing the Universe expansion history. The difference is that dark energy is not negligible in the early times, although in quantity bound by the primordial nucleosynthesis. The merit of our quintessence model lies in the dynamics of the scalar field that attract the Universe towards its current acceleration for a wide range of initial conditions. Moreover, with only one additional parameter λ, the model allows for a large variety of possible evolution of the dark energy equation of state w_ϕ while maintaining it bound at high redshift.

Besides the homogeneous background at zero order, we are now studying in the next section how the parameter λ influences the growth of matter perturbations at first order.

2.4 Cosmological perturbations in λCDM

2.4.1 Linear perturbation theory

(a) Metric perturbations

According to the standard cosmological model, the primordial universe, albeit highly uniform, contained small inhomogeneities that have been evolving via gravitational instability. After the matter-radiation equality, the radiation pressure could not resist the gravitational pull any more and the inhomogeneities of pressureless matter have been growing, particularly the dominant cold dark matter component. Overdense regions become more overdense as time goes by. The inhomogeneities eventually become non linear and undergo gravitational collapse that brings forth the large scale structures observed today in the universe such as filaments, clusters and galaxies.

The evolution of the primordial fluctuations in the cosmological fluid within an expanding FLRW universe can be studied by the linear perturbation theory as long as the perturbations to the homogeneous background are small enough [35]. The inhomogeneities in the density field produce a change in the metric that also becomes inhomogeneous. Like any physical quantities, the universe spacetime metric can be expanded into spatial average and small linear perturbations,

$$g_{\mu\nu}(\vec{x},t) = \bar{g}_{\mu\nu}(t) + \delta g_{\mu\nu}(\vec{x},t), \tag{2.53}$$

where $\bar{g}_{\mu\nu}(t)$ represents the background metric in the inhomogeneous universe and $\vec{x}$ is a comoving spatial coordinate. Its line element is given by the flat FLRW model (A.4) in conformal time,

$$ds^2 = a^2(\tau)\left(-d\tau^2 + \delta_{ij}dx^i dx^j\right). \tag{2.54}$$

In order to perturb the 10 components of the background metric, the symmetric metric perturbation can be written in this most generic way [36] ,

$$\delta g_{\mu\nu} = a^2(\tau)\left(-2Ad\tau^2 + 2B_i dx^i d\tau + h_{ij}dx^i dx^j\right), \tag{2.55}$$

parametrising the 10 degrees of freedom. They are represented by functions of space and time. In the time component, the scalar field $A(\vec{x},\tau)$ is called lapse function. In the cross time-space component, the 3-vector field $B_i(\vec{x},\tau)$ is called shift vector. The rank-2 symmetric tensor field $h_{ij}(\vec{x},\tau)$ corresponds to the 6 components of the perturbations spatial part. The Euclidian trace of the spatial perturbation is noted $h \equiv h^i_i = \delta^{ij}h_{ij}$. At linear order, the metric of the inhomogeneous universe is thus,

$$ds^2 = a^2(\tau)\left[-\left(1+2A\right)d\tau^2 + 2B_i dx^i d\tau + \left(\delta_{ij}+h_{ij}\right)dx^i dx^j\right]. \tag{2.56}$$

The inverse of the metric is given by,

$$g^{\mu\nu} = \bar{g}^{\mu\nu} + \delta g^{\mu\nu}, \qquad \delta g^{\mu\nu} = -\bar{g}^{\mu\sigma}\bar{g}^{\nu\lambda}\delta g_{\sigma\lambda}. \tag{2.57}$$

The perturbations are conveniently decomposed into a set of independent scalar, vector and tensor components (called SVT decomposition). Given that the SVT components do not couple at first order, they evolve independently of each other. This feature allows them to be treated separately. The whole evolution of the full perturbation is then a simple linear superposition of the evolution of the independent SVT components. The 3-vector field B_i is divided into two parts: a curl-free vector as the gradient of a given scalar field B, and a divergenceless vector $\nabla.\bar{B} = 0$,

$$B_i = B_{,i} + \bar{B}_i. \tag{2.58}$$

Similarly, the rank-2 symmetric tensor h_{ij} is decomposed into a scalar component C that carries the trace of the spatial metric perturbation ($C = -h/6$) and a symmetric and traceless perturbation tensor E_{ij},

$$h_{ij} = -2C\delta_{ij} + 2E_{ij}, \tag{2.59}$$

that can in turn be divided into a scalar component E, a divergenceless vector E_i and a divergenceless and traceless tensor $\bar{E}_{ij}$,

$$E_{ij} = \left(\nabla_i\nabla_j - \frac{1}{3}\delta_{ij}\Delta\right)E + \bar{E}_{(i;j)} + \bar{E}_{ij}, \qquad \nabla.\bar{E} = 0. \tag{2.60}$$

Finally, it is usual to define a new scalar ψ called curvature perturbation that combines the 2 scalar components of the tensor (trace and Laplacian),

$$\psi = C + \frac{1}{3}\nabla^2 E. \tag{2.61}$$

According to the above SVT decomposition, the perturbed metric reads,

$$\delta g_{\mu\nu} = a^2\begin{bmatrix} -2A & B_{,i} \\ B_{,i} & -2\psi\delta_{ij} + 2E_{,ij} \end{bmatrix} + a^2\begin{bmatrix} 0 & \bar{B}_i \\ \bar{B}_i & 2\bar{E}_{(i;j)} \end{bmatrix} + a^2\begin{bmatrix} 0 & 0 \\ 0 & 2\bar{E}_{ij} \end{bmatrix}. \tag{2.62}$$

The vector mode (the second term) of the perturbed metric decays with the expansion and the tensor perturbations (the third term) are gravitational waves. In the present analysis, we thus restrict ourselves to the scalar perturbations (the first term) that are those that involve density and pressure perturbations. Furthermore, in the following, we derive the equations of the linear perturbations for the cold dark matter δ_c and the scalar field φ that give their time evolution in the synchronous gauge. A gauge is a way of slicing the spacetime in equal-time hypersurfaces on which the perturbations vary. Fixing the gauge is to impose a restriction that fixes the time slicing, yet genuine observable quantities are gauge independent. In the synchronous gauge, the perturbations are only in the space part of the metric. It is defined by

imposing that $\delta g_{00} = \delta g_{0i} = 0$, and thus $A = B_i = 0$. Since the shift vector vanishes, the threads (1D timelike curves defined by constant x^i) are orthogonal to the slices (constant τ). In that gauge, the scalar component of the inhomogeneous line element reduces to,

$$ds^2 = a^2(\tau)\left[-d\tau^2 + (\delta_{ij} + h_{ij})\, dx^i dx^j\right], \tag{2.63}$$

$$= a^2(\tau)\left\{-d\tau^2 + \left[(1-2\psi)\,\delta_{ij} + 2E_{,ij}\right] dx^i dx^j\right\}. \tag{2.64}$$

From now on, we choose to adopt CLASS notation that respects Ref. [37] to ease the modifications of the code,

$$h = -6C = h^i_i, \qquad \eta = \psi = C + \frac{1}{3}\nabla^2 E, \qquad \mu = 2E. \tag{2.65}$$

It follows from Eq. (2.59) that the scalar mode of the spatial perturbations metric can be rewritten as,

$$h_{ij}\left(\vec{x},\tau\right) = \frac{1}{3}h\left(\vec{x},\tau\right)\delta_{ij} + \left(\partial_i\partial_j - \frac{1}{3}\delta_{ij}\nabla^2\right)\mu\left(\vec{x},\tau\right). \tag{2.66}$$

In Ref. [37] one works in Fourier space[2], where Eqs. (2.65) imply that,

$$\mu = -6\eta - h, \tag{2.67}$$

and using Eq. (2.66), one obtains the scalar mode of the perturbations metric $h_{ij}(\vec{k},\tau)$ in terms of the variables $h(\vec{k},\tau)$ and $\eta(\vec{k},\tau)$ [37],

$$\begin{aligned} h_{ij}(\vec{k},\tau) &= \frac{1}{3}h(\vec{k},\tau)\delta_{ij} + \left(-\frac{k_i k_j}{k^2} + \frac{1}{3}\delta_{ij}\right)\left[-6\eta(\vec{k},\tau) - h(\vec{k},\tau)\right] \\ &= \hat{k}_i\hat{k}_j h(\vec{k},\tau) + \left(\hat{k}_i\hat{k}_j - \frac{1}{3}\delta_{ij}\right)\, 6\eta(\vec{k},\tau), \end{aligned} \tag{2.68}$$

where $\vec{k} = k\hat{k}$. Finally, one obtains a parametrisation of the synchronous metric perturbations in coordinate space like in Ref. [37],

$$\begin{aligned} h_{ij}\left(\vec{x},\tau\right) &= \int h_{ij}(\vec{k},\tau)e^{i\vec{k}.\vec{x}}d^3k \\ &= \int d^3k\; e^{i\vec{k}.\vec{x}}\left[\hat{k}_i\hat{k}_j h(\vec{k},\tau) + \left(\hat{k}_i\hat{k}_j - \frac{1}{3}\delta_{ij}\right)\, 6\eta(\vec{k},\tau)\right]. \end{aligned} \tag{2.69}$$

By computing the perturbed Einstein tensor defined in Eq. (A.9) in the synchronous gauge in Fourier space, we obtain the two components that are relevant for our analysis in the Newtonian limit,

$$\delta G^0_0 = a^{-2}(2k^2\psi + 6\mathcal{H}\dot{C}) = a^{-2}(2k^2\eta - \mathcal{H}\dot{h}), \tag{2.70}$$

$$\delta G^i_i = a^{-2}(6\ddot{C} + 2k^2\psi + 12\mathcal{H}\dot{C}) = a^{-2}(-\ddot{h} + 2k^2\eta - 2\mathcal{H}\dot{h}). \tag{2.71}$$

[2] with the convention $\left(\partial_i\partial_j - \frac{1}{3}\delta_{ij}\nabla^2\right) \to \left(-\frac{k_i k_j}{k^2} + \frac{1}{3}\delta_{ij}\right)$ applying to the scalar component E.

The dot denotes the derivation with respect to conformal time: a Fourier mode of physical wavelength $\frac{2\pi}{k}a$ crosses the Hubble radius, $r_H = \frac{1}{H}$, when $k \sim \mathcal{H}$, where the conformal Hubble parameter is,

$$\mathcal{H} = \frac{\dot{a}}{a} = aH. \tag{2.72}$$

(b) Fluid and scalar field perturbations

For the perturbations in the cosmological fluid, the dimensionless density contrast δ_i (or excess function field) conveniently describes the fluctuations in the energy density field of a given cosmological species[3] i,

$$\delta_i \equiv \frac{\delta\rho_i}{\bar{\rho}_i} = \frac{\rho_i(\vec{x},t) - \bar{\rho}_i(t)}{\bar{\rho}_i(t)}. \tag{2.73}$$

The density contrast measures the deviation of the field $\rho_i(\vec{x},t)$ from the mean density in the Universe $\bar{\rho}_i(t) = \langle\rho_i(\vec{x},t)\rangle$ which coincides with the unperturbed background density. The perturbations of the corresponding pressure field are defined as,

$$\delta p_i(\vec{x},t) = p_i(\vec{x},t) - \bar{p}_i(t). \tag{2.74}$$

Similarly, noting $\varphi = \delta\phi$, the perturbations of the scalar field are,

$$\varphi = \phi(\vec{x},t) - \bar{\phi}(t). \tag{2.75}$$

Perturbations are said to be small when $\delta_i < 1$, $\delta p_i/\bar{p}_i < 1$ and $\varphi/\bar{\phi} < 1$.

The perturbed metric is sourced by a perturbed fluid whose energy-momentum tensor can be expanded from the background $\bar{T}^\nu_\mu$ defined in Eq. (A.15),

$$T^\nu_\mu = \bar{T}^\nu_\mu + \delta T^\nu_\mu, \qquad \delta T^\nu_\mu = (\delta\rho + \delta p)\,\bar{u}^\mu\bar{u}_\nu + \delta p\, g^\nu_\mu + (\bar{\rho}+\bar{p})(\delta u_\nu \bar{u}^\mu + \delta u^\mu \bar{u}_\nu), \tag{2.76}$$

where we have neglected the contribution from anisotropic stress and heat conduction. δu^μ is the four-velocity perturbation in the perturbed metric,

$$u^\mu = \bar{u}^\mu + \delta u^\mu, \qquad u_\mu u^\mu = -1 \qquad \bar{u}_\mu = (-a, 0). \tag{2.77}$$

Noting that $\delta u^i \equiv v^i/a$, where $v^i \equiv dx^i/d\tau$ is the peculiar velocity of the fluid with respect to the expansion, the velocity perturbation takes the following form in the synchronous gauge,

$$\delta u^\mu = a^{-1}(0, v^i), \qquad \delta u_\mu = a(0, v_i), \tag{2.78}$$

and the vector v_i can also be decomposed into a scalar part and vectorial part[4]. Inserting Eq. (2.78) into

[3] We will be using the indices γ, b, c and ϕ respectively for photons, baryons, cold dark matter and the scalar field.

[4] The scalar part in the decomposition of the velocity vector is defined by $v_j = -v_{,j}$ which becomes $-i\frac{k_j}{k}v$ by convention in Fourier space as in Ref. [38].

Eq. (2.76) one obtains,

$$\begin{aligned} T^{\nu}_{\mu} &= \bar{T}^{\nu}_{\mu} + \delta T^{\nu}_{\mu}, \\ &= \begin{bmatrix} -\bar{\rho} & 0 \\ 0 & \bar{p}\delta^{i}_{j} \end{bmatrix} + \begin{bmatrix} -\delta\rho & (\bar{\rho}+\bar{p})v_i \\ -(\bar{\rho}+\bar{p})v_i & \delta p \delta^{i}_{j} \end{bmatrix}. \end{aligned} \tag{2.79}$$

Every cosmological specie i adds to the perturbations in the density and pressure fields, so we can write,

$$\delta\rho = \sum \delta\rho_i = \sum \bar{\rho}_i \delta_i, \qquad \delta p = \sum \delta p_i. \tag{2.80}$$

Since we are discussing the perturbations after decoupling, we assume that the content of the universe is dominated by a barotropic pressureless fluid and the scalar field, both of them approximated by a perfect fluid, in consistency with Ref. [29]. In addition, baryons are neglected as they only constitute a small proportion of the whole matter fluid. They will not make a difference in the present analysis of the λCDM model behaviour at the linear perturbation level. This is indeed a fair approximation because the formation of large scale structure originated mainly from cold dark matter perturbations. The baryon growth was suppressed for a long time during the matter-plasma epoch since they were tightly coupled to photons exercising a radiation pressure that overwhelmed gravity.

Using Eq. (2.5) and (2.6), the density and pressure perturbations of the scalar field are,

$$\delta\rho_\phi = \frac{\dot{\phi}\dot{\varphi}}{a^2} + V_{,\phi}\varphi, \tag{2.81}$$

$$\delta p_\phi = \frac{\dot{\phi}\dot{\varphi}}{a^2} - V_{,\phi}\varphi. \tag{2.82}$$

Therefore, in our model the relevant components of the perturbed energy-momentum tensor are,

$$\delta T^0_0 = -\delta\rho = -\left(\delta_c\bar{\rho}_c + \delta_b\bar{\rho}_b + \delta_r\bar{\rho}_r + \delta\rho_\phi\right) = -\left(\delta_c\bar{\rho}_c + \frac{\dot{\phi}\dot{\varphi}}{a^2} + V_{,\phi}\varphi\right), \tag{2.83}$$

$$\delta T^i_i = \delta^i_i \delta p_\phi = 3\left(\frac{\dot{\phi}\dot{\varphi}}{a^2} - V_{,\phi}\varphi\right). \tag{2.84}$$

(c) Equations of motion of the perturbations

It is now possible to solve the perturbed Einstein field equations, writing the first-order separately, as the zeroth-order part corresponds to the background evolution,

$$\delta G^{\nu}_{\mu} = \kappa^2 \delta T^{\nu}_{\mu}, \qquad \kappa^2 \equiv 8\pi G = 1. \tag{2.85}$$

The time-time and trace space-space components give two independent equations,

$$2k^2\eta - \mathcal{H}\dot{h} = -\left(a^2\delta_c\bar{\rho}_c + \dot{\phi}\dot{\varphi} + a^2 V_{,\phi}\varphi\right), \tag{2.86}$$

$$-\ddot{h} + 2k^2\eta - 2\mathcal{H}\dot{h} = 3\left(\dot{\phi}\dot{\varphi} - a^2 V_{,\phi}\varphi\right), \tag{2.87}$$

in Fourier space[5]. The first equation is the Hamiltonian constraint involving the density fluctuations. It is a relativistic Poisson equation that corresponds to the background Friedmann equation. The second one is the pressure constraint. The corresponding background equation is the Raychaudhuri equation. Their combination gives the equation of motion for the evolution of the perturbations metric trace,

$$\boxed{\ddot{h} + \mathcal{H}\dot{h} + a^2\delta_c\rho_c + 2\left(2\dot{\phi}\dot{\varphi} - a^2 V_{,\phi}\varphi\right) = 0.} \tag{2.88}$$

It is worthwhile noting that there are two additional equations relating to the metric perturbations. They stem from the resolution of the other Einstein field components and respectively involve velocity and shear. They are the following for the species concerned here,

$$k^2\dot{\eta} = \frac{1}{2}a^2\left(\dot{\phi}k^2\varphi + \bar{\rho}_c\theta_c\right), \tag{2.89}$$

$$\ddot{h} + 6\ddot{\eta} + 2\mathcal{H}\left(\dot{h} + 6\dot{\eta}\right) - 2k^2\eta = 0, \tag{2.90}$$

where the latter is the sheer-free version. They are not useful for the approximation in the Newtonian limit that we are to analyse later in the present chapter, yet the numerical Boltzmann code incorporates Eq. (2.90) along with radiation and baryons.

Besides, the conservation of energy-momentum $\nabla_\mu T^\mu_\nu = 0$ provides for the equations of motion of the fluid perturbations. We will work them out in detail below since they are the ones that will be impacted by the coupling with dark matter explored in Chapter 4. Here, in the absence of interaction between cosmological species, the conservation applies to the individual stress-energy tensor. At first order in the perturbations we have [39],

$$\begin{aligned}\delta(\nabla_\mu T^\mu_\nu) &= 0 \\ &= \delta\left(\partial_\mu T^\mu_\nu\right) - \bar{\Gamma}^\alpha_{\nu\mu}\delta T^\mu_\alpha + \bar{\Gamma}^\mu_{\alpha\mu}\delta T^\alpha_\nu - \delta\Gamma^\alpha_{\nu\mu}\bar{T}^\mu_\alpha + \delta\Gamma^\mu_{\alpha\mu}\bar{T}^\alpha_\nu.\end{aligned} \tag{2.91}$$

The components $\nu = 0$ and $\nu = i$ give respectively the continuity and Euler equations, using the Christofell symbols of the background metric $\bar{\Gamma}$ in Eq. (A.13) and those scalar components of the perturbed affine connections,

$$\delta\Gamma^0_{00} = 0, \qquad \delta\Gamma^0_{i0} = 0, \qquad \delta\Gamma^i_{0i} = \frac{\dot{h}}{2}. \tag{2.92}$$

Since cold dark matter is composed of particles with low thermal velocities, it can be considered pressureless. Putting $\bar{p} = \delta p = 0$ in Eq. (2.79), and noting the velocity divergence $\theta \equiv \partial_j v^j = ik_j v^j = kv$, the component $\nu = 0$ yields,

$$\dot{\delta\rho_c} + \bar{\rho}_c\theta_c + 3\mathcal{H}\delta\rho_c + \frac{1}{2}\dot{h}\bar{\rho}_c = 0. \tag{2.93}$$

[5] δ_c is to be understood as $\delta_c(\vec{k}, t)$, dropping the under-script k.

As $\delta\dot{\rho}_c = \dot{\bar{\rho}}_c\delta_c + \bar{\rho}_c\dot{\delta}_c$, and $\dot{\bar{\rho}}_c = -3\mathcal{H}\bar{\rho}_c$ according to Eq. (A.21), the continuity equation of the cold dark matter perturbation reads,

$$\boxed{\dot{\delta}_c + \theta_c + \frac{\dot{h}}{2} = 0.} \tag{2.94}$$

The presence of the metric perturbation in the continuity equation of cold dark matter accounts for the gravitational interaction. Similarly, the component $\nu = i$ yields,

$$\bar{\rho}_c\dot{v}_i + \dot{\bar{\rho}}_c v_i - 0 + 4\mathcal{H}\bar{\rho}_c v_i - 0 + 0 = 0, \tag{2.95}$$

and by taking the divergence, one obtains,

$$\bar{\rho}_c\dot{\theta}_c + \dot{\bar{\rho}}_c\theta_c + 4\mathcal{H}\bar{\rho}_c\theta_c = 0. \tag{2.96}$$

By plugging $\dot{\bar{\rho}}_c = -3\mathcal{H}\bar{\rho}_c$ into it, the Euler equation reads,

$$\boxed{\dot{\theta}_c + \mathcal{H}\theta_c = 0.} \tag{2.97}$$

Moreover, the choice of the initial timelike hypersurface is arbitrary in the synchronous gauge, leaving a residual degree of freedom. An additional condition should be imposed to completely fix the gauge. It is usual to set $\theta_c(k, \tau_{ini}) = 0$ as in CLASS which saves one equation: since $\theta_c = 0$ at all times according to Eq. (2.97), h can be obtained by integrating Eq. (2.94). The synchronous gauge is therefore comoving with cold dark matter.

As regards the scalar field, the linearised equation of motion for the quintessence fluctuation φ is also obtained with the component $\nu = 0$ of Eq. (2.91),

$$\dot{\delta\rho}_\phi + 3\mathcal{H}\left(\delta\rho_\phi + \delta p_\phi\right) + \left(\rho_\phi + p_\phi\right)\left(\theta_\phi + \frac{\dot{h}}{2}\right) = 0, \tag{2.98}$$

where,

$$\begin{aligned}
\theta_\phi \equiv -\frac{ik_i(\delta T^i_0)}{\rho_\phi + p_\phi} &= k^2\frac{\varphi}{\dot{\phi}}, \\
\delta\rho_\phi + \delta p_\phi &= \frac{2}{a^2}\dot{\phi}\dot{\varphi}, \\
\rho_\phi + p_\phi &= \frac{\dot{\phi}^2}{a^2}, \\
\dot{\delta\rho}_\phi &= \frac{\ddot{\phi}\dot{\varphi} + \dot{\phi}\ddot{\varphi}}{a^2} - \frac{2\mathcal{H}\dot{\phi}\dot{\varphi}}{a^2} + V_{,\phi}\dot{\varphi} + \dot{\phi}V_{,\phi\phi}\varphi.
\end{aligned} \tag{2.99}$$

Further using the Klein-Gordon Eq. (2.11) in conformal time, one obtains the perturbed Klein-Gordon equation which corresponds to the equation of motion of φ,

$$\ddot{\varphi} + 2\mathcal{H}\dot{\varphi} + \left(k^2 + a^2 V_{,\phi\phi}\right)\varphi - \dot{\delta}_c\dot{\phi} = 0, \tag{2.100}$$

or equivalently,

$$\boxed{\ddot{\varphi} + 2\mathcal{H}\dot{\varphi} + \left(k^2 + a^2 V_{,\phi\phi}\right)\varphi + \frac{\dot{h}\dot{\phi}}{2} = 0,} \tag{2.101}$$

where we need,

$$\dot{\delta}_c = -\frac{1}{2}\dot{h}. \tag{2.102}$$

2.4.2 Full numerical results and analytic approximation in the Newtonian limit

It is not necessary to modify the code of the CLASS perturbations module to get numerical results. The version publicly available already implements an uncoupled scalar field in a generic way, contrary to the background module that we had to adapt to our specific potential. We use it to numerically solve the full set of perturbation equations, by duly evolving every cosmological species in the real universe (photons, neutrinos, baryons, dark matter and scalar field), on the basis of adiabatic initial conditions. In particular, we numerically compute the evolution of the dark matter fluctuation δ_c and compare it with the asymptotic expressions that we derive below in the Newtonian limit for the periods respectively dominated by matter and dark energy.

The initial relative amplitudes of the various species are given by thermodynamic considerations in the primordial universe. By considering that the temperature changes in a way that heat transfer is compensating entropy, the conservation of entropy imposes that the density perturbations are related to the evolution of the background. Therefore,

$$\frac{\delta\rho_m}{\dot{\bar{\rho}}_m} = \frac{\delta\rho_r}{\dot{\bar{\rho}}_r}, \tag{2.103}$$

and, by applying the energy conservation (A.21) to dark matter, baryons and photons, the initial conditions read [37],

$$\delta_c = \delta_b = \frac{3}{4}\delta_\gamma. \tag{2.104}$$

As for the scalar field, vanishing initial perturbations are imposed since quintessence should reach the attractor soon enough. CLASS sets the initial conditions as a truncated series in powers of conformal time to the order $\mathcal{O}(k^3\tau^3)$. The comoving scales that are observable today (through the CMB anisotropy or matter power spectra) were all beyond the Hubble radius in the radiation-dominated era. Their corresponding perturbations are free from small scales interactions and reflect the original fluctuations that grew with inflation according to the standard cosmological model. On super-horizon-sizes, $\mathcal{H} \propto 1/\tau$

since $a \propto \tau^2$. Therefore $k\tau \ll 1$ corresponds to the super-horizon limit. In CLASS, the adiabatic initial condition for the photon perturbations on a given scale k for a flat universe is set as,

$$\delta_\gamma = -\frac{(k\tau)^2}{3} + \frac{\omega}{15}\frac{(k\tau)^3}{k} = -\frac{(k\tau)^2}{3}\left(1 - \frac{\omega\tau}{5}\right), \qquad \omega \equiv \frac{\Omega_m}{\sqrt{\Omega_r}}H_0 = a\frac{\rho_m}{\sqrt{\rho_r}}. \tag{2.105}$$

This is valid at leading order in $k\tau$ and $\omega\tau$. It relates to the leading order $k\tau$ in Ref. [37] by normalizing the arbitrary dimensionless constant $C = 1/2 = \mathcal{R}/2$, where $\mathcal{R}$ is the initial spatial curvature perturbation which is conserved on super-Hubble scales and used to fix adiabatic initial conditions.

As illustrated in Figure 2.8, the evolution of dark matter perturbations, computed with CLASS, decelerates with increasing values of the parameter λ compared to ΛCDM. This is clearly perceptible on smaller scales in the Newtonian limit, as in Ref. [40]: it is on the sub-horizon scales in the matter era that the evolution of the perturbations is essentially different from a scalar free universe. Our numerical results are in line with the analytic expression of the equation of motion for the dark matter density contrast. Deriving Eq. (2.94) and inserting Eq. (2.88), the density contrast evolves according to the following differential equation,

$$\ddot{\delta}_c + \mathcal{H}\dot{\delta}_c - \frac{a^2}{2}\bar{\rho_c}\delta_c - \left(2\dot{\phi}\dot{\varphi} - a^2 V_{,\phi}\varphi\right) = 0. \tag{2.106}$$

In the limit of small scales within the Hubble horizon, $k \gg \mathcal{H}$, the derivatives of φ and the potential term can be neglected in Eq. (2.100) as in Ref. [41], which brings us to,

$$k^2\varphi - \dot{\delta}_c\dot{\phi} = 0, \tag{2.107}$$

which can be rewritten in terms of derivatives with respect to the number of e-folds,

$$\varphi = \frac{\mathcal{H}^2}{k^2}\lambda\delta_c', \tag{2.108}$$

as $\phi' = \lambda$. Substituting into Eq. (2.106) and neglecting $\frac{\mathcal{H}^2}{k^2} \ll 1$, as well as the derivative of φ and the potential term (being of higher order), the density contrast in the Newtonian approximation evolves as,

$$\delta_c'' + \left(1 + \frac{\mathcal{H}'}{\mathcal{H}}\right)\delta_c' - \frac{1}{2}\frac{a^2\bar{\rho_c}}{\mathcal{H}^2}\delta_c = 0. \tag{2.109}$$

Remembering that we have defined the abundance parameter in Eq. (A.22) as,

$$\Omega_c \equiv \frac{a^2\bar{\rho_c}}{3\mathcal{H}^2}, \tag{2.110}$$

we find that the form of the evolution equation for δ_c on small scales does not differ from ΛCDM,

$$\delta_c'' + \left(1 + \frac{\mathcal{H}'}{\mathcal{H}}\right)\delta_c' - \frac{3}{2}\Omega_c\delta_c = 0, \tag{2.111}$$

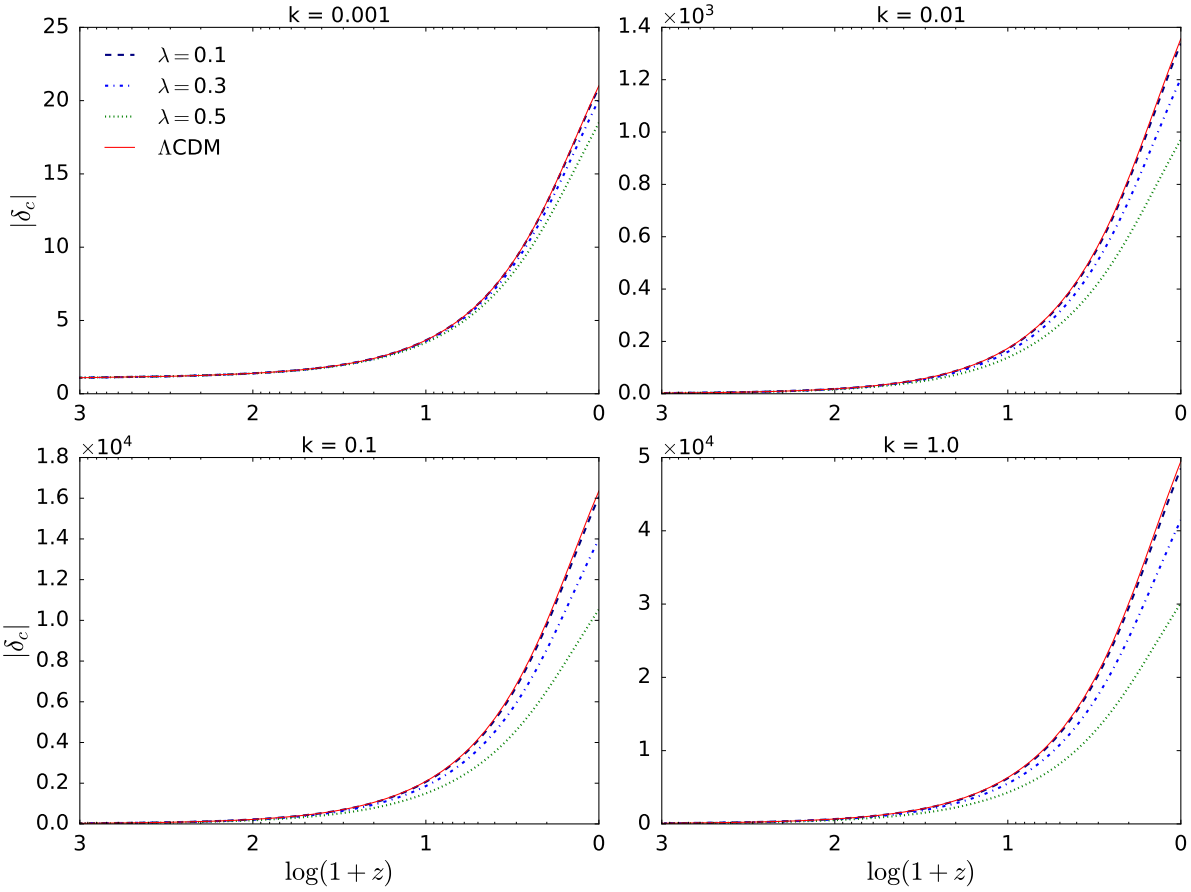

Figure 2.8: λCDM cosmological evolution of dark matter fluctuations during matter era for various scales in [h Mpc^{-1}], computed with our modified CLASS code on the basis of Planck 2018 cosmological parameters results [5]. The initial conditions are adiabatic with $\mathcal{R} = 1$ normalization. The model suppresses the growth of perturbations that are significantly affected by increasing λ on smaller scales.

where, according to Eq. (2.40),

$$\Omega_c = 1 - \Omega_\phi = 1 - \frac{\lambda^2/3}{w_\phi + 1}, \tag{2.112}$$

and,

$$\frac{\mathcal{H}'}{\mathcal{H}} = \frac{\mathcal{H}\mathcal{H}'}{\mathcal{H}^2} = -\frac{1}{2} - \frac{3}{2} w_{\text{eff}} = -\frac{1}{2} - \frac{3}{2} w_\phi \Omega_\phi = -\frac{1}{2} - \frac{\lambda^2}{2} \frac{w_\phi}{w_\phi + 1}. \tag{2.113}$$

Finally, we obtain the general expression of the evolution equation for the dark matter density contrast, valid on small scales in both matter and quintessence dominated eras, from which we can extract interesting features,

$$\delta_c'' + \left(\frac{1}{2} - \frac{\lambda^2}{2} \frac{w_\phi}{w_\phi + 1} \right) \delta_c' - \frac{3}{2} \left(1 - \frac{\lambda^2/3}{w_\phi + 1} \right) \delta_c = 0, \tag{2.114}$$

where the expression of the dark energy equation of state w_ϕ is given in Eq. (2.41). Both the friction term (the second one called Hubble drag working against the growth) and the dynamical term (the third

one representing the gravity pull) are affected by the presence of early dark energy. We are going now to asymptotically derive analytic solutions in the limit of the deep matter dominated epoch, as well as when dark energy dominates. We will be able to compare them with the growth rate obtained numerically with CLASS.

Deep in the scaling regime with matter, $w_\phi \sim 0$ and Eq. (2.114) reduces to,

$$\delta_c'' + \frac{1}{2}\delta_c' - \frac{3}{2}\left(1 - \frac{\lambda^2}{3}\right)\delta_c = 0. \tag{2.115}$$

Whereas the Hubble drag is identical to the standard term during the matter dominated epoch ($w_{\text{eff}} = 0$ in both models), the gravitational pull is different. In the ΛCDM model, the dynamical term is sourced with $\Omega_c \sim 1$ all along the matter epoch, up until the universe begins to accelerate. For the quintessence model in the matter era, the potential well is comparatively decreased due to the scalar field kinetic energy. Therefore, in comparison with the standard cosmological model, in which the sub-Hubble scales grow at the same rate as the background expansion, the presence of early dark energy slackens off the growth of dark matter perturbations. The effect becomes significant for high values of λ. Assuming a power-law solution of the form $\delta_c \propto e^{mN}$, Eq. (2.115) imposes that,

$$m^2 + \frac{1}{2}m - \frac{3}{2}\left(1 - \frac{\lambda^2}{3}\right) = 0. \tag{2.116}$$

Similarly to Ref. [40], we obtain that the growing mode corresponds to,

$$m_+ = \frac{1}{4}\left[-1 + \sqrt{24\left(1 - \frac{\lambda^2}{3}\right) + 1}\right]. \tag{2.117}$$

The damping solution is uninteresting as it becomes negligible with respect to the growing mode. When $\lambda = 0$, the standard ΛCDM model is retrieved, in which $m_+ = 1$ and $\delta_c \propto a$. We necessarily have $0 < m_+ < 1$ given that $|\lambda| < \sqrt{2}$ to allow for cosmic acceleration. This means that the perturbations do grow, but at a slower pace due to the existence of the scalar field. In order to emphasize the deviation from the standard rate, it is common to define the growth parameter f as,

$$f \equiv \frac{d\ln\delta}{dN} \quad \text{or} \quad f \equiv \frac{\delta'}{\delta}, \tag{2.118}$$

which is plotted in Figure 2.9 on a small scale from the numerical results computed with CLASS. These results are coherent with the approximation of the growth rate given by the analytic expression of (2.117) as we can see that indeed $f \sim m_+$ in the late matter era.

At later times, beyond the domination of matter when the expansion of the universe begins to accelerate, both models have the same behaviour. The dark energy density freezes once the second exponential term dominates the scalar field potential. The equation of state dramatically decreases towards

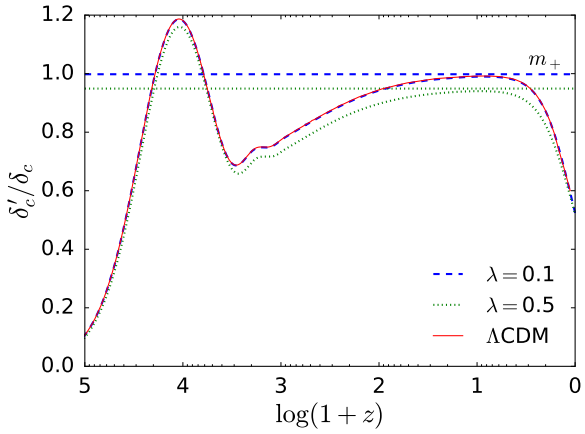

Figure 2.9: The growth rate function $f = \delta_c'/\delta_c$ of the dark matter fluctuation is numerically computed with our modified CLASS code on the basis of Planck 2018 cosmological parameters results [5]. The scale considered is $k = 0.1\ h$ Mpc^{-1}, around matter-radiation equality. In the deep matter era, after a transient period, the growth parameter $f \sim m_+$ is in line with the analytic and approximated expression of the growth rate derived in Eq. (2.117).

$w_\phi \sim -1 + \lambda^2/3$, pulling further down the gravitational source term which quickly fades out. For $z \gg z_\lambda$, the equation of dark matter perturbations (2.114) is governed by the Hubble drag,

$$\delta_c'' + \left(2 - \frac{\lambda^2}{2}\right)\delta_c' = 0, \tag{2.119}$$

whose general solution is composed of a constant mode and a swiftly decaying mode because $|\lambda| < 2$,

$$\delta_c(k, N) = A(k) + B(k)\, e^{\left(\frac{\lambda^2}{2} - 2\right)N}. \tag{2.120}$$

The standard case with a cosmological constant is retrieved when $\lambda = 0$, i.e. $\delta_c \propto a^{-2}$. During quintessence domination, the growth of perturbations stops, $f \to 0$: the density contrast of dark matter freezes at a constant value as shown by Eq. (2.120).

The evolution of the dark matter density contrast differs from ΛCDM, depending on the value of λ. The existence of the scalar field suppresses the subhorizon growing mode, thus also suppresses structure formation. In the next chapter, we will be seeing whether the parametrisation gives reliable predictions about the formation of large scale structures in the Universe, as well as about the CMB anisotropies.

Chapter 3

Observational constraints on λCDM

3.1 Effects on observable quantities

3.1.1 Redshift-luminosity distance relation

The luminosity distance numerically computed with CLASS can be confronted with SNIa brightness observations, as exemplified in Figure 3.1 with the Pantheon sample [42]. SNIa can be considered as standard candles that have fixed absolute magnitude inferred by the observation of their luminosity decay rate. They therefore can be used to probe the luminosity distance as a function of redshift using the distance modulus μ defined by,

$$\mu = m - M = 5\log(d_L) + 25, \tag{3.1}$$

where m and M are respectively the apparent and absolute magnitudes of the supernova, and d_L is the luminosity distance (A.8) measured in Megaparsec. The most distant supernovae are located in remote regions where relativistic corrections to the Euclidian space are important. In the λCDM model, the theoretical luminosity distance is given by,

$$d_L(z) = \frac{1+z}{H_0}\int_0^z \frac{dz}{E(z)}, \tag{3.2}$$

$$E(z) = \left[\frac{3}{3-\lambda^2}\Omega_{m_0}(1+z)^3 + \left(1 - \frac{3}{3-\lambda^2}\Omega_{m_0}\right)(1+z)^{\lambda^2}\right]^{1/2}. \tag{3.3}$$

Parameter λ influences the Hubble expansion in the model, and we can see in Figure 3.1 that a broad range of values is able to reproduce the shape of the observed redshift - luminosity distance relation, thus reproducing very well the cosmic evolution of the standard ΛCDM background. On the other hand, we can also conclude that the magnitude does not exhibit a strong dependence on λ. Its effect is almost negligible $< 1.5\%$, even for the highest possible values of the parameter. Nevertheless, the supernovae

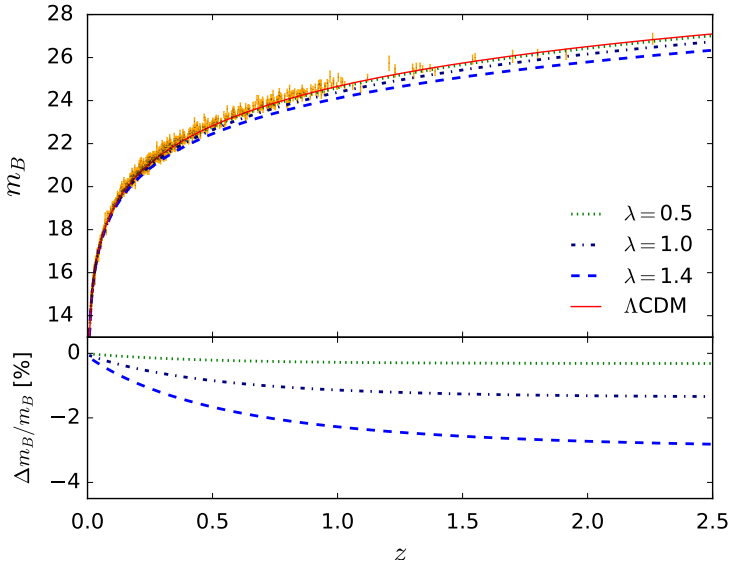

Figure 3.1: Top panel: Comparison between supernova brightness observations from the Pantheon sample data points (plotted in orange) and luminosity distance computed with our modified CLASS code on the basis of Planck 2018 cosmological parameters results [5]. Bottom panel: Relative deviation from ΛCDM. We note that acceptable values of λ are not making significant deviation from the standard redshift-luminosity distance relation. The λCDM model reproduces noticeably well the expansion history of the universe background.

magnitude may help constrain λ by confronting the luminosity distance predicted by the model with the observations.

3.1.2 Linear matter power spectrum

(a) Matter power spectrum as indicator of structure formation

Matter distribution in the Universe can be quantified by measuring the correlation function or the power spectrum of observed galaxies. The observed structure forms from the quantum fluctuations in the energy density field that existed in the early universe. Inflation produced from quantum fluctuations a field of macroscopic primordial perturbations that is thus a statistical realization of initial conditions. Since the fluctuations are the result of a stochastic process, the density at any point, and also at any moment, obeys a distribution of probability. The resulting density contrast δ is therefore a stochastic field that follows a probability distribution at any time, which we assume Gaussian. It is fully specified by the n-point correlation functions. For instance, the two-point correlation function is defined by the probability distribution function ξ averaged over an ensemble of possible universes $\xi(\vec{x}, \vec{x}') \equiv \langle \delta(\vec{x}) \delta(\vec{x}') \rangle$. Assuming statistical homogeneity and isotropy, the one-point probability distribution function $\langle \delta(\vec{x}) \rangle$ is independent of $\vec{x}$ and the two-point correlation function is invariant under spatial translations and rotations. It only depends on the distance between the two points considered $r = |\vec{x} - \vec{x}'|$. Therefore,

$\xi(r) = \langle \delta(\vec{x})\delta(\vec{x}+\vec{r})\rangle$.

Given the impossibility to compare our Universe with others, the probability distribution functions are instead estimated with spatial averages over large volumes under the ergodic hypothesis. It assumes that the Universe is a representative volume that includes all possible realizations. Accordingly, $\langle\delta\rangle = 0$ and the appropriate quantities for characterizing the fluctuations become their variance and two-point correlation function corresponding to the covariances. The two-point correlation function quantifies the clustering of the density field, i.e. the degree of collapse. It is thus a good estimation for the formation of structure. The correlation function can be measured by counting galaxy pairs and comparing it with the number count in a random sample of mock galaxies. Several estimators of the correlation function do exist. They are based on different comparison methods between the observations and the random sample.

Whereas the number density of galaxies traces the density contrast, the relation between the over-density size and the correlation function is not exclusive. Instead of sizes based on separations between points, the Fourier modes are used to define on the density field a group of independent characteristic sizes (or scales) $\vec{k}$ with wavelengths $2\pi/k$. The two-point correlation function is thus computed by expanding the density contrast field in a Fourier series over a large and finite volume V that is conventionally set to unity,

$$\delta\left(\vec{x},t\right) = \frac{V}{(2\pi)^3}\int \delta_k(\vec{k},t)\, e^{+i\vec{k}.\vec{x}}\, d^3k, \qquad \delta_k(\vec{k},t) = \frac{1}{V}\int \delta(\vec{x},t)\, e^{-i\vec{k}.\vec{x}}\, d^3x. \tag{3.4}$$

In harmonic space, the correlation function thus reads,

$$\xi(r,t) = \frac{V}{(2\pi)^3}\int \langle|\delta_k(\vec{k},t)|^2\rangle\, e^{-i\vec{k}.\vec{r}}\, d^3k, \tag{3.5}$$

$$P(k,t) = \langle|\delta_k(\vec{k},t)|^2\rangle = \frac{1}{V}\int \xi(r,t)\, e^{i\vec{k}.\vec{r}}\, d^3r, \tag{3.6}$$

where $P(k,t)$ is called the power spectrum of the density perturbations, which is the Fourier transform of the correlation function $\xi(r,t)$. It is an indicator of structure formation as it gives the amplitude of clustering as a function of independent characteristic scales represented by the set of Fourier modes. It has dimensions of volume but can be redefined in the dimensionless power spectrum,

$$\mathcal{P}(k,t) \equiv \frac{V}{(2\pi)^3}4\pi k^3 P(k,t) = \frac{2}{\pi}k^3\int_0^\infty \xi(r,t)\frac{\sin kr}{kr}r^2 dr, \tag{3.7}$$

which is used to define the variance of the density contrast field per natural logarithm interval,

$$\sigma^2(t) \equiv \langle\delta(\vec{x},t)^2\rangle = \int_0^\infty \mathcal{P}(k,t)\frac{dk}{k}. \tag{3.8}$$

The clustering properties are observationally determined by the variance of number counts in cells. In this case, a smooth density contrast is used as a convolution with a given (top-hat or Gaussian) window

function $W(R, r)$ that swiftly vanishes beyond $r > R$. The corresponding variance of the smooth density on scale R is defined as,

$$\sigma_R^2(t) = \int_0^\infty W^2(R, k)\mathcal{P}(k, t)\frac{dk}{k}. \tag{3.9}$$

The scale $R = 8$ Mpc/h is of particular importance as it is the scale where today's observed power spectrum of dark matter has an amplitude close to 1, which is the boundary between linear and non-linear scales. The value of $\sigma_8(z = 0)$ for a given cosmological model reflects the present clustering level.

(b) Predicting the matter power spectrum

Large Scale Structure observations probe the power spectrum during matter or dark energy domination, when radiation is subdominant. They customary refer to the total density contrast of the non-relativistic matter sources δ_m defined as[1],

$$\delta_m = \frac{\delta\rho_m}{\bar{\rho}_m} = \frac{\delta\rho_b + \delta\rho_c}{\bar{\rho}_b + \bar{\rho}_c} = \frac{\bar{\rho}_b\delta_b + \bar{\rho}_c\delta_c}{\bar{\rho}_b + \bar{\rho}_c}. \tag{3.10}$$

The power spectrum is also a quantity that can be theoretically computed from the linear perturbation theory that gives the equations for the evolution of the density contrast in a given cosmological model, as seen in Subsection 2.4.1. CLASS computes the linear matter power spectrum of the non-relativistic matter density perturbations δ_m at a given redshift [43],

$$P(k, z) = \left[\frac{\delta_m(k, z)}{\mathcal{R}(k)}\right]^2 \frac{2\pi^2}{k^3}\mathcal{P}_\mathcal{R}(k), \qquad \mathcal{P}_\mathcal{R}(k) = A_s(k/k_*)^{n_s-1}. \tag{3.11}$$

The function in brackets (called transfer function) accounts for the linear evolution of the perturbations, irrespectively of the initial conditions. It depends on $\mathcal{R}$ which is the spatial curvature perturbation on an initial comoving hypersurface, conserved on super-Hubble scales and normalized to $\mathcal{R} = 1$. $\mathcal{P}_\mathcal{R}(k)$ is the primordial power spectrum that represents the initial conditions for the Gaussian matter fluctuations in the aftermath of inflation. It is as a power-law parametrised by an amplitude A_s, normalized at a pivot scale $k_* \sim 0.05$ Mpc^{-1}, and by a slope n_s called spectral index giving the relative amplitudes between scales. Instead of A_s, the amplitude of the matter power spectrum can be normalized by the root mean square fluctuation σ_8 on the scale of $k = 2\pi/8$ hMpc^{-1} at $z = 0$. A_s (or σ_8) and n_s are two additional free parameters of the model that complement those three corresponding to the background evolution. The relation between σ_8 and A_s depends on the evolution of the power spectrum from early times to $z = 0$, and hence it depends on all cosmological parameters. CLASS uses a shooting mechanism to

[1] δ is to be indifferently understood as $\delta_k(\vec{k}, t)$ or $\delta(\vec{x}, t)$ depending on the context, i.e. on whether the harmonic or real space is considered.

get σ_8 by iteration as a derived parameter when it is the amplitude of the primordial spectrum A_s that is assumed.

(c) Numerical results for the λCDM model

Figure 3.2 depicts the predictions for the linear matter power spectrum that we calculate with our modified CLASS version. It illustrates how the parametrisation of the scalar field affects the computed matter power spectrum. The overall shape is consistent with a typical ΛCDM scenario. The turn around scale is about the wave-number $k_{\rm eq}$ that corresponds to the size of the horizon at the matter-radiation equality, which remains the same in both the standard and the λCDM models. Using the Friedmann equation (1.2) at the time of equality given in Eq. (2.49),

$$\begin{aligned} k_{\rm eq} = \mathcal{H}_{\rm eq} &= H_0 a_{\rm eq} \left(\Omega_{m_0} a_{\rm eq}^{-3} + \Omega_{r_0} a_{\rm eq}^{-4}\right)^{1/2}, \\ &= \sqrt{2} H_0 \frac{\Omega_{m_0}}{\sqrt{\Omega_{r_0}}}. \end{aligned} \tag{3.12}$$

The location of the peak is sensitive to today's abundance of matter Ω_{m_0}, given that Ω_{r_0} is a nearly fixed quantity in the models at stake. For instance, larger Ω_{m_0} entails a shorter radiation epoch, thus a shorter Hubble radius at equality and the peak consequently would move to the larger k (smaller scales). Since we have chosen the fiducial values of the ΛCDM parameters, the location is not affected by the existence of the scalar field in the simulations.

The main difference with the standard model is due to the presence of early dark energy that reduces the growth rate of fluctuations during matter domination, in consistency with the analysis of the previous section. The reduction is independent of k for all sub-Hubble scales, leading to a suppression of power beyond equality. The parameter λ thus affects the global amplitude of the matter power spectrum on those scales. We expect less structure formation as illustrated by the lower values of σ_8 in Table 3.1.

Table 3.1: Predicted σ_8 values at $z = 0$ computed with our modified CLASS code on the basis of Planck 2018 cosmological parameters results [5], normalizing the amplitude of the primordial power spectrum at large scale to $A_s = 2.215 \times 10^{-9}$.

λ	σ_8
0.01	0.848
0.10	0.833
0.20	0.790
0.30	0.722
0.50	0.540
ΛCDM	0.848

We find that the amplitude of the matter power spectrum is a signature of the λCDM model and would discriminate it against the cosmological constant. It can be observationally measured through astrophysical structure formation surveys such as galaxy clustering or weak lensing. It is also possible to

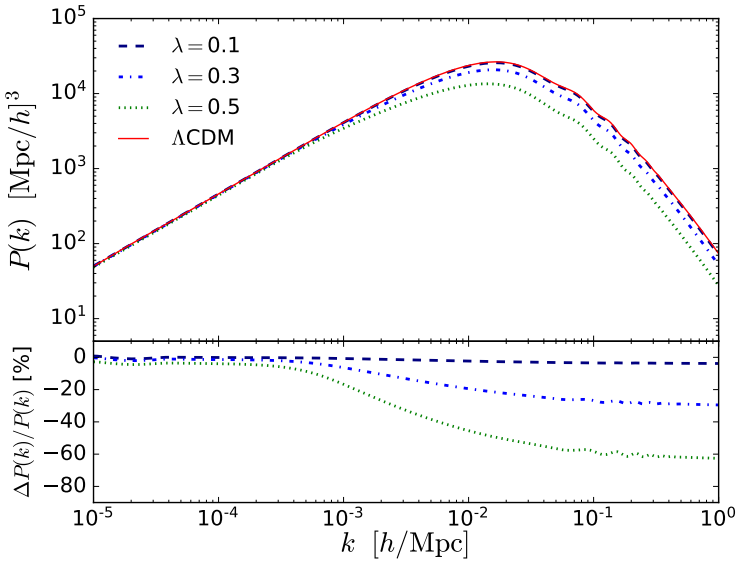

Figure 3.2: Linear matter power spectrum at redshift $z = 0$ in the λCDM model, predicted by our modified CLASS code on the basis of Planck 2018 cosmological parameters results [5]. The overall amplitude of the power spectrum pointedly goes down when dark energy increases, except for the largest scales that are less impacted. In terms of growth amplitude parameters, we expect smaller predicted σ_8. Alternatively, the primordial perturbations amplitude A_s must be larger to account for today's current structures.

measure the power spectrum through cosmological observations with the CMB temperature anisotropies map. We will be looking into the behaviour of the λCDM model with respect to the CMB in the next subsection.

3.1.3 Cosmic Microwave Background anisotropies

The CMB is composed of those photons that were emitted at the epoch of recombination when the Universe had a temperature of about $3,000$ K. Astrophysical sources began to emit additional photons at reonization around $z \sim 10 - 20$. Whereas the temperature fluctuations must be computed through the full Einstein-Boltzmann formalism because the equations of the matter components are coupled to each other, this subsection only aims to present the basics of the CMB physics. It will enable us to qualitatively describe how the CMB anisotropies are affected by the presence of quintessence. We will later confront the anisotropies predicted by the λCDM model with the Planck observations to infer and constrain the cosmological parameters value.

(a) Origin of the anisotropies

After the primordial nucleosynthesis, the Universe was composed of an opaque plasma that essentially consisted of relativistic photons and non-relativistic electrons, as well as Hydrogen and Helium nuclei (in addition to decoupled relativistic neutrons). At the time, it was the electromagnetic interac-

tions that ensured equilibrium among the plasma components. Photons were tightly coupled to electrons through Thomson scattering. Carrying opposite charges, the electrons were tightly coupled to the baryons through Coulomb scattering. Baryons and photons essentially interacted through gravitation, as well as cold dark matter. The ionization of Hydrogen and Helium ensured the efficiency of the electromagnetic interactions. While the Universe expanded, its temperature decreased and reached the threshold of $3,000$ K under which the scattering rate of these interactions was insufficient to maintain the plasma in equilibrium. At that time ($z \sim 1080$), electrons recombined with nuclei and given the paltry number of free electrons with which to scatter, photons decoupled and began to free-stream through the Universe which became transparent. The shape of the Planck spectrum of the radiation observed today on the entire celestial sphere is frozen but redshifted by the expansion. The corresponding temperature is relatively uniform. It reaches now $T_\gamma \sim 2.726\ K$ which corresponds to millimetres wavelengths, and to $\sim 10\ \mu\mathrm{m}$ in the infrared at the time of emission.

There are though small fluctuations in the temperature across the sky in the order of 10^{-5}. The energy distribution, i.e. the temperature, of these photons is defined by their emission conditions that depend on the plasma and dark matter inhomogeneities at the redshift of recombination. Therefore, the anisotropy of the radiation detected today in a given direction reflects the inhomogeneities of the radiation (or equivalently the baryons) on the corresponding point of emission from the last interactions. This is why it is commonly said that the primordial radiation that is observed today is an imprint of the last scattering surface at the beginning of the matter dominated epoch. The primary temperature anisotropies have various contributions that can be modelled by three fields:

- The local gravitational potential Φ: Photons that suffered the last scattering from inside a potential well ($\Phi < 0$) experience a gravitational redshift by climbing out of it.
- The matter peculiar velocity v: Photons scattered by matter approaching us ($v < 0$) are blueshifted through Doppler effect.
- The fluid density fluctuation δ, which is the most important term: The temperature of photons emitted from within an overdense region ($\delta > 0$) is higher since overdensity regions are hotter.

Consequently, the equation of the temperature contrast can be expressed as,

$$\frac{\delta T}{T}(\hat{r}) = \Phi(\vec{r}) - \hat{r}.\vec{v}(\vec{r}) + \frac{1}{3}\delta(\vec{r}), \tag{3.13}$$

where $\vec{r}$ is the proper distance to the last scattering surface. The three fields Φ, $\vec{v}$ and δ take their value at the recombination time ($z \sim 1080$ and $r \sim 6000\ h^{-1}$Mpc).

In order to confront the theoretical temperature contrast field with CMB observations, the temperature anisotropies are usually expanded on the celestial sphere on the basis of spherical harmonics Y_{ml},

$$Y_{ml}(\theta,\phi) = Ne^{im\phi}P_l^m(\cos\theta), \qquad N = (-1)^m\sqrt{\frac{2l+1}{4\pi}\frac{(l-m)!}{(l+m)!}}, \tag{3.14}$$

where P_l^m are the associated Legendre polynomials and $l = \pi/\theta$[rad] are the multipole moments. The temperature contrast is decomposed on this basis,

$$\frac{\delta T}{T}(\theta,\phi) = \sum_{l=0}^{\infty}\sum_{m=-l}^{l} a_{lm}Y_{lm}(\theta,\phi), \tag{3.15}$$

where a_{lm} are the multi-polar moments specified by ,

$$a_{lm} = \int Y_{lm}^*(\theta,\phi)\frac{\delta T}{T}(\theta,\phi)d\Omega, \tag{3.16}$$

where $d\Omega$ is the solid angle element. Since inflation predicts that the temperature fluctuations field is Gaussian, the anisotropies can be characterized by their angular correlation function. It is the angular power spectrum of the temperature contrast C_l^{TT}, called the power spectrum of temperature anisotropies in harmonic space, which is used to confront the theoretical models with the observations,

$$C_l^{TT} \equiv \left\langle |a_{lm}|^2 \right\rangle = \int d\Omega d\Omega' Y_{lm}(\theta,\phi)\left\langle \frac{\delta T}{T}^*(\theta,\phi)\frac{\delta T}{T}(\theta',\phi')\right\rangle Y_{lm}^*(\theta',\phi'). \tag{3.17}$$

(b) Predicted CMB power spectrum

Figure 3.3 provides examples of predicted dimensionless temperature anisotropy angular power spectra that we numerically compute with CLASS as an observational output for the λCDM and ΛCDM theoretical models. It depicts the shape of the CMB spectrum in light of Eq. (3.13). The power spectra are flat on large scales (the Sachs-Wolfe plateau) as the fluctuations of Φ, $\vec{v}$ and δ are frozen on angular scales larger than the horizon at decoupling. On angular scales smaller than the sound horizon, $l > 200$, the peaks are the result of the baryons and photons tight coupling fluctuations that oscillated acoustically within the plasma before recombination. There is a cut off from $l \sim 1000$ caused by the damping of perturbations on small scales. This is due to the Silk damping and thickness effects that mix the photons coming from different points inside the last scattering surface (not treated here).

We expect that the presence of the scalar field affects the peaks' location, particularly the first and dominant one. It corresponds to the largest scale with oscillations that reached maximum compression at decoupling. Its location is given by the angular scale $\theta = \pi/l_a$ that depends on both the size of the sound horizon at decoupling, $r_s(z_*)$, and the comoving angular diameter distance to the last scattering surface, $r(z_*) = (1+z_*)d_A(z_*)$,

$$l_a \equiv \pi\frac{r(z_*)}{r_s(z_*)}, \tag{3.18}$$

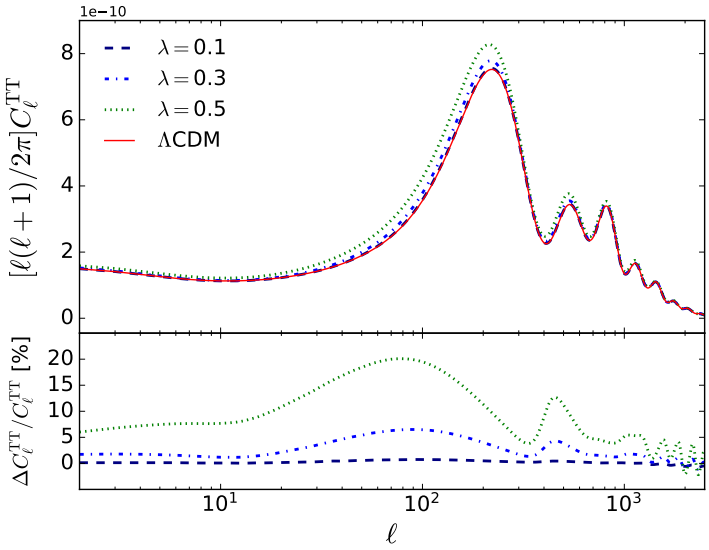

Figure 3.3: Top panel: CMB dimensionless angular power spectrum in the λCDM model, predicted by our modified CLASS code on the basis of Planck 2018 cosmological parameters results [5]. Bottom panel: Relative deviation from ΛCDM. Increasing values of λ enhance power on every scale. For the smallest value in the figure, the model is almost indistinguishable from the standard one (deviations $< 5\%$).

where z_* is the redshift at decoupling. The two effects are competing. On the one hand, the sound horizon at decoupling is the maximum distance a perturbation can propagate from $a = 0$ to $a = a_{\rm dec} = a_*$,

$$r_s(z_*) = \int_0^{a_*} \frac{da}{a^2} \frac{c_s}{H\,(a)} \sim 100\ \text{Mpc}/h, \tag{3.19}$$

where c_s is the adiabatic sound velocity in the plasma with inhomogeneous pressure. It can be written with the help of the baryonic fraction $f_b = \Omega_b/\Omega_m$ (~ 0.133 in the concordance model) as,

$$c_s = \left(\frac{\delta\bar{p}}{\delta\bar{\rho}}\right)^{1/2} = \frac{c}{\sqrt{3}} \left(1 + \frac{3 f_b}{4} \frac{a}{a_{\rm eq}}\right)^{-1/2}. \tag{3.20}$$

Whereas the presence of the scalar field does not change the baryonic fraction nor the time of equality given by Eq. (2.49), it affects the expansion rate which becomes larger as early dark energy density adds to the total energy density during the radiation dominated epoch. As a consequence, quintessence slightly decreases the size of the sound horizon at decoupling, slightly shifting the peak to smaller scales (to the right). On the other hand, the comoving angular diameter distance to the CMB surface also depends on the cosmic expansion history after decoupling,

$$\begin{aligned} r\,(z_*) &= c \int_0^{z_*} \frac{dz}{H\,(z)} \\ &= \frac{c}{H_0} \int_0^{z_*} dz \left[\frac{3}{3-\lambda^2}\Omega_{m_0}\,(1+z)^3 + \left(1 - \frac{3}{3-\lambda^2}\Omega_{m_0}\right)(1+z)^{\lambda^2}\right]^{-1/2}, \end{aligned} \tag{3.21}$$

which is the formula valid for flat space, neglecting radiation. Since the Hubble expansion increases with increased dark energy, the distance to the CMB surface decreases, as well as the respective multipole, shifting the position of the first peak to larger scales (to the left). This effect dominates the first one given the larger expansion history to date.

Moreover, the peaks' amplitude are also sensitive to λ as a result of the Early-time Integrated Sachs-Wolfe effect. As the universe expands and becomes increasingly dominated by matter, the gravitational potential Φ decays. The time variation of the gravitational potential adds an extra Sachs-Wolfe contribution to the temperature contrast seen in Eq. (3.13) with the term,

$$2\int \dot{\Phi} dt, \tag{3.22}$$

because the net gravitational shift is not null as the potential evolves during the time a photon takes to cross it. Since the scalar metric perturbation acts as a gravitational potential, the Einstein equation that relates the metric to a density perturbation is the comoving, perturbed and linearised Poisson-like equation that reads,

$$\nabla^2\Phi = -k^2\Phi\left(\tau, k\right) = \frac{3}{2}\mathcal{H}^2\left(\tau\right)\Omega_m\left(\tau\right)\delta_c\left(\tau, k\right). \tag{3.23}$$

At the beginning of matter domination, it takes a while for the sub-sound horizon metric fluctuations to freeze and the Early Integrated Sachs-Wolfe effect is maximal for scales crossing the sound horizon at the time of decoupling. In our quintessence model, matter density is decreased with increasing λ due to the presence of early dark energy at that epoch (see Figure 2.6). This enables the radiation to produce a stronger contribution to the Sachs-Wolfe plateau that notably boosts even more the first peak. Later, deep inside the matter domination epoch, $\Omega_m \sim 1$, $\mathcal{H} \propto a^{-1/2}$ and $\delta_c \propto a$ imply that $\Phi \sim$ constant from the Poisson equation in ΛCDM. Conversely, in λCDM, since $\delta \propto a^{m_+}$ where m_+ is given in Eq. (2.117), the potential Φ is no longer constant and its time variation increases the temperature anisotropies following the term in Eq. (3.22).

Finally, a similar effect happens during dark energy domination in the late Universe when the potential is again no longer constant, giving rise to the so called late-time Integrated Sachs-Wolfe effect that tilts the plateau on large scales. The CMB photons that cross evolving potentials of large scale structures are gaining energy while they get in, and loosing energy while escaping. When dark energy becomes important, the potential decays over the time the photons go through the large scale structure. Their energy net balance is positive, increasing their temperature and hence enhancing the low-l tail of the CMB power spectrum. However, as shown in Figure 3.3, the shape of the plateau on those large scales is only moderately affected by the quintessence model against ΛCDM.

3.1.4 Baryon Acoustic Oscillations

While the Baryon Acoustic Oscillations (BAO) is a feature that is detected in both the matter correlation function and power spectrum, they are used to obtain constraints on the cosmological parameters at background level. During the ionized plasma epoch, the tight coupling between the baryon fluid (free electrons and nuclear particles) and photons before recombination prevented the growth of baryonic structures until the last scattering. It also produced baryon-photon acoustic oscillations that were happening before photon decoupling. These oscillations called BAO are density waves travelling in the baryon-photon plasma at sound speed. At decoupling, the sound speed vanished as the plasma dissolved, and therefore the waves ceased. The latter left an overdensity of baryonic matter at the maximum distance (called sound horizon) the wave could travel from the Big Bang to decoupling. In fact, the decoupling of photons and baryons did not coincide. Given that they were outnumbered, the baryons were tracking photon perturbations for a little while after photon decoupling, until a time known as baryon drag. After the baryon drag time, during the transparency epoch, baryons collapsed into gravitational potential wells since they did not undergo Thomson scattering and were hence not subject to radiation pressure any longer. As two collisionless species subject only to gravity, the baryon perturbation eventually reached equilibrium with cold dark matter, growing at the same pace. The baryon overdensity remained frozen on the sound horizon scale at baryon drag, corresponding to the comoving scale defined in Eq. (3.19) depending on ω_b and ω_m,

$$r_s(\tau_{drag}) = \int_0^{a(\tau_{drag})} \frac{da}{a^2} \frac{c_s}{H(a)}. \tag{3.24}$$

This acoustic feature is detected in both the matter correlation function and power spectrum. They combine dark matter fluctuations with the small amplitude oscillation of the baryon fluctuations that become imprinted in them. The overdensity thus appears as a single secondary peak in the matter correlation function at the sound horizon distance. This means that there is an excess correlation around every galaxy at a separation of 150 Mpc from it (in the concordance model). Since the sound wave propagated isotropically in the primordial plasma, the peak can be measured at different 3-dimensional space directions. Being a standard ruler, we use the BAO peak as a geometric probe. Observationally, the angular size is measured from the wave number where the peak appears. It provides for a measure of a quantity called volume distance D_V that combines angular and redshift separations, respectively orthogonal to the line of sight (as the background evolution causes distortion in the transverse direction [44]) and along the line of sight,

$$D_V(z) \equiv \left[(1+z)^2 d_A(z)^2 \frac{c\, z}{H(z)}\right]^{1/3}, \tag{3.25}$$

where H is the Hubble rate in Eq. (2.39) and d_A is the angular diameter distance defined in Eq. (A.7).

The latter can be computed with the luminosity distance in Eq. (3.3) which has a dependence on λ,

$$d_A = \frac{d_L}{(1+z)^2}. \tag{3.26}$$

We use BAO to constrain d_A and H, and thus the background parameters of the model including λ.

3.2 CLASS-MontePython pipeline

So far, we have been estimating the observational signatures that the λCDM model could leave on predicted observables, both at background and perturbations levels, and at low and high redshift. To facilitate the direct comparison between models, and assess the sensitivity of the scalar field parametrisation, we normalized the numerical results by assuming the fiducial values for the ΛCDM parameters at $z = 0$. They are thus likely inconsistent with observational data. This is why, we turn now our focus on the observations themselves to statistically constrain the model, particularly λ which is key to our parametrisation, by carrying-out a Monte Carlo Markov Chain analysis. We want to fit our theoretical model of quintessence λCDM by finding the parameters values that best fit observation data, and their corresponding uncertainties. To this end, we set up a pipeline interfacing the Boltzmann code Cosmic Linear Anisotropy Solving System (CLASS) [45, 46] with the Monte Carlo code MontePython [47, 48] to infer and constrain the cosmological parameters.

3.2.1 Computing predictions with CLASS

We use CLASS to compute cosmological observable quantities that are predicted by our theoretical model which consists in a flat universe containing radiation, massless neutrinos, baryons, cold dark matter and our parametrised scalar field. It is a code programmed in C language that numerically evolves the background and linear perturbation quantities. CLASS solves the full system of Einstein-Boltzmann coupled equations for all cosmological species and for a large range of scales and scale factor. In particular, it computes the density perturbations in the radiation-baryonic plasma and their time evolution to construct the predicted linear Matter Power Spectrum and CMB angular power spectrum that we compare with astrophysical and cosmological observations.

As far as quintessence is concerned, the publicly available versions of CLASS only provide for a scalar field potential of the form $V(\phi) = [(\phi - B)^\alpha + A]\, e^{-\lambda\phi}$, proposed in Ref. [49]. We therefore must modify the source code to implement the double exponential potential (2.43) of the λCDM model. The modifications concern the CLASS modules *background.c*, *background.h* and *input.c*, *input.h*. The perturbation modules remain unchanged at this stage since the corresponding scalar field equations are entirely valid for λCDM. These modules (as well as the background ones) will have to be modified at a later stage to adapt them to the coupling with dark matter that we will be envisaging in Chapter 4.

It is always possible to renormalise the potential mass scales A (2.44) and B (2.45) with today's value ϕ_0 of the scalar field. We decided to fix $\phi_0 = 0$ in order to avoid numerical limitations related to using exponentially large numbers during the computations. ϕ_0 can be set to zero without loss of generality because it is the relative field displacement which is relevant as regards the cosmological evolution, and not today's value that is just a matter of redefining the initial condition for ϕ. For the quintessence model originally foreseen in the public code, CLASS imposes by default a hard coded shooting mechanism to tune the initial conditions. In the case of our potential, we do not implement any shooting in order to keep λ a free parameter. Given that we possess the analytic expression of the mass scales, it is not necessary to numerically adjust them to today's Friedmann constraints. We just slightly tune the initial conditions of the scalar field ϕ_i in order to ensure that dark energy is sub-dominant at the outset of the evolution. Our approach is consistent with Ref. [40] where the initial conditions are set in the aftermath of inflation. The precise initial conditions are unimportant by virtue of the existence of attractor solutions that are reached unavoidably, as described in Section 2.3. For the same reason, we decide to set $\dot{\phi}_i = 0$. It follows that we implement in CLASS the following initial conditions at the beginning of the evolution ($z = 10^{14}$),

$$\phi_i \sim -\frac{\lambda}{3} \ln \frac{10^{-10} \rho_i^{rad}}{A}, \qquad \dot{\phi}_i = 0, \tag{3.27}$$

where ρ_i^{rad} is the initial energy density of radiation and A is the mass scale of the dominant exponential at the time. The scalar field thus enters the attractor during the radiation dominated era, before BBN. In the present work, we limit ourselves to these initial conditions. It might be worth investigating further the possibility of escaping the primordial nucleosynthesis constraint that applies to early dark energy models by considering non-vanishing initial kinetic energy conditions. These would allow the scalar field to reach the attractor in the matter era.

3.2.2 Bayesian inference with MontePython

(a) Bayesian estimation of cosmological parameters

In the Bayesian approach, the random variable is the vector of theoretical parameters for a given cosmological model [50]. The vector is thus a set of unobserved variables which is subject to a probability distribution. The latter needs to be computed as a conditional probability given the observed data, which is also considered as random variables. To this end, a joint probability $P(m, d)$ is defined, where d stands for the data (i.e the estimated physical property) and m for the model (i.e the values of the parameters). The joint probability is the probability of the parameters value given the data. It satisfies $P(m, d) = P(m|d)P(d)$ and also $P(m, d) = P(d|m)P(m)$. In this approach, the Bayesian Inference hence considers two spaces: in the one hand, the data space where the random variables d live with the

conditional probability $P(d|m)$, and on the other hand, the parameter space where the random variables m live with the conditional probability $P(m|d)$. They are connected through the Bayes theorem that states,

$$P(m|d) = \frac{P(d|m)P(m)}{P(d)}, \tag{3.28}$$

where $P(m|d)$ is the distribution in the parameter space, called posterior distribution, which is our aim. $P(m)$ is called the prior. It corresponds to the probability of the parameters values and does not hinge on the observations. The prior can have already been inferred through previous experiments or from inherent properties of the model. $P(d|m)$ is the distribution in data space and corresponds to the probability of obtaining the data on the basis of the parameters values. Whereas the frequentist method studies the properties of the data space, the Bayesian approach uses $P(d|m)$ to deduce $P(m|d)$. Moreover, it assumes that the probability of the observation, considering a parameter value, is connected to the likelihood of that value to occur. Therefore $P(d|m)$ is called the likelihood $\mathcal{L}(m)$ of the parameters, although this quantity lies in the data space. Finally, $P(d)$ is the probability of the observation data aside the parameters values. It is obtained by marginalization over all parameters, and thus is independent of them,

$$P(d) = \int_m P(d|m)P(m)\, dm. \tag{3.29}$$

It is therefore a normalization constant, yet it depends on the cosmological model itself. Its value, called evidence, can be used as a criteria for comparing different models. The value of the evidence may be renormalized to unity when a single model is considered.

As regards the data space, the measured data represents a sample of the distribution, the moments of which can be computed. In general, for large amount of data, the full distribution should be Gaussian. As regards the parameter space, the posterior can be computed from the likelihood using the Bayes theorem, provided that the prior is known and the evidence is renormalized. Fitting a theoretical model consists in identifying the posteriors that best fit the data. It requires us to find the set of parameters values that minimize chi-square χ^2, or equivalently maximize the likelihood, i.e. the probability of obtaining the data assuming our model.

In order to estimate the parameters values, as well as their uncertainties, we seek to determine the posterior distribution in the parameter space, by sampling it thanks to a Monte Carlo stochastic method using the MontePython code.

(b) MontePython parameter inference package

MontePython includes several algorithms to sample the parameter space as a group of points in the same proportion as in the full distribution. We use the Markov Chain Monte Carlo (MCMC) algorithm called Metropolis-Hastings that draws stochastic jumps in the parameter space from a Gaussian proposal density used as an auxiliary distribution.

Each selected point in the parameter space is automatically passed to CLASS as an input of the cosmological model. On this basis, CLASS computes the related observable quantity (such as the luminosity distance as a function of z) and passes it back to MontePython. The latter contains several datasets of observations to compute the likelihood of the CLASS output. The likelihood is the probability of getting the measured data given the parameters values corresponding to the point selected by the random jump. Every point is then accepted or rejected depending on its likelihood evaluated against the data and compared with the likelihood of the precedent point. The use of a covariance matrix of the posterior distribution can optimize the proposal densities, generating an optimal acceptance rate of the order of 0.25. The optimal jumping step size is approximatively 2σ of the considered parameter distribution.

The sequence of the drawn points that are accepted is called a Markov chain and targets regions of higher likelihood. The resulting chain is a correlated sample of the posterior in the parameter space. The latter possibly includes nuisance parameters accounting for the measurements bias. The Markov chain eventually converges to the wanted probability distribution although the initial samples may correspond to a different one, particularly when the starting point is within a low density region. The points before convergence are removed by the code in the burn-in phase to throw away the initial samples. Chains may require a long time to converge, particularly when the jumps are small. The quality of the convergence is estimated by the Gelman-Rubin test $R-1$. It can be loosely defined as the variance of the chain means divided by the mean of the variances. A set of chains can be considered converged when this estimator is small enough, typically < 0.05 for every parameter [51]. In Appendix B, the values quoted for assessing the convergence of the chains is the worst, i.e. the largest, value among the parameters.

3.3 Datasets supporting the statistical analysis

3.3.1 Pantheon sample

As far as the background expansion is concerned, we use the supernovae likelihood based on the Pantheon sample [52] to fit the model. As Pantheon is technically not part of the MontePython code, we have to install it ad-hoc. The sample is the largest compilation of SNIa to date, containing a total of 1048 brightness data points ranging from $0.01 < z < 2.3$. It compiles the measurement of their apparent magnitude $m(z)$, which corresponds to the observed peak magnitude in the rest-frame B band, along

with a certain uncertainty. The observable is the luminosity distance computed with CLASS to predict the theoretical distance modulus $\mu_{class}(z)$ defined in Eq. (3.1) for each supernova in the sample, knowing its redshift. The supernova absolute magnitude $M \sim -19.3$ in the B-band is considered as a nuisance parameter that needs to be varied in the statistical inference together with the cosmological parameters. The distance estimator is then just $\hat{\mu}(z) = m(z) - M$ for every data point. Based on Ref. [53], the fit of a given cosmological model to supernovae measurements in the Pantheon sample is done in the MontePython code by maximizing the log-likelihood $\ln \mathcal{L} = \chi^2/2$, where χ^2 is defined by the following function over the residuals,

$$\chi^2 = (\hat{\mu} - \mu_{class})^t \, C^{-1} \, (\hat{\mu} - \mu_{class}) \,, \tag{3.30}$$

where the vector $\hat{\mu}(z)$ contains the data points. $\mu_{class}(z)$ is the vector of the corresponding CLASS predictions for the different redshifts, computed on the basis of the model's parameters. C is the provided covariance matrix that consists of the variances of each data point (diagonal terms) and the correlation between them (off-diagonal terms).

3.3.2 BOSS measurements

In combination with SNIa observations, we use BAO measurements to constrain the model at background level. The BAO peak is detected at different angular separations through samples of galaxies at different redshift to obtain independent data points. We choose those from the BOSS 2014 dataset from $0.106 < z < 2.36$ provided in MontePython. It includes five data points related to the quantity D_V in Eq. (3.26), and respectively collected from the 6DF galaxy survey [54], the BOSS LOWZ data release 11 galaxy samples [55], the BOSS LyaQSO (2 points) [56] and the SDSS DR7 Main Galaxy Sample [57]. In addition, anisotropic measurements are also used.

In order to predict the theoretical estimator $D_{V_{class}}(z)$ for each point in the dataset, CLASS computes the angular distance $d_A(z)$, the radial distance $z/H(z)$ (as well as the sound horizon at baryon drag $r_s(\tau_{drag})$ when the data point consists in the relative BAO distance defined as $r_{BAO} \equiv r_s(\tau_{drag})/D_V(z)$). The χ^2 contribution is then calculated by MontePython over the data points and their associated uncertainties σ_z,

$$\chi^2 = \sum_z \left[\frac{\hat{D}_V(z) - D_{V_{class}}(z)}{\sigma_z} \right]^2 . \tag{3.31}$$

3.3.3 Planck observations

Following the results of the simulations in 3.1.3, we use CMB anisotropies angular power spectra measured by the Planck satellite mission to constrain our cosmological models at perturbation level at

high redshift. We choose the recent three likelihoods released in 2018 [58] based on temperature T power spectra from Planck data. In order to enhance the determination of the parameters as in [5], we also use the combined data on the curl-free component E of the anisotropies polarization produced by Thomson scattering during the plasma epoch. The patterns are measured by the Wilkinson Microwave Anisotropy Probe (WMAP). As they are both technically not part of the MontePython code, we had to install them ad-hoc.

The datasets are composed of points for the temperature and polarization cross-correlation TT, TE and EE angular spectra on high multipoles that are complemented by measurements on lower multipoles for EE and TT. It is worthwhile noting that we use the lite version of the Planck likelihoods of the higher multipoles which includes marginalization over the foreground and instrumental effects. In the lite likelihoods, all the nuisance parameters are fixed except for the Planck absolute calibration $A_{\rm planck}$. We deliberately choose the lite version to limit the statistical analysis to a lower dimensional parameter space, enhancing convergence pace and sparing computational time. The Planck likelihoods we use are composed of a total of 667 data points: 215 points for the TT spectrum, plus 199 in each EE and TE, plus 27 data points in each low-l TT and EE datasets.

The high-multipole likelihood (called *Plik*), is a Gaussian approximation of the probability distributions of the temperature and polarization cross-correlation angular spectra. The polarization likelihood at low-l (*SimAll*) has a quadratic maximum form whereas the temperature likelihood (*Commander*) relies on a Gibbs-sample based Blackwell-Rao likelihood [59] to account for the non-Gaussian shapes. The covariance matrices are semi-analytic and calculated on the basis of a fiducial cosmology.

3.3.4 KIDS-450 survey

Weak gravitational lensing, also known as cosmic shear, relates to light deflection caused by gravity [60]. It is produced by the gravitational potentials of Large Scale Structures that deflect the propagation of photons emitted by astrophysical sources such as galaxies. Gravitational lensing can therefore be used to probe matter distribution at a given redshift that can be compared with the matter power spectrum predicted by cosmological models. It is mainly sensitive to Ω_m and the amplitude σ_8, with a well defined degeneracy encapsulated in the combination $S_8 = \sigma_8\sqrt{\Omega_m/0.3}$, and hence allows to constrain our λCDM model.

We make use of the Kilo-Degree Survey-450 (KiDS-450) weak lensing dataset [61] that contains the measurement of galaxies' ellipticity with 450 deg^2 imaging. The observed ellipticities consist in the intrinsic ellipticity of the galaxies combined with the shear caused by the lensing potential. The data vector is composed of 130 points sampled in four tomographic redshift bins: $0.1-0.3$, $0.3-0.5$, $0.5-0.7$ and $0.7-0.9$. We need to add two extra nuisance parameters in the Bayesian analyses to account for

the measurements' bias: the uncertainty in the amplitude of the Intrinsic Alignment ($A_{\rm IA}$), as well as the uncertainty on the dark matter power spectrum amplitude related to the feedback from baryons ($A_{\rm bary}$).

Moreover, since part of the measurements corresponds to the non-linear regime of structure formation, it is necessary to apply a correction to the predicted linear matter power spectrum for the small scales concerned. We use in CLASS the HALOFIT model [62] valid for ΛCDM as a fitting formula to infer the non-linear matter power spectrum. The model is calibrated to reproduce the small-scale power spectra computed by N-body simulations. Finally, the likelihood used in MontePython is based on Ref. [63].

3.4 Analysis of the results

3.4.1 Operational description of the runs

MontePython works with three types of parameters. The cosmological ones are those that we want to fit as free parameters of the models at stake. Depending on the kind of dataset in the MCMC chains, either for the homogeneous background evolution or at perturbative level, we sample with flat priors all or part of the six free parameters in the standard spatially flat cosmology having a power-law spectrum of adiabatic scalar perturbations: the density of baryonic matter ω_b, the density of cold dark matter ω_c, the angular scale of the sound horizon at last scattering $100\theta_s$ (which is the ratio of the sound horizon at decoupling to the angular diameter distance to the last scattering surface) or the Hubble parameter h, the optical depth to reionization τ_{reio}, the amplitude of the initial fluctuations $\ln 10^{10} A_s$, and the scale dependence of this amplitude n_s, plus the free parameter λ. The nuisance parameters are those that are forced to vary for some particular datasets, such as Pantheon (M), Planck ($A_{\rm planck}$) or KiDS ($A_{\rm IA}$ and $A_{\rm bary}$), to marginalize over systematics effects. MontePython also provides for derived parameters on demand to infer constraints on them, particularly those parameters of the late-universe that are model-dependent: the Hubble constant H_0, the matter density parameter Ω_m and the matter fluctuation amplitude σ_8. They are not varied as such as they depend on the free cosmological parameters.

We execute MontePython in the *run* mode to compute the chains with an input parameter file whose extension is *.param* that specifies the experiment dataset to use and the varying parameters of the model, along with their prior expected mean value and uncertainty. Since the convergence is increased by running MontePython with a covariance matrix, we use the *superupdate* sampling option, which is particularly suitable for models that contain many parameters requiring more time to complete the runs. This option allows to on the fly periodically improve the covariance matrix as proposal density to increase convergence performance, and periodically adapt the jumping factor to target the 25% acceptance rate [64].

We analyse the chains with the *info* execution mode of MontePython. It computes the convergence of the chains and produces statistical information on the posteriors, including credible intervals, 1-dimensional probability distributions and plots of the 2-dimensional marginalized iso-likelihood contours at 1σ and 2σ Confidence Levels (CL). The full plots can be found in Appendix B.

3.4.2 Comparing constraints from Pantheon, BOSS and Planck

The constraints we extract on background parameters from the cosmic expansion, as well as from the perturbed universe at high redshift, are summarized in Table 3.2. Additional cosmological parameters do not need to be fit with the Pantheon and BOSS datasets since the related observables depend only on λ, Ω_m and H_0. The free parameters specific to Planck are reported in the next subsection.

Table 3.2: Constraints on the λCDM model at background level. We note the usual tension on the value of H_0 between the early universe measurements ~ 67 and those obtained in the local universe ~ 70.

	Pantheon+BOSS			Planck		
Parameter	mean$\pm\sigma$	95% lower	95% upper	mean$\pm\sigma$	95% lower	95% upper
λ	$-0.04^{+0.41}_{-0.39}$	-0.77	0.69	$0.000^{+0.052}_{-0.052}$	-0.100	0.100
Ω_m	$0.283^{+0.050}_{-0.024}$	0.181	0.359	$0.3181^{+0.0086}_{-0.0094}$	0.3003	0.3363
H_0	$70.3^{+2.9}_{-5.0}$	62.37	79.58	$67.18^{+0.64}_{-0.64}$	65.90	68.46
$-\ln\mathcal{L}$	515.737			502.192		
χ^2	1031			1004		

The expression of the double exponential potential in equation (2.43) reveals the existence of a symmetry for our scalar field parameter λ with respect to zero by making $\phi \to -\phi$. This symmetry is identifiable in the λ-Ω_m and λ-H_0 planes of Figure 3.4. Although, to spare computational time, we could be sampling the positive side of the λ posterior parameter space only, we decided to let it free at this stage in order to reveal the approximate Gaussian shape of the probability distribution for this posterior.

The posterior bounds $-0.77 < \lambda < 0.69$ at 2σ Confidence Level (CL) obtained with the combination of Pantheon and BOSS are rather wide and allow too large quantities of early dark energy that are incompatible with the tighter BBN ceiling discussed in Section 2.3. On the other hand, the observations of the Universe at high redshift are considerably more constraining, as shown in Figure 3.4. Those extracted from the CMB anisotropies with Planck data significantly lower the 95% CL upper bounds to $|\lambda| < 0.1$. The CMB likelihoods further constrain the posterior λ since large values of early dark energy have significant impact on the angular power spectrum, as was illustrated in section 3.1.3, and are thus statistically disfavoured by the fitting. In both cases, the expected value of $|\lambda|$ is compatible with zero, i.e. with a cosmological constant.

As regards λ degeneracies with other cosmological parameters, Figure 3.4 shows the existence of

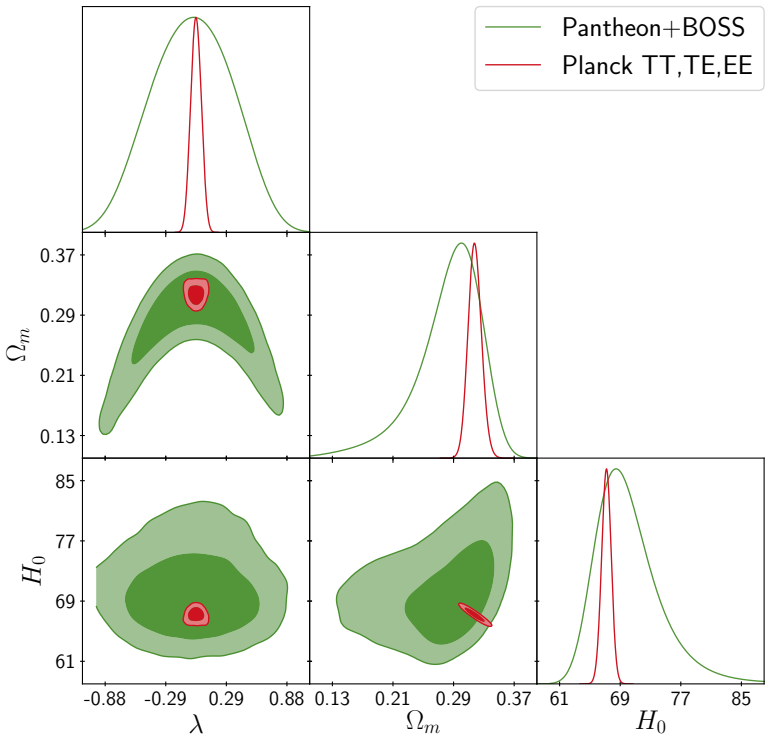

Figure 3.4: Plots at the top of the triangle: Probability distribution for marginalized parameters (λ and the common derived parameters). Confidence contours plots showing the marginalized 2-dimensional likelihood. The Pantheon+BOSS contours contain those of Planck. The formers allow for a region in parameter space with larger values of the Hubble constant. Conversely, the latter substantially reduce the allowed areas.

a strong anti-correlation to Ω_m at background level. In coherence with the explicit expression of the luminosity distance in Eq. (3.3), increasing values of quintessence lead to decreasing values of matter for a given distance. However, they are moderately correlated in the Planck datasets within the smaller credible intervals that are inferred.

3.4.3 Comparing models with Planck

Table 3.3 compares the inferred values of the cosmological parameters between quintessence and the standard model that we also run in our Bayesian analysis. They remarkably agree, hinting that within the λ credible intervals, the quintessence model is undistinguishable from a cosmological constant. All the six common parameters constraints are highly consistent with the Planck results for the standard model, which is though characterized by one parameter less. Statistically, a good fit would roughly correspond to the minimum χ^2 equalling the number of data points. The chi-square normalised by the number of degrees of freedom $N_{\rm dof} = N_{\rm datapoints} - N_{\rm parameters}$ called reduced $\chi^2_{\rm red} \equiv \chi^2/N_{\rm dof}$, is a useful quantity to compare the merit of the two models. ΛCDM is slightly better as it corresponds to the lowest reduced chi-square. Yet the observations do not convincingly discriminate the two models. They notably foresee a similar constraint on today's dark energy abundance.

Table 3.3: Comparison between quintessence λCDM with standard ΛCDM using Planck. The first five parameters are derived while the following seven are those that we use as sampling parameters with flat priors in the MCMC. The last one is the single nuisance parameter of the lite version.

	λCDM		ΛCDM	
Parameter	best-fit	mean$\pm\sigma$	best-fit	mean$\pm\sigma$
Ω_m	0.3139	$0.3167^{+0.0085}_{-0.0093}$	0.3138	$0.3166^{+0.0086}_{-0.0089}$
H_0	67.37	$67.18^{+0.64}_{-0.64}$	67.47	$67.28^{+0.62}_{-0.64}$
σ_8	0.8121	$0.8095^{+0.0087}_{-0.0081}$	0.8118	$0.8122^{+0.0077}_{-0.0077}$
$10^{+9}A_s$	2.106	$2.104^{+0.033}_{-0.036}$	2.106	$2.103^{+0.032}_{-0.036}$
$z_{\rm reio}$	7.74	$7.72^{+0.80}_{-0.82}$	7.86	$7.70^{+0.79}_{-0.81}$
λ	0.013	$0.000^{+0.052}_{-0.052}$	n.a.	n.a
$100\ \omega_b$	2.238	$2.236^{+0.015}_{-0.015}$	2.237	$2.236^{+0.015}_{-0.015}$
$\omega_{\rm cdm}$	0.1201	$0.1205^{+0.0014}_{-0.0015}$	0.1198	$0.1203^{+0.0014}_{-0.0014}$
$100 * \theta_s$	1.04200	$1.04200^{+0.00034}_{-0.00031}$	1.04200	$1.04200^{+0.00031}_{-0.00030}$
$\ln 10^{10}A_s$	3.047	$3.046^{+0.016}_{-0.017}$	3.047	$3.046^{+0.016}_{-0.017}$
n_s	0.9659	$0.9650^{+0.0045}_{-0.0045}$	0.9667	$0.9653^{+0.0045}_{-0.0045}$
$\tau_{\rm reio}$	0.0548	$0.0546^{+0.0075}_{-0.0083}$	0.0560	$0.0545^{+0.0074}_{-0.0084}$
$A_{\rm planck}$	1.0010	$1.0010^{+0.0026}_{-0.0025}$	1.0010	$1.0010^{+0.0025}_{-0.0026}$
χ^2_{red}	1.521		1.519	

Moreover, λ should be anti-correlated to the late-time fluctuation amplitude parameter σ_8. We have already concluded in Subsection 2.4.2 that the pace of the perturbations growth is sensitive to the existence of early dark energy. Figure 3.5 confirms a weak anti-correlation between λ and σ_8 which decreases the level of clustering in the universe relatively to ΛCDM. The level of clustering is slightly less constrained in the quintessence model on the σ_8-H_0 and σ_8-Ω_m symmetric planes, allowing for slightly lower values of σ_8 than in ΛCDM.

3.4.4 Obtaining specific constraints with KiDS-450

To further the analysis, we test the λCDM model with the KiDS-450 observations in the perturbed universe at lower redshift. Unfortunately, the poor Metropolis-Hasting convergence of the Markov chains, which is far worse than Pantheon-BOSS or Planck, does not allow to obtain conclusive constraints. This issue occurs despite that we have restricted the λ prior to positive values, taking advantage of the existing symmetry, and limited the varying parameters to $\{h, \Omega_m, A_s\}$ on top of the two nuisance parameters. We had to therefore opt for the Nested-Sampling algorithm, implemented as MultiNest in MontePython [65–67], to sample the parameter space in order to cope with the posteriors' non-Gaussian shapes. Additional computational power would be necessary to maintain the number of live points beyond the default value of 400, and reach better results within affordable runtime. Nevertheless, we decide

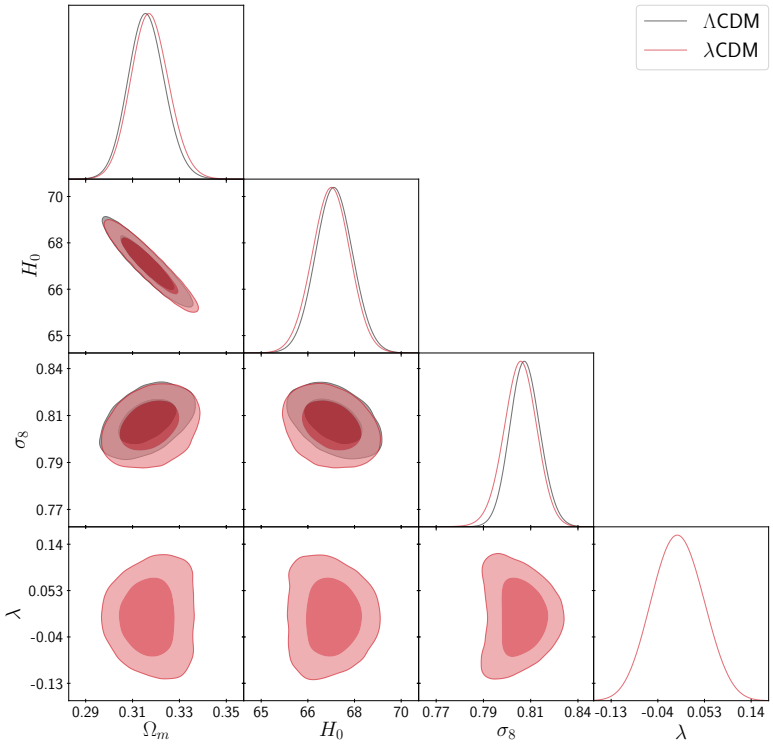

Figure 3.5: Probability distribution for marginalized parameter (plots at the top of the triangle) and contour plots showing the marginalized 2-dimensional constraints obtained with the Planck dataset alone. Contours include 68% and 95% of the probability.

to present hereafter some preliminary results, bearing in mind that they have to be taken with caution. The constraints on the derived parameters are summarized in Table 3.4.

Table 3.4: Comparison between quintessence λCDM with standard ΛCDM using KiDS.

	λCDM		ΛCDM	
Parameter	best-fit	mean$\pm\sigma$	best-fit	mean$\pm\sigma$
λ	0.62	$0.52^{+0.24}_{-0.18}$	n.a.	n.a
Ω_m	0.60	$0.57^{+0.13}_{-0.16}$	0.334	$0.335^{+0.074}_{-0.056}$
σ_8	0.498	$0.540^{+0.075}_{-0.096}$	0.70	$0.72^{+0.063}_{-0.11}$
S_8	0.708	$0.730^{+0.048}_{-0.049}$	0.743	$0.745^{+0.045}_{-0.044}$
χ^2_{red}	2.655		2.641	

As for the posterior λ, a vanishing value of the parameter is not favoured by KiDS observations, unlike Pantheon, BAO and Planck. We obtain the following weak constraint at 1σ CL,

$$\lambda = 0.52^{+0.24}_{-0.18}. \tag{3.32}$$

As λCDM suppresses power, we find that the abundance of matter Ω_m increases dramatically and the level of clustering measured by σ_8 is reduced compared to the standard cosmological constant model. In Figure 3.6, we note that while the 2-D marginalized contours overlap, the likely values of Ω_m and σ_8 in the λCDM model are respectively shifted to higher and lower values, yet with little impact on the

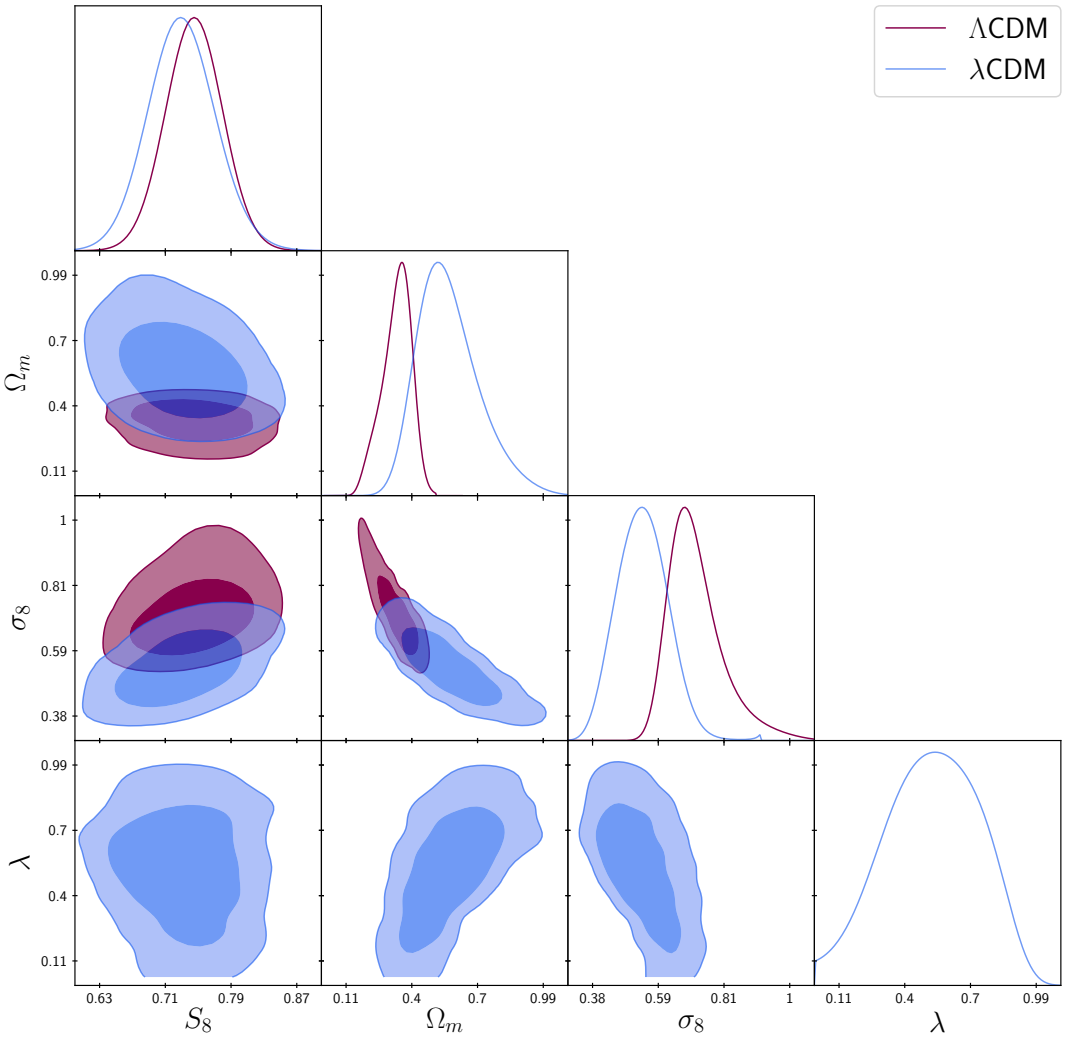

Figure 3.6: Probability distribution for marginalized parameter (plots at the top of the triangle) and contour plots showing the marginalized 2-dimensional constraints obtained with the KiDS dataset. Contours include 68% and 95% of the probability.

degenerated combination S_8.

The present analysis will have to be deepened in future works since the posteriors values in the ΛCDM model do not match those in Ref. [61]. Whereas the constraints on the parameter combination S_8 is of the same order, Ω_m and σ_8 are respectively higher and lower. While we have limited the flat prior on h to $[0.64, 0.82]$ as in Ref. [61], it was not possible in our analysis to derive credible intervals for this posterior. Finally, Figure 3.7 compares KiDS with the Planck constraints. The posterior distributions of the derived cosmological parameters are all in tension.

3.4.5 Discussion on the parameters estimation

We are in a position to conclude that the model consisting in parametrising the scalar field supposedly responsible for the recent acceleration of the universe is a plausible alternative to ΛCDM. It is a simple

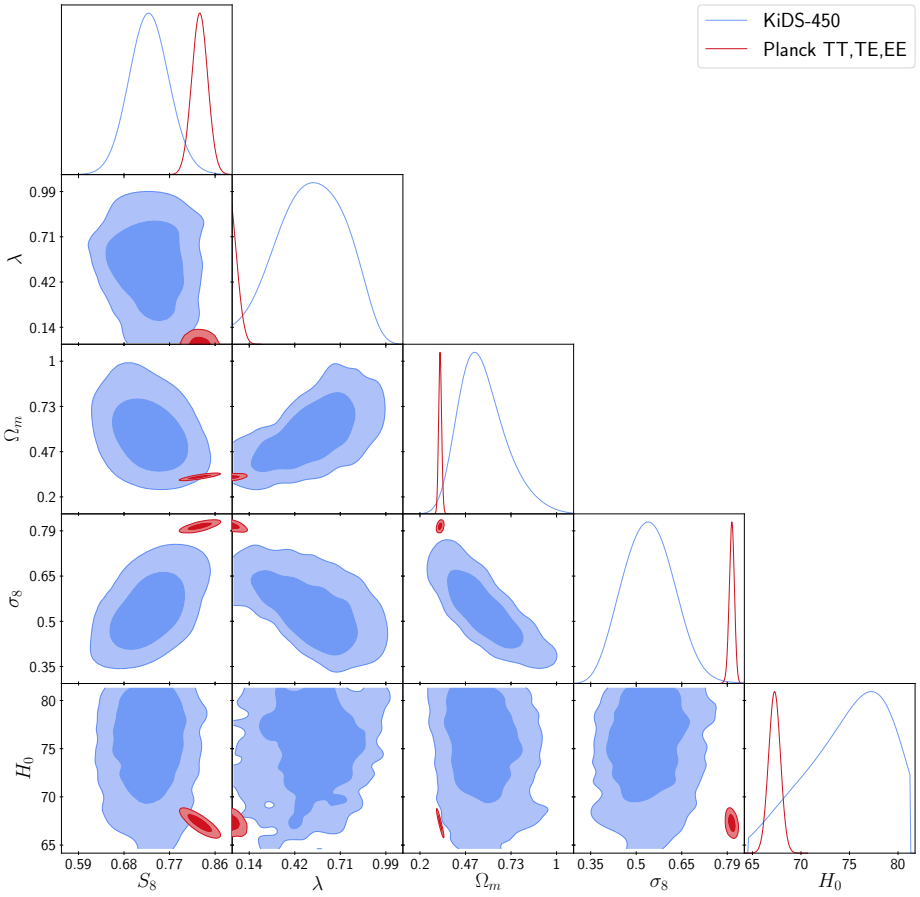

Figure 3.7: Comparison of the constraints on λCDM between Planck and KiDS. Probability distribution for marginalized parameter (plots at the top of the triangle) and contour plots showing the marginalized 2-dimensional constraints. Contours include 68% and 95% of the probability.

model that only adds one single parameter (against several in other dark energy parametrisations as seen in section 1.2) to account for the dynamics of dark energy with time. Its behaviour successfully matches observational data which bring similar statistical constrains on the standard cosmological parameters.

While the Bayesian inference done with Planck finds a preference for a vanishing value of the additional parameter, compatible with the existence of a cosmological constant, we are able to constrain the upper limit to $|\lambda| < 0.052$ and $|\lambda| < 0.10$ respectively at 68% and 95% CL from the most recent CMB anisotropies measurements. However, the weak lensing observations at lower redshift are not compatible with a vanishing value: $|\lambda| = 0.52^{+0.24}_{-0.18}$. All posterior distributions are also in tension between KiDS and Planck. In the next chapter, we will be contemplating a possible extension of our parametrisation by allowing interactions within the dark sector through a constant coupling β, adding an additional degree of freedom to the model.

Chapter 4

$\lambda\beta$CDM coupled quintessence model

The unknown nature of both dark energy and dark matter allows us to propose models that assume interactions between them [68]. The fact that their energy densities are comparable in the present epoch might even be a sign of an interaction. For the sake of simplicity, we consider a constant coupling β that parametrises the interaction between cold dark matter and the quintessence field ϕ described in the previous chapters. This is the kind of conformal coupling that appears in the Einstein frame where the matter fields depend on the scalar field [69]. Radiation is neglected given that we are studying the behaviour of cosmological models in the deep matter or dark energy dominated epochs. A similar coupling with radiation would vanish anyway since the trace of the radiation energy-momentum tensor is null. It is further assumed that dark energy does not interact with baryons due to local gravity constraints. Since baryons are subdominant, their presence only makes little difference for the evolution of the background. However, we keep them in the cosmological fluid for the sake of completeness.

4.1 Evolution of the background

Since baryons do not interact, they are conserved separately. The baryonic fluid evolves according to the regular continuity equation,

$$\nabla_\mu T^{(b)}{}^\mu_\nu = 0 \qquad \Rightarrow \qquad \dot{\rho}_b + 3H\rho_b = 0. \tag{4.1}$$

As regards the dark sector, energy flows among quintessence and dark matter through their coupling. Therefore, in spite of not being individually divergenceless, the dark sector energy momentum tensor is jointly conserved through the Bianchi identities, preserving General Relativity covariance,

$$\nabla_\mu \left(T^{(\phi)}{}^\mu_\nu + T^{(c)}{}^\mu_\nu \right) = 0, \tag{4.2}$$

and,

$$\nabla_\mu T^{(\phi)}{}^{\mu}_{\nu} = -\beta T_c \nabla_\mu \phi = +\beta \rho_c \nabla_\mu \phi, \tag{4.3}$$

$$\nabla_\mu T^{(c)}{}^{\mu}_{\nu} = +\beta T_c \nabla_\mu \phi = -\beta \rho_c \nabla_\mu \phi, \tag{4.4}$$

where $\kappa = 1$ and $T_c = -\rho_c + 3p_c = -\rho_c$ is the trace of the energy-momentum tensor of cold dark matter, which is pressureless by definition. Using Eq. (A.20) the time component $\nu = 0$ yields,

$$\dot{\rho}_\phi + 3H(\rho_\phi + p_\phi) = -\beta \rho_c \dot{\phi}, \tag{4.5}$$

$$\dot{\rho}_c + 3H\rho_c = +\beta \rho_c \dot{\phi}, \tag{4.6}$$

where the dot denotes derivation with respect to cosmic time. The combination of Eq. (4.5) with (2.5) and (2.6) gives the Klein-Gordon equation according to which coupled quintessence evolves. The motion of the interacting scalar field thus satisfies,

$$\ddot{\phi} + 3H\dot{\phi} + V_{,\phi} = -\beta \rho_c. \tag{4.7}$$

The regular uncoupled equations are recovered in the limit of the coupling constant $\beta = 0$.

In accordance with the same procedure described in Ref. [29], we uncover, for the first time, the coupled quintessence potential corresponding to $\phi' = \lambda$. This model is called $\lambda\beta$CDM in the rest of the document. The main steps of the derivation are described below where a prime denotes differentiation with respect to the number of e-folds. Using that notation, the species considered evolve as,

$$\rho_b' + 3\rho_b = 0, \tag{4.8}$$

$$\rho_c' + 3\rho_c = \beta \rho_c \phi' \quad \Rightarrow \quad \rho_c' + 3\rho_c = \beta \rho_c \lambda, \tag{4.9}$$

$$\rho_\phi' + 3H^2\phi'^2 = -\beta \rho_c \phi' \quad \Rightarrow \quad \rho_\phi' + 3H^2\lambda^2 = -\beta \rho_c \lambda. \tag{4.10}$$

The direct integration of equations (4.8) and (4.9) gives respectively the solution for the baryon and dark matter energy densities,

$$\rho_b = \rho_{b_0}\, e^{-3N}, \tag{4.11}$$

$$\rho_c = \rho_{c_0}\, e^{(-3+\beta\lambda)N} = \rho_{c_0}\, e^{-3N+\beta(\phi-\phi_o)} = \rho_{c_0}\, e^{(-\frac{3}{\lambda}+\beta)(\phi-\phi_o)}. \tag{4.12}$$

The interaction within the dark sector alters the evolution of the cosmological background as the dilution of dark matter depends on the transfer of energy with quintessence. It deviates from the regular dilution $\rho_c \propto a^{-3}$ to become $\rho_c \propto a^{-3+\beta\lambda}$ as illustrated in Figure 4.1. Correspondingly, the expansion of the universe during the matter domination epoch is modified by the coupling. The scale factor law becomes $a \propto t^{2/(3-\beta\lambda)}$, neglecting baryonic matter, instead of $a \propto t^{2/3}$ in the standard case. These alterations are consistent with those found in [70].

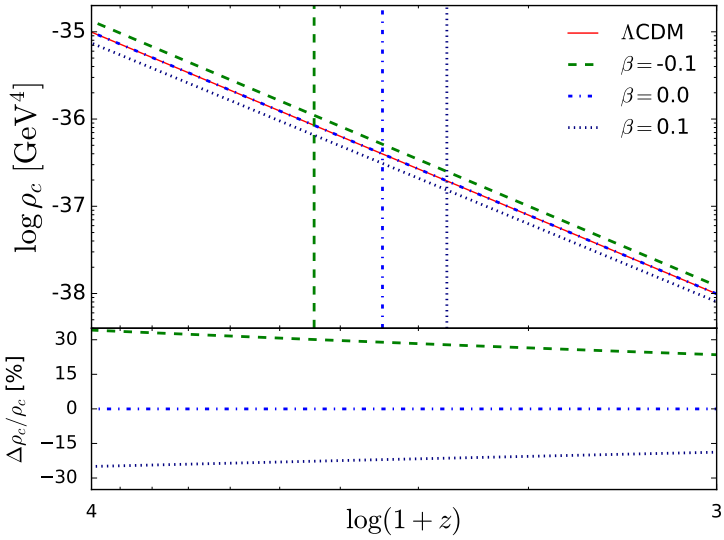

Figure 4.1: Dark matter dilution in $\lambda\beta$CDM between equality (identified by the vertical lines) and decoupling, when $\lambda = 0.3$, computed with our modified CLASS code on the basis of Planck 2018 cosmological parameters results [5]. The coupling strength β affects the dilution of dark matter. The effect is stronger when $\beta\lambda < 0$, i.e. when energy is being injected into quintessence.

The source term $Q = \beta\rho_c\lambda$ represents the stress-energy exchange among the interacting fluids. As $\rho_c \to 0$ the source term vanishes with time. Moreover, the direction of the energy exchange depends on the sign of Q, which means that it depends both upon the evolution of the dark energy scalar field imposed by the sign of λ and on the sign of the coupling β. There is therefore a symmetry with respect to the sign of the product $\beta\lambda$ which determines the direction of the energy flow. If the value of the scalar field increases with time ($\lambda = \phi' > 0$), then the coupling pumps energy from the scalar field component into the dark matter fluid when $\beta > 0$. Consequently, the energy being granted to dark matter slows its dilution. When $\beta < 0$, the energy lost by dark matter conversely accelerates its dilution. The opposite holds for a decreasing scalar field ($\lambda = \phi' < 0$).

As regards the quintessence energy density, Eq. (4.10) can be rewritten by substituting Eq. (4.11) and (4.12) into the Friedmann equation applied to a flat universe, $3H^2 = \rho_b + \rho_c + \rho_\phi$. Hence, the density of dark energy satisfies the following differential equation,

$$\rho'_\phi + \lambda^2\rho_\phi = \left(-\lambda^2 - \beta\lambda\right)\rho_{c_0}\, e^{(-3+\beta\lambda)N} - \lambda^2\rho_{b_0}\, e^{-3N}, \tag{4.13}$$

whose solution is,

$$\rho_\phi = e^{-\int_0^N \lambda^2\, dx}\left\{\rho_{\phi_0} - \int_0^N dx\left[\left(\lambda^2 + \beta\lambda\right)\rho_{c_0}\, e^{(-3+\beta\lambda)x} + \lambda^2\rho_{b_0}\, e^{-3x}\right] e^{\int_0^x \lambda^2 dy}\right\}, \tag{4.14}$$

which is equivalent to,

$$\rho_\phi = \left(\rho_{\phi_0} + \frac{\lambda^2+\beta\lambda}{-3+\beta\lambda+\lambda^2}\,\rho_{c_0} + \frac{\lambda^2}{-3+\lambda^2}\,\rho_{b_0}\right) e^{-\lambda^2 N} \\ - \frac{\lambda^2+\beta\lambda}{-3+\beta\lambda+\lambda^2}\,\rho_{c_0}\,e^{(-3+\beta\lambda)N} - \frac{\lambda^2}{-3+\lambda^2}\,\rho_{b_0}\,e^{-3N}. \tag{4.15}$$

According to Eq. (2.5), the scalar field potential can be found with,

$$V(\phi) = \rho_\phi - \frac{1}{2}\dot{\phi}^2 = \rho_\phi - \frac{1}{2}H^2\phi'^2 = \rho_\phi - \frac{1}{2}H^2\lambda^2, \tag{4.16}$$

where,

$$H^2 = \frac{1}{3}\left[\rho_\phi + \rho_{c_0}\,e^{(-3+\beta\lambda)N} + \rho_{b_0}\,e^{-3N}\right]. \tag{4.17}$$

Therefore,

$$V(\phi) = \left(1 - \frac{\lambda^2}{6}\right)\rho_\phi - \frac{\lambda^2}{6}\left[\rho_{c_0}\,e^{(-3+\beta\lambda)N} + \rho_{b_0}\,e^{-3N}\right]. \tag{4.18}$$

Substituting Eq. (4.15) into the above equation with $N = (\phi - \phi_0)/\lambda$, we obtain the following potential,

$$V(\phi) = Ae^{\left(-\frac{3}{\lambda}+\beta\right)\phi} + Be^{-\lambda\phi} + Ce^{-\frac{3}{\lambda}\phi}, \tag{4.19}$$

where the mass scales are given by,

$$A = \frac{1}{2}\frac{\lambda^2+2\beta\lambda}{3-\lambda^2-\beta\lambda}\rho_0\Omega_{c_0}\,e^{\left(\frac{3}{\lambda}-\beta\right)\phi_0}, \tag{4.20}$$

$$B = \frac{1}{6}(6-\lambda^2)\rho_0\left(\Omega_{\phi_0} + \frac{\lambda^2+\beta\lambda}{\lambda^2-3+\beta\lambda}\Omega_{c_0} + \frac{\lambda^2}{\lambda^2-3}\Omega_{b_0}\right)e^{\lambda\phi_0}, \tag{4.21}$$

$$C = \frac{1}{2}\frac{\lambda^2}{3-\lambda^2}\rho_0\Omega_{b_0}\,e^{\frac{3}{\lambda}\phi_0}. \tag{4.22}$$

It is worthwhile noting that the coupling essentially affects the quintessence potential when the latter is driven by the steeper exponential in the early times, when ϕ is subdominant. Once the shallower potential takes the lead, the coupling does not impact the potential any longer. Nor does it affect the quintessence equation of state w_ϕ in the long term. The equation of state satisfies,

$$\rho_\phi(1+w_\phi) = \rho_\phi + p_\phi = \dot{\phi}^2 = H^2\phi'^2 = H^2\lambda^2, \tag{4.23}$$

and therefore,

$$w_\phi = -1 + \frac{\lambda^2}{3}\left[1 + \frac{1}{\rho_\phi}\left(\rho_c^o\,e^{(-3+\beta\lambda)N} + \rho_b^o\,e^{-3N}\right)\right]. \tag{4.24}$$

In early times, during the matter era we have $w_\phi \to 0$, and for late times, as the scalar field dominates the evolution we obtain $w_\phi \to -1 + \frac{\lambda^2}{3}$. The dark energy equation of state tends to the same values as in the λCDM case. Moreover, today's equation of state remains unchanged despite the coupling existence, as shown in Figure 4.2,

$$w_0 = -1 + \frac{\lambda^2}{3\Omega_{\phi_0}}. \tag{4.25}$$

Dynamically, the cosmological behaviour of the model can be studied by adopting the very same approach described in pages 190-193 of Ref. [3], yet with a different cosmological scenario due to the fact that our scalar field potential includes the coupling strength β and differs from the single exponential postulated there. The baryonic term of the potential is neglected here for the sake of simplicity. This can be done to a good approximation given that baryons are subdominant. Nevertheless we include them in the numerical simulations, along with radiation. Firstly, at the early times, the potential is driven by the steeper exponential term $e^{(-\frac{3}{\lambda}+\beta)\phi}$ and quintessence provisionally scales with radiation,

$$w_\phi = w_{\text{eff}} = \frac{1}{3}, \qquad \Omega_\phi = 1 - \Omega_r = \frac{4}{\left(\frac{3}{\lambda} - \beta\right)^2}. \tag{4.26}$$

It is subsequently attracted to a stable scaling solution in the matter era during which Ω_ϕ and w_ϕ are also constant,

$$w_\phi = -\frac{\beta}{\lambda + \beta}, \qquad \Omega_\phi = \frac{\lambda}{3}\left(\beta + \lambda\right). \tag{4.27}$$

As the coupling strength $\beta > 0$ increases, the value of the equation of state w_ϕ tends to -1 for $\lambda > 0$ during matter domination. This is to be expected because the transfer of energy towards dark matter decreases the kinetic energy of the scalar field that can become negligible compared to its potential energy in the limit of very strong interaction. During that period, the effective equation of state of the whole cosmological fluid in the universe is,

$$w_{\text{eff}} = -\frac{\lambda\beta}{3}, \tag{4.28}$$

which is close to zero, approaching matter's, for small values of the parameters. Finally, once the shallower exponential term $e^{-\lambda\phi}$ takes the lead in driving the scalar field, dark energy density freezes and accelerates the Universe like for the λCDM case when $\lambda^2 < 2$, independently of the coupling. This feature comes as a novelty compared with [3]. In the latter, the non-existence of the extra exponential term in the potential prevents the late acceleration without the coupling for small λ.

The viability of our cosmological scenario is confirmed numerically in Figure 4.2 by using a version of CLASS where we modified the code of the background module to accommodate the $\lambda\beta$CDM potential

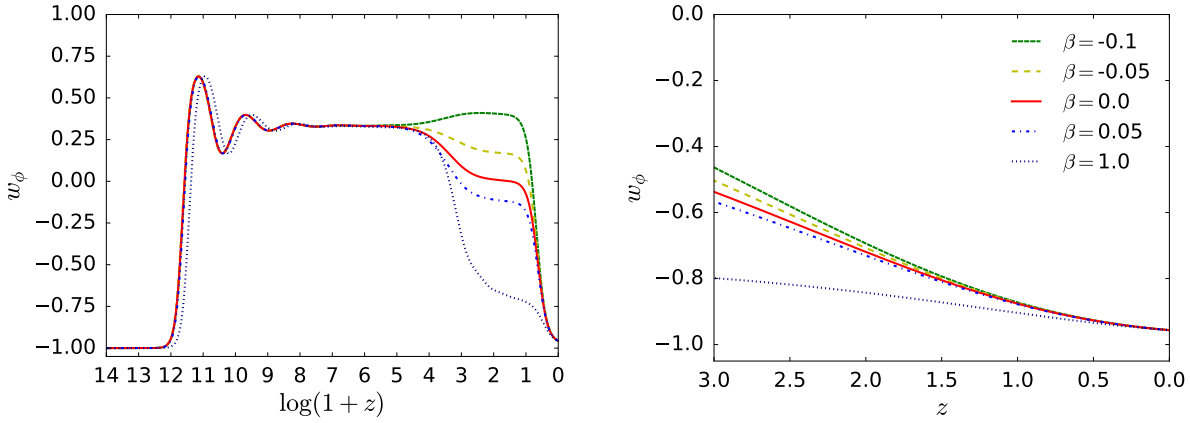

(a) Dark energy equation of state evolution

(b) Zoom in at lower redshift

Figure 4.2: Panel (a): Dark energy equation of state in $\lambda\beta$CDM for $\lambda = 0.3$, computed with our modified CLASS code on the basis of Planck 2018 cosmological parameters results [5]. The coupling turns on during matter domination and turns off when the scalar field starts slow-rolling. Panel (b): The extra degree of freedom β entails additional evolution possibilities at low redshift for a given parameter λ.

in Eq. (4.19), as well as the new dark matter dilution law (4.12) and scalar field equation of motion (4.7). In particular, it shows the consistency of the numerical results with the theoretical scalar field equation of state given in Eq. (4.27) that depends on the values of λ and β as the universe evolves.

Moreover, in order for the cosmological model to satisfy $-1 \leq w_\phi \leq +1$ and $0 \leq \Omega_\phi \leq 1$, the values of the parameters are constrained by the following bounds,

$$0 \leq \lambda \leq \sqrt{6} \quad \Rightarrow \quad -\frac{\lambda}{2} \leq \beta \leq \frac{3-\lambda^2}{\lambda}, \tag{4.29}$$

$$-\sqrt{6} \leq \lambda \leq 0 \quad \Rightarrow \quad \frac{3-\lambda^2}{\lambda} \leq \beta \leq -\frac{\lambda}{2}. \tag{4.30}$$

Using Eq. (4.26), these bounds can be combined with the ceiling $\Omega_\phi < 0.045$ imposed by BBN on the dark energy abundance during radiation domination. We expect that the constraint on λ from BBN in Eq. (2.48) is slightly relaxed for scenarios where dark matter grants energy to the scalar field.

In terms of background evolution, a major difference with the uncoupled λCDM model lies in the time of matter-radiation equality which is affected by the existence of the coupling. Instead of $a_{\rm eq} = \Omega_{r_0}/\Omega_{m_0}$, it now approximatively satisfies,

$$\Omega_{m_0} a_{\rm eq}^{-3+\beta\lambda} \simeq \Omega_{r_0} a_{\rm eq}^{-4} \quad \Longleftrightarrow \quad a_{\rm eq} \simeq \frac{\Omega_{r_0}}{\Omega_{m_0}} \left(\frac{\Omega_{m_0}}{\Omega_{r_0}}\right)^{\beta\lambda/(1+\beta\lambda)}, \tag{4.31}$$

neglecting the fact that baryons still dilute as a^{-3} in order to get an analytic form of the equality time. The exact equation would be $\Omega_{c_0} a_{\rm eq}^{1+\beta\lambda} + \Omega_{b_0} a_{\rm eq} = \Omega_{r_0}$, leading to $\sim 3\%$ deviation with the approximation in Eq. (4.31). The approximate relative change in the scale factor of matter-radiation equality is given by,

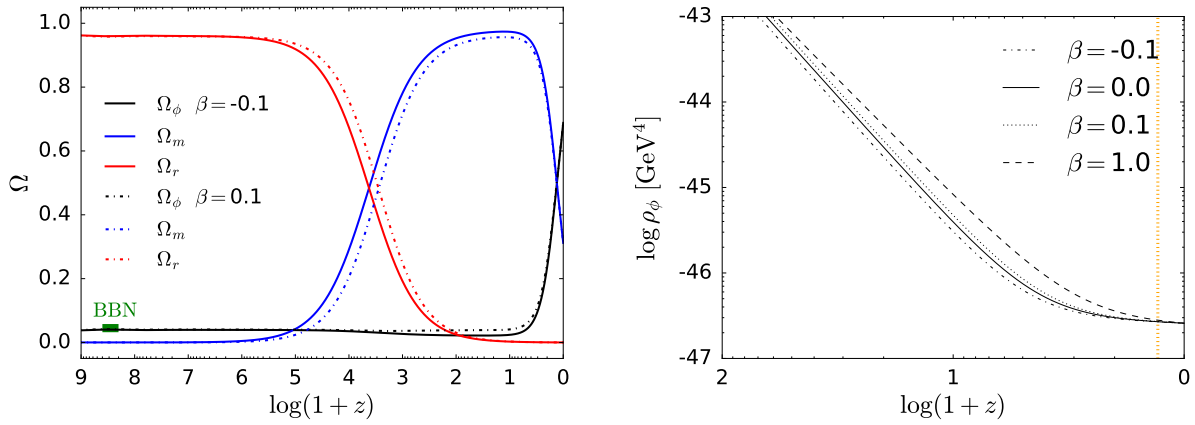

(a) Background evolution of the fractional energy densities

(b) Background evolution of the scalar field energy density

Figure 4.3: $\lambda = 0.3$. Panel (a): The coupling strength β influences the matter-radiation equality. Panel (b): The coupling regulates the dilution of quintessence: when energy is being pumped into dark matter ($\beta > 0$) the energy density of the scalar field increases during matter domination to converge to today's observed value, and vice versa. The vertical line in yellow represents matter-dark energy transition.

$$\frac{\Delta a}{a} = -1 + \left(\frac{\Omega_{m_0}}{\Omega_{r_0}}\right)^{\beta\lambda/(1+\beta\lambda)}. \tag{4.32}$$

As identified in Figure 4.1 and 4.3, when the product $\beta\lambda > 0$, the matter-radiation equality occurs later because of the modified dilution of dark matter in Eq. (4.12), and vice versa. Assuming that the models evolve towards the same fiducial cosmology, the density of dark matter was necessarily lower at early times with the coupling. Therefore, if $\beta\lambda = 0.01$ and $\beta\lambda = 0.03$ for instance, the radiation domination lasts longer by about 8% and 27% respectively. We are to see in section 4.3 that this difference alters the Hubble radius at equality and thus has an impact on both the location of the turn around scale in the matter power spectrum and the peak structure of the CMB temperature anisotropies.

By affecting the Hubble expansion rate, the coupling changes the expansion history of the universe background, and hence should leave observational marks. In the $\lambda\beta$CDM model, we find that the theoretical luminosity distance reads,

$$\begin{aligned} d_L(z) &= \frac{1+z}{H_0}\int_0^z \frac{dz}{E(z)}, \\ E^2(z) &= \frac{3}{3-\lambda^2}\Omega_{b_0}(1+z)^3 + \frac{3}{3-\lambda^2-\beta\lambda}\Omega_{c_0}(1+z)^{3-\beta\lambda} \\ &\quad + \left(\Omega_{\phi_0} + \frac{\lambda^2+\beta\lambda}{\lambda^2-3+\beta\lambda}\Omega_{c_0} + \frac{\lambda^2}{\lambda^2-3}\Omega_{b_0}\right)(1+z)^{\lambda^2}. \end{aligned} \tag{4.33}$$

It reduces to Eq. (3.3) when $\beta = 0$. We use our modified version of CLASS to simulate the predicted redshift - luminosity distance relation. The plot in Figure 4.4 shows that the sensitivity to the coupling strength β at low redshift is negligible. Let us confirm in the next section whether the coupling brings noticeable effects on the formation of structures, and at high redshift on the CMB power spectrum.

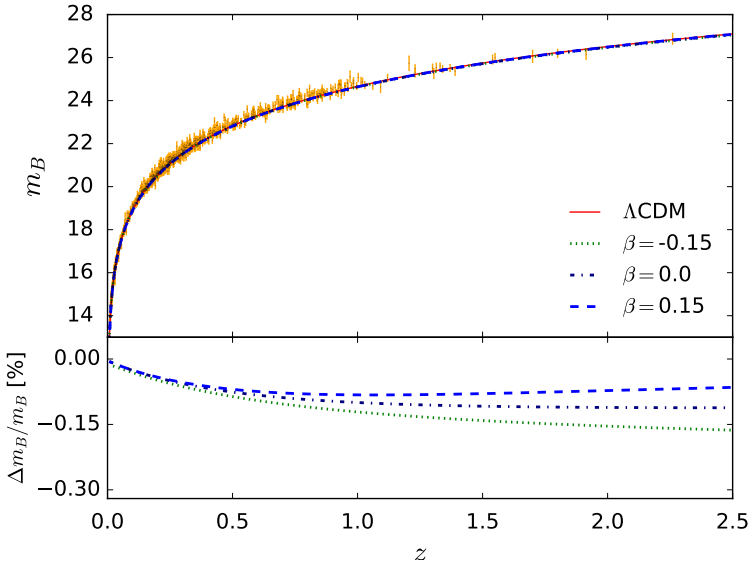

Figure 4.4: top panel: Redshift - luminosity distance relation predicted by the $\lambda\beta$CDM model for $\lambda = 0.3$. The observed Pantheon sample data points are in orange. Bottom panel: Relative deviation from ΛCDM. The effective coupling β produces insignificant deviation at low redshift.

4.2 Evolution of cosmological perturbations

The coupling within the dark sector affects the evolution of cosmological perturbations. Stress-energy transfers allowed by the interaction between components of the cosmological fluid add extra source terms in the equations of motion as in Ref. [71]. They are obtained following the same method as in Subsection 2.4.1 but with the joint conservation Eq. (4.4). For a constant coupling strength β, the continuity equation (2.93) in conformal time is changed into,

$$\dot{\delta\rho_c} + 3\mathcal{H}\delta\rho_c + \bar{\rho}_c\theta_c + \frac{1}{2}\dot{h}\bar{\rho}_c = \beta\left(\bar{\rho}_c\dot{\varphi} + \delta\rho_c\dot{\phi}\right), \tag{4.34}$$

with $\dot{\delta\rho_c} = (-3\mathcal{H}\bar{\rho}_c + \beta\bar{\rho}_c\dot{\phi})\delta_c + \bar{\rho}_c\dot{\delta}_c$ according to Eq. (4.6). Therefore, the equation of motion for the density contrast of coupled dark matter reads,

$$\boxed{\dot{\delta}_c + \theta_c + \frac{\dot{h}}{2} = \beta\dot{\varphi}.} \tag{4.35}$$

Similarly, the Euler equation of dark matter (2.97) is to be adapted. In Fourier space and β constant, Eq. (2.95) becomes,

$$\bar{\rho}_c\dot{v}_i + \dot{\bar{\rho}}_c v_i + 4\mathcal{H}\bar{\rho}_c v_i = -\beta\left(\delta\rho_c\nabla_i\bar{\phi} + \bar{\rho}_c\nabla_i\varphi\right), \tag{4.36}$$

where $\nabla_i\bar{\phi} = 0$ since the scalar field is considered spatially homogeneous. Taking the divergence and using Eq. (4.6), we obtain,

$$\dot{\theta}_c + \mathcal{H}\theta_c = \beta\left(k^2\varphi - \dot{\phi}\theta_c\right), \tag{4.37}$$

and then,

$$\boxed{\dot{\theta}_c + \mathcal{H}\theta_c = \beta\dot{\phi}\left(\theta_\phi - \theta_c\right).} \tag{4.38}$$

We also impose the same condition $\theta_c(k, \tau_{ini}) = 0$ we applied in Eq. (2.97) to define the initial timelike hypersurface of the synchronous gauge. Contrary to the λCDM model, this condition is now insufficient to fix the gauge completely because the coupling makes cold dark matter velocity divergence θ_c evolve with time in compliance with Eq. (4.38). Therefore, we modified the code of the CLASS perturbations modules to implement the two equations (4.35) and (4.38) with varying θ_c, and evolve the perturbation equations in a synchronous gauge that still possesses one remaining degree of freedom. The coupling, that can be interpreted as a force, has the effect of changing the dark matter geodesics. Since the gauge is not comoving with dark matter any longer, it is necessary to further transform δ_c into the gauge-invariant quantity δ_c^C [36] that enters the matter density contrast Eq. (3.10) that CLASS uses to predict the power spectra observables that are physically independent from the choice of the synchronous gauge. By considering the coordinate transformation $x^\mu \to \tilde{x}^\mu \equiv x^\mu + \xi^\mu$, the gauge transformation of a scalar perturbation s is given by $\delta\tilde{s} = \delta s - \dot{s}\,\xi^0$, and applying it to the density contrast, the comoving slicing is obtained by,

$$\delta_c^C = \delta_c - \frac{\dot{\bar{\rho}}_c}{\bar{\rho}_c}\,\xi^0. \tag{4.39}$$

With $\xi^0 = v + B$ and Eq. (4.9), we get,

$$\delta_c^C = \delta_c + \mathcal{H}\left(3 - \beta\phi'\right)\frac{\theta_c}{k^2}, \tag{4.40}$$

the latter being valid in Fourier space with the similar convention adopted in Ref. [38][1], and $B = 0$ in the synchronous gauge. Only the largest scales are impacted since the two density contrasts coincide when $k \to \infty$. It is worth noting the difference with Ref. [72] which instead uses $\delta_c^C = \delta_c + 3\mathcal{H}\theta_c/k^2$ as gauge-invariant variable, since in their specific case the dark matter continuity equation remains unchanged by the coupling. In practice, we modify the existing gauge transformation performed by the public version of CLASS [73],

$$\delta_m^C = \frac{\delta\rho_m}{\bar{\rho}_m} + 3\frac{\mathcal{H}}{k^2}\theta_m, \tag{4.41}$$

into the following gauge-invariant matter density contrast,

[1] The scalar part in the decomposition of the velocity vector is defined by $v_j = -v_{,j}$ which becomes $-i\frac{k_j}{k}v$ by convention in Fourier space. We also recall that $\theta = ik^j v_j = kv$

$$\boxed{\delta_m^C = \frac{\delta\rho_m}{\bar{\rho}_m} + \left(3 - \frac{\beta\phi'\rho_c}{\rho_c + \rho_b}\right)\frac{\mathcal{H}}{k^2}\theta_m,} \tag{4.42}$$

to account for baryonic matter. Furthermore, when it comes to numerically plot the time evolution of δ_c, the quantities are provided in the Newtonian gauge δ_c^N by CLASS. We have therefore to change the gauge transformation ensured by the code [37] to adapt it to the existence of the coupling, taking account of the modified form of the continuity equation (4.6),

$$\delta_c^N = \delta_c + \alpha\frac{\dot{\bar{\rho}}_c}{\bar{\rho}_c}, \tag{4.43}$$

with

$$\alpha = \frac{\dot{h} + 6\dot{\eta}}{2k^2}. \tag{4.44}$$

We hence obtain the following gauge transformation,

$$\boxed{\delta_c^N = \delta_c + \alpha\mathcal{H}\left(-3 + \beta\phi'\right).} \tag{4.45}$$

Given that the existing version of the code uses the constraint equation (2.102) which is no longer valid, we further modify it to integrate the metric perturbation h from the adiabatic initial conditions that can be found in Ref. [37],

$$h = \frac{1}{2}(k\tau)^2. \tag{4.46}$$

We limit that initial condition to the leading order because the next one, being $\mathcal{O}(k^4\tau^4)$, is discarded since the series are truncated to the $\mathcal{O}(k^3\tau^3)$ order. The adiabatic initial condition of dark matter also differs from λCDM. Using the coupled dark matter continuity equation (4.6) with the regular photons energy conservation (A.21), we obtain that initially,

$$\frac{\delta_c\bar{\rho}_c}{\dot{\bar{\rho}}_c} = \frac{\delta_\gamma\bar{\rho}_\gamma}{\dot{\bar{\rho}}_\gamma} \quad \Leftrightarrow \quad \boxed{\delta_c = \frac{3}{4}\left(1 - \frac{\beta\phi'}{3}\right)\delta_\gamma.} \tag{4.47}$$

As for quintessence, we keep the same previous rationale as in the uncoupled case to set vanishing initial perturbations. The linear perturbation equation is obtained with Eq. (2.98) taking account of the joint conservation (4.7),

$$-\left[\dot{\delta\rho}_\phi + 3\mathcal{H}\left(\delta\rho_\phi + \delta p_\phi\right) + \left(\rho_\phi + p_\phi\right)\left(\theta_\phi + \frac{\dot{h}}{2}\right)\right] = \beta\left(\rho_c\dot{\varphi} + \delta\rho_c\dot{\phi}\right). \tag{4.48}$$

By substituting the coupled Klein-Gordon equation (4.7) and re-using Eq. (2.99), we find the following equation of motion for the coupled quintessence fluctuations, as in Ref. [70],

$$\boxed{\ddot{\varphi} + 2\mathcal{H}\dot{\varphi} + \left(k^2 + a^2 V_{\prime\phi\phi}\right)\varphi + \frac{\dot{h}\dot{\phi}}{2} = -\beta a^2 \rho_c \delta_c.} \tag{4.49}$$

We modify the code of the CLASS perturbations module to implement this equation.

The numerical results that we obtain with our modified version of CLASS are plotted in Figure 4.5. They are consistent with the adapted Eq. (2.114) that we are going to analytically derive below in the Newtonian limit for our specific $\lambda\beta$CDM model, as in Ref. [41, 74]. We first differentiate Eq. (4.35) and insert the two equations (4.38) and (2.88),

$$\ddot{\delta}_c - \mathcal{H}\beta\dot{\varphi} + \mathcal{H}\dot{\delta}_c - \frac{3}{2}\mathcal{H}^2\Omega_c\delta_c - 2\dot{\phi}\dot{\varphi} + a^2 V_{,\phi}\varphi = \beta\ddot{\varphi} - \beta k^2\varphi. \tag{4.50}$$

In Ref. [41], it was demonstrated that the existence of the coupling only makes a difference for the sub-horizon during the matter dominated era. For those scales within the horizon we can consider that $k \to \infty$. In our approximation, we also neglect the higher order terms, i.e. the derivatives of φ and the potential term. Therefore, Eq. (4.49) reduces to,

$$k^2\varphi + \frac{\dot{h}\dot{\phi}}{2} = -3\beta\mathcal{H}^2\Omega_c\delta_c. \tag{4.51}$$

Being of higher order, we can also neglect the velocity divergence terms in Eq. (4.35) to approximate $\dot{h}/2 = -\dot{\delta}_c$. It follows that,

$$k^2\varphi = -3\beta\mathcal{H}^2\Omega_c\delta_c + \dot{\delta}_c\dot{\phi}, \tag{4.52}$$

which we insert into Eq. (4.50). Similarly neglecting the higher orders, we find the equation of motion of the coupled dark matter,

$$\ddot{\delta}_c + \left(\mathcal{H} + \beta\dot{\phi}\right)\dot{\delta}_c - \frac{3}{2}\mathcal{H}^2\Omega_c\left(1 + 2\beta^2\right)\delta_c = 0. \tag{4.53}$$

Let us now consider our parametrisation where $\phi' = \lambda$. We rewrite the last equation with the number of e-folds instead of conformal time to ease the comparison with Eq. (2.114) of the uncoupled model,

$$\delta_c'' + \left(1 + \frac{\mathcal{H}'}{\mathcal{H}} + \beta\lambda\right)\delta_c' - \frac{3}{2}\left(1 - \frac{\lambda^2/3}{w_\phi + 1}\right)\left(1 + 2\beta^2\right)\delta_c = 0, \tag{4.54}$$

where the analytic expression of w_ϕ, parametrised with λ and β, is given in Eq. (4.24). We obtain the following equation of motion for the dark matter fluctuation, valid on small scales during matter and dark energy dominated eras,

$$\delta_c'' + \left(\frac{1}{2} - \frac{\lambda^2}{2}\frac{w_\phi}{w_\phi + 1} + \beta\lambda\right)\delta_c' - \frac{3}{2}\left(1 - \frac{\lambda^2/3}{w_\phi + 1}\right)\left(1 + 2\beta^2\right)\delta_c = 0. \tag{4.55}$$

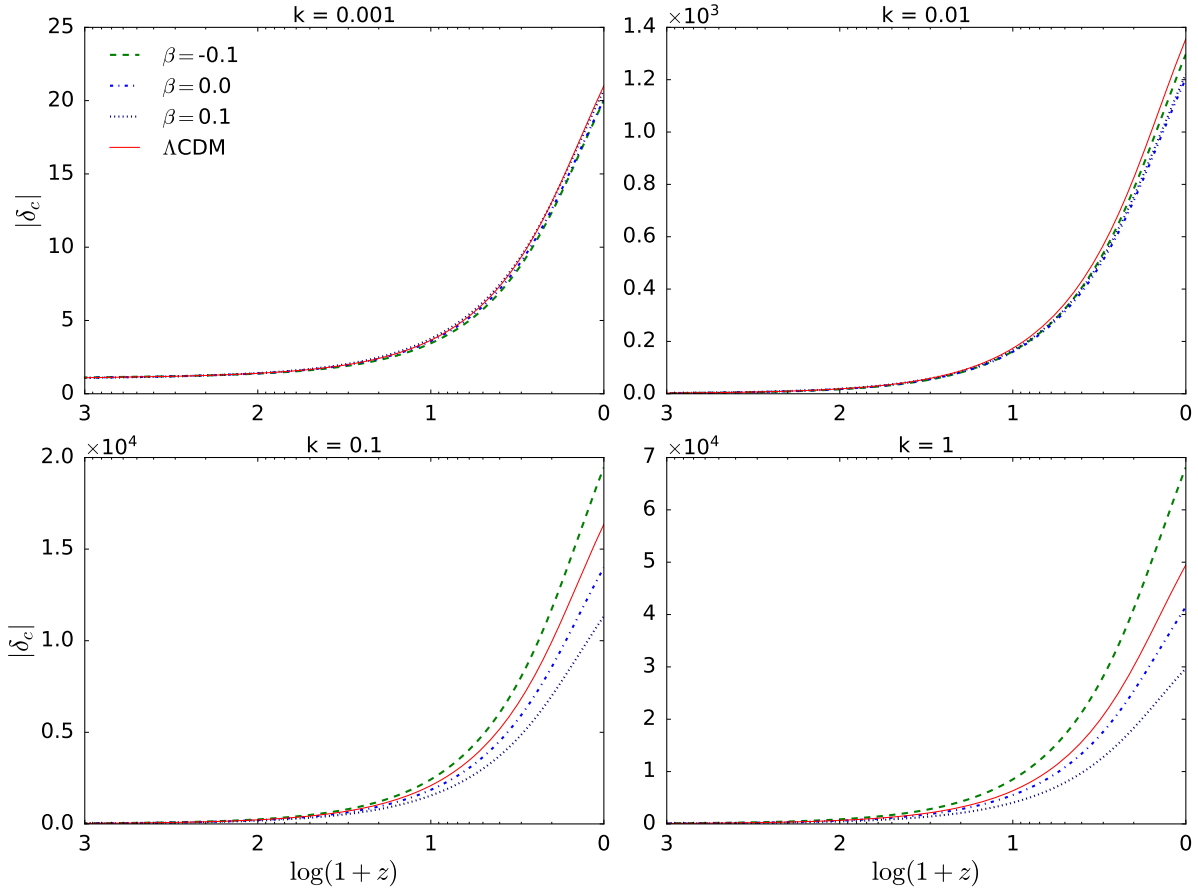

Figure 4.5: Evolution of dark matter fluctuations in $\lambda\beta$CDM for $\lambda = 0.3$ and various scales k in units of h Mpc^{-1}, computed with our modified CLASS code on the basis of Planck 2018 cosmological parameters results [5]. The initial conditions are adiabatic with $\mathcal{R} = 1$ normalization. Smaller scales are affected by faster or slower growth depending on the sign of the effective coupling β.

We find, like in Ref. [28], that the coupling brings three competing effects to the evolution of the linear perturbations. Firstly, the value of the equation of state w_ϕ is not zero during the scaling regime in the matter era, $w_\phi = -\beta/(\lambda+\beta)$ according to Eq. (4.27). Thus at that epoch, the dynamical term is changed into,

$$\Omega_c = 1 - \frac{\lambda^2}{3} - \frac{\lambda\beta}{3}. \tag{4.56}$$

Secondly, the coupling systematically enhances the gravity pull by adding an extra source to the potential acting on dark matter. Re-establishing the Newton constant, the source term becomes,

$$\nabla^2\Phi = -k^2\Phi = 4\pi G\left(1 + 2\beta^2\right) a^2 \bar{\rho}_c \delta_c, \tag{4.57}$$

as if we had a different effective potential along with a specific effective gravitational constant between dark matter particles: $G_{\text{eff}} \equiv G\left(1 + 2\beta^2\right)$. It encompasses standard gravity supplemented by a long-range force which is generated by the coupling and mediated by the scalar field. This effect always

contributes to the growth of perturbations during matter domination and hence counterbalances the presence of early dark energy. Whichever is the direction of the energy transfer, the coupling consistently plays the role of a gravitational source as if dark matter particles were subject to an additional force. It is to be noted though that since $w_\phi \to -1 + \lambda^2/3$ during the acceleration period, the source term vanishes anyway, independently of the coupling existence.

Thirdly, the friction term is affected by the dark sector interaction which increases or decreases the Hubble drag depending on the direction of the energy transfer determined by the sign of $\beta\lambda$. Similarly to the gravitational potential, we can identify an effective Hubble rate as $\mathcal{H}_{\rm eff} \equiv \mathcal{H}\,(1+\beta\lambda)$ that influences the clustering of matter particles.

As illustrated by our numerical results in Figure 4.5, when energy flows from dark matter to dark energy ($\beta\lambda < 0$), the growth of matter fluctuations is enhanced. All three individual effects contribute to it: the source term is increased by the higher density of dark matter whereas the Hubble drag term decreases, easing the clustering of matter which is further facilitated by the extra long range gravitational force induced by the coupling. On the other flow direction when quintessence is loosing energy, the lower dark matter density at early times combined with the increased expansion rate fight fluctuations growth against the coupling force. The winner depends on the value of the pair (β, λ) as we are to confirm below.

It is possible to derive a general power-law solution to Eq. (4.55) of the form $\delta_c \propto e^{mN}$ in the deep matter era, when $w_\phi = -\beta/(\lambda+\beta)$ according to Eq. (4.27). During that epoch, Eq. (4.55) reduces to,

$$\delta_c'' + \frac{1}{2}\left(1+3\lambda\beta\right)\delta_c' - -\frac{3}{2}\left(1-\frac{\lambda^2}{3}-\frac{\lambda\beta}{3}\right)\left(1+2\beta^2\right)\delta_c = 0, \tag{4.58}$$

and m satisfies,

$$m^2 + \frac{1}{2}\left(1+3\lambda\beta\right)m - \frac{3}{2}\left(1-\frac{\lambda^2}{3}-\frac{\lambda\beta}{3}\right)\left(1+2\beta^2\right) = 0, \tag{4.59}$$

whose positive solution is,

$$m_+ = \frac{1}{4}\left[-1-3\lambda\beta + \sqrt{24\left(1-\frac{\lambda^2}{3}-\frac{\lambda\beta}{3}\right)(1+2\beta^2) + (1+3\lambda\beta)^2}\right]. \tag{4.60}$$

This approximated analytic expression of the growth rate, which is valid on small scales in the deep matter domination era, is consistent with Ref. [41]. We compare it with the numerical results obtained with our modified CLASS code in Figure 4.6. They match very well in the matter dominated era.

In figure 4.7, we notice that growth is suppressed ($m_+ < 1$) or enhanced ($m_+ > 1$) relatively to the ΛCDM model ($m_+ = 1$) depending on the strength and sign of the coupling. Whereas early dark energy systematically reduces the growth for all values of λ, a given value of the coupling strength β either reduces or enhances the growth with respect to the uncoupled model. There is an exception for small

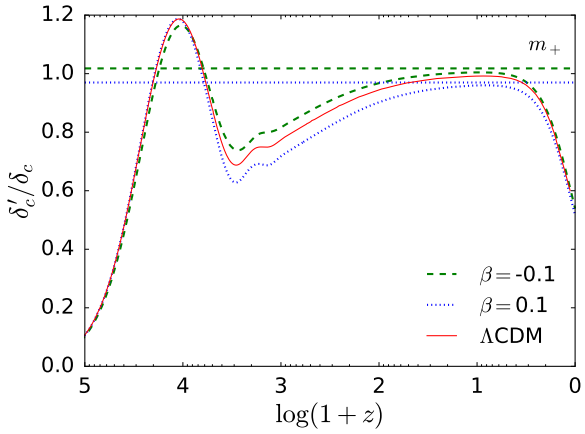

Figure 4.6: The growth rate funtion $f = \delta_c'/\delta_c$ of the dark matter fluctuations is numerically computed with our modified CLASS code on the basis of Planck 2018 cosmological parameters results [5] for the instance $\lambda = 0.3$. The scale considered is $k = 0.1$ h/Mpc. In the deep matter era, the growth parameter $f \sim m_+$ is in line with the analytic and approximated expression of the growth rate derived in Eq. (4.60).

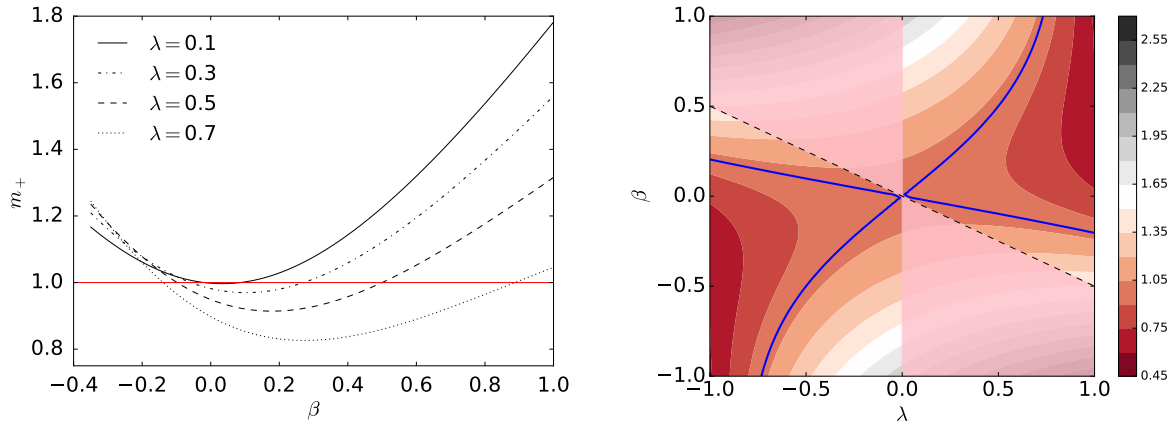

(a) Effect of the coupling on the growth of perturbations

(b) Exponent m_+ contour plot

Figure 4.7: Panel (a): The value of the coupling β determines whether the growth is suppressed or enhanced relatively to ΛCDM. The plot is based on the analytic expression of m_+ in Eq. (4.60). Panel (b): The blue lines represent $m_+ = 1$. The dashed black line represents the $-\lambda/2$ boundary imposed to β in Eq. (4.29) and (4.30). The values of β are not allowed in the pink shaded region.

values of λ, for which the coupling consistently enhances dark matter fluctuation. During the subsequent period when quintessence dominates, we have $w_\phi \to -1 + \lambda^2/3$ and we can write,

$$\delta_c'' + \left(2 - \frac{\lambda^2}{2} + \beta\lambda\right)\delta_c' = 0, \tag{4.61}$$

whose solution is similar to Eq. (2.120), but changed by the existence of the coupling,

$$\delta_c(k, N) = A(k) + B(k)\, e^{\left(\frac{\lambda^2}{2} - 2 - \beta\lambda\right)N}. \tag{4.62}$$

In the next subsection we will be outlining the corresponding effects on the power spectra, besides those relative to the position of the characteristic scales.

4.3 Numerical results for matter and CMB anisotropies power spectra

According to Section 4.1, the interaction between the scalar field and dark matter alters the time of matter-radiation equality compared to the standard and uncoupled models. This difference modifies the Hubble radius at equality and thus influences the turn around scale in the matter power spectrum. Using Eq. (3.12), we obtain that it is now approximatively given by,

$$k_{\rm eq} = \sqrt{2} H_0 \frac{\Omega_{m_0}}{\sqrt{\Omega_{r_0}}} \left(\frac{\Omega_{r_0}}{\Omega_{m_0}} \right)^{\beta\lambda/(1+\beta\lambda)} , \tag{4.63}$$

again neglecting baryons. Assuming the concordance model [5], the turn around scale moves to the larger k (smaller scales) when $\beta\lambda < 0$. As the horizon is smaller at equality, only those perturbations on the smaller scales have time to enter it and grow during radiation domination. Additionally, the coupling further fosters the fluctuation growth during the subsequent matter-dominated era (Cf. the predictions in Figure 4.5). As a result, power increases on small scales because growth is enhanced, as depicted in Figure 4.8. We thus expect higher predicted σ_8 as exemplified in table 4.1. On very large scales though, dark energy suppresses power. The converse situation holds when $\lambda\beta > 0$ which provides for a larger horizon at equality.

Table 4.1: Predicted σ_8 values at $z = 0$ computed with our modified CLASS code on the basis of Planck 2018 cosmological parameters results [5], normalizing the amplitude of the primordial power spectrum at large scale to $A_s = 2.215 \times 10^{-9}$. The results are obtained with $\lambda = 0.3$.

β	σ_8
-0.10	1.016
-0.05	0.840
0.00	0.722
$+0.05$	0.643
$+0.10$	0.592
ΛCDM	0.848

As regards the baryon oscillations, their predicted imprint should become more visible with increasing coupling strength that lowers the fractional energy density of dark matter at the time of the primordial plasma. Consequently, the oscillations are fostered by the increased share of baryons.

The peaks location of the CMB angular power spectrum are, also, shifted by the existence of the interaction. This is due, firstly, to the modified scale factor expansion law that changes the sound horizon at decoupling Eq. (3.19). Secondly through the Hubble parameter, since the interaction alters the comoving angular distance to the last scattering surface, as it has a dependence on the cosmic expansion from decoupling to the present time. The combination of these give rise to diverse effects regarding the peak structure, allowing to observationally constrain the value of the two parameters λ and β.

Moreover, the amplitude on the small scales of the CMB temperature power spectrum increases (decreases) with stronger positive (negative) coupling strength, as long as $\lambda > 0$. Symmetric effects

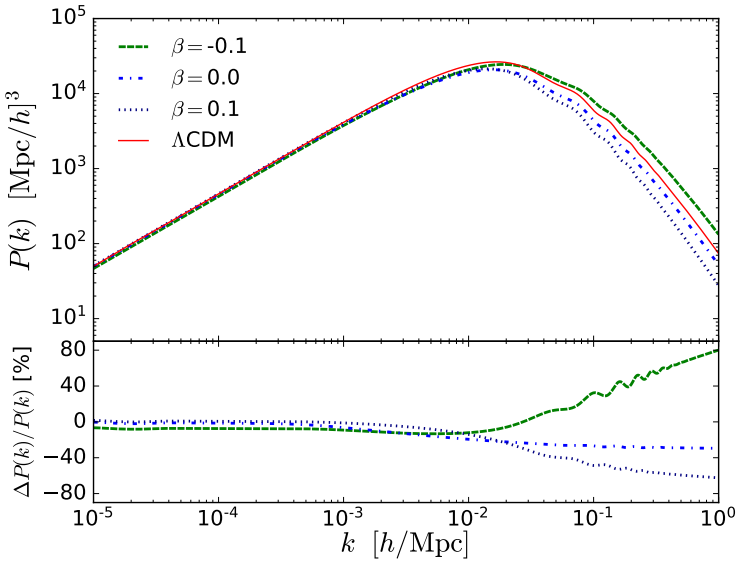

Figure 4.8: Predicted linear matter power spectrum at redshift $z = 0$ in the $\lambda\beta$CDM model for $\lambda = 0.3$, computed with our modified CLASS code on the basis of Planck 2018 cosmological parameters results [5].

hold for $\lambda < 0$. When $\beta > 0$, the reduced amount of dark matter at the time of the primordial plasma allows radiation to produce a stronger contribution to the Sachs-Wolfe plateau, through the gravitational potential decay according to 3.1.3. It further rises the first and subsequent peaks. On the contrary with $\beta < 0$, the enhanced dark matter physical density inhibits radiation effects, lowering the amplitude of every peak, as in Figure 4.9.

Besides, we notice too that the ratio of the angular power spectrum amplitude between the second and third acoustic peak is sensitive to the coupling. The height of the second peak can become smaller than the third when the interaction pumps energy away from dark matter ($\beta < 0$). As dark matter increasingly dominates matter density in the primordial plasma, the baryons are falling into deeper potentials, further amplifying the odd peaks which reproduce the maximum compression of the baryon-photon oscillations.

Finally, on very large scales, the plateau tilt is impacted by the interaction. Positive coupling strength suppresses CMB temperature anisotropies on those scales because the late-time ISW effect is weaker as quintessence has been loosing energy. It is the other way around when quintessence acquires energy from dark matter ($\beta < 0$).

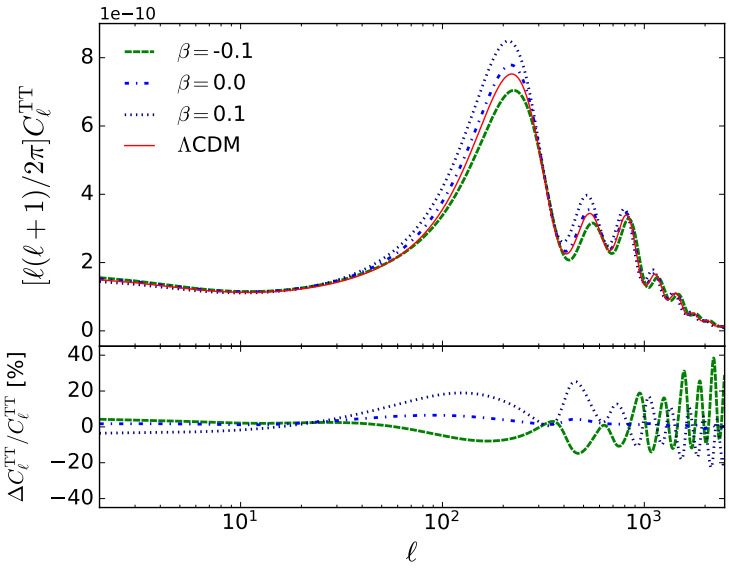

Figure 4.9: Predicted CMB dimensionless angular power spectrum in the $\lambda\beta$CDM model with $\lambda = 0.3$, computed with our modified CLASS code on the basis of Planck 2018 cosmological parameters results [5].

4.4 Observational constraints on $\lambda\beta$CDM

Since we have concluded from Figure 4.4 that the coupling between quintessence and dark matter does not affect much the homogeneous cosmic evolution at low redshift, it is seemingly irrelevant to try to constrain the model with low redshift datasets at background level. We have already drawn a similar conclusion regarding the λCDM model by testing it with the Pantheon and BOSS datasets in Section 3.4. We thus decide to skip the SNIa and BAO observations in the present MCMC fit.

4.4.1 Planck constraints

We seek to constrain the parameters at perturbation level given the larger influence the coupling brings on the predicted power spectra. Regarding the Planck mission CMB measurements, we restrict the statistical analysis to the lite version of the cross-correlation temperature anisotropies TT because of computational limitations due to the additional degree of freedom β. For the very same reason, we limit the number of free cosmological parameters to $\{\lambda, \beta, \Omega_c, h, A_s\}$ on top of the nuisance parameter. We fix the others to their fiducial values. Taking advantage of the symmetry with regards to the product $\lambda\beta$ identified in Section 4.1, we decide to only sample the positive side of the λ posterior space to spare computational time. This approach is also appropriate when using the Metropolis-Hasting algorithm because it gives better results with single peaked probabilities. Moreover, in Ref. [75] it is claimed that an interesting constraint on β is found by tackling the tension on the Hubble constant between local and Planck measurements. Accordingly, we also present in Table 4.2 the statistical analysis by combining

the Planck dataset with the Hubble Space Telescope (HST) Gaussian prior on the Hubble constant. That combination mainly increases the upper limit found on the coupling.

Table 4.2: Constraints on $\lambda\beta$CDM with Planck and Planck+HST.

	Planck			Planck+HST		
Parameter	mean$\pm\sigma$	95% lower	95% upper	mean$\pm\sigma$	95% lower	95% upper
λ	$0.040^{+0.012}_{-0.040}$	0.000	0.113	$0.0332^{+0.0076}_{-0.0330}$	0.0000	0.1052
β	$0.018^{+0.011}_{-0.045}$	-0.037	0.108	$0.031^{+0.016}_{-0.058}$	-0.033	0.135
Ω_m	$0.3091^{+0.0035}_{-0.0036}$	0.3021	0.3162	$0.3072^{+0.0034}_{-0.0035}$	0.3003	0.3143
H_0	$67.8^{+0.3}_{-0.3}$	67.2	68.4	$68.0^{+0.3}_{-0.3}$	67.4	68.6
σ_8	$0.8610^{+0.0073}_{-0.0200}$	0.8244	0.9103	$0.8673^{+0.0063}_{-0.0260}$	0.8254	0.9394
S_8	$0.874^{+0.011}_{-0.020}$	0.835	0.920	$0.8776^{+0.0089}_{-0.0260}$	0.8361	0.9480
$-\ln\mathcal{L}$	113.76			118.388		
$\chi^2_{\rm red}$	0.964			1.004		

We note that the incorporation of the additional degree of freedom does not alter the fact that a vanishing value of the posterior λ, corresponding to the cosmological constant, is preferred by the CMB temperature anisotropies measurement. The upper bound is also rather in line with the λCDM model. As regards the coupling strength, the observations of Planck and HST give the following weak constraints at 1σ CL,

$$\beta = 0.018^{+0.011}_{-0.045} \qquad (\text{Planck}), \tag{4.64}$$

$$\beta = 0.031^{+0.016}_{-0.058} \qquad (\text{Planck} + \text{HST}), \tag{4.65}$$

meaning that we cannot exclude a vanishing coupling. Figure 4.10 compares our two models and shows that the existence of the coupling makes σ_8 increase. However, it is necessary to continue running Markov chains to improve the convergence towards the targetted probability distribution of the two posteriors λ and β.

4.4.2 KiDS constraints

Similarly to our approach in Section 3.4, we endeavour to constrain the $\lambda\beta$CDM model with weak lensing observations. The results, reported in Table 4.3, indicate a preference for non-vanishing values of our two parameters, with the following likelihood peak at 1σ CL,

$$\lambda = 0.70^{+0.28}_{-0.15}, \qquad \beta = -0.080^{+0.041}_{-0.057}. \tag{4.66}$$

The inferred λ value is compatible with the more relaxed ceiling imposed on early dark energy at BBN discussed in Section 2.3. The favoured negative value of the coupling β represents a transfer of energy

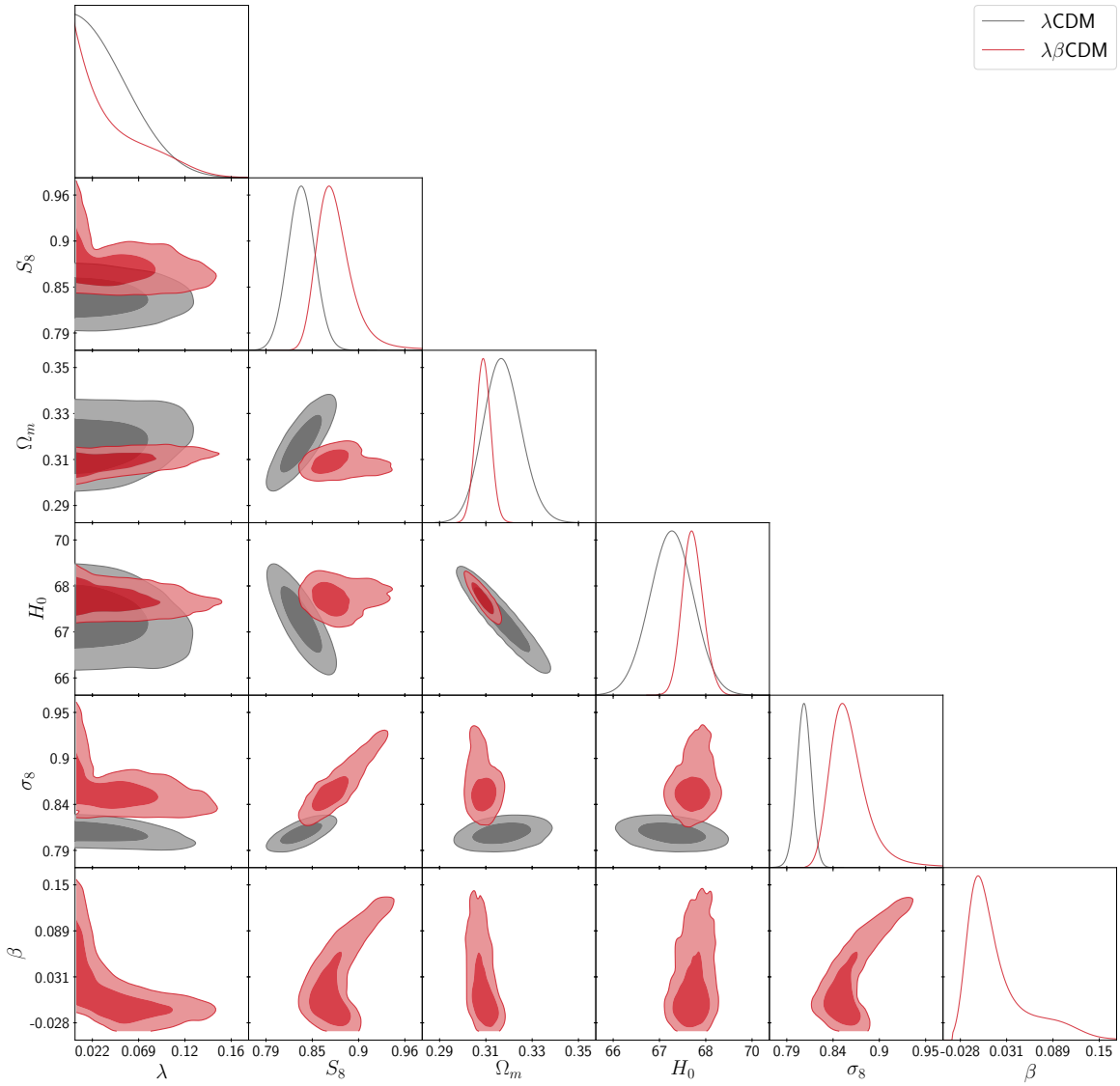

Figure 4.10: Constraints obtained with Planck. Probability distribution for marginalized parameter (plots at the top of the triangle) and contour plots showing the marginalized 2-dimensional constraints. Contours include 68% and 95% of the probability. The cut-off value of β that we have identified in Eq. (4.29) is clearly visible on the corresponding plots.

from the dark matter fluid to the quintessence component. Today's amplitude of the matter power spectrum increases compared to the uncoupled scenario whereas the S_8 combination is just slightly affected by the coupling as the abundance of matter Ω_m decreases (see Figure 4.11).

Table 4.3: Constraints on $\lambda\beta$CDM with KiDS.

Parameter	best-fit	mean$\pm\sigma$	95% lower	95% upper
λ	0.97	$0.70^{+0.28}_{-0.15}$	0.28	1.08
β	-0.088	$-0.080^{+0.041}_{-0.057}$	-0.175	0.028
Ω_m	0.328	$0.462^{+0.088}_{-0.180}$	0.185	0.807
σ_8	0.80	$0.63^{+0.14}_{-0.13}$	0.36	0.88
S_8	0.8389	$0.749^{+0.067}_{-0.060}$	0.621	0.878

$-\ln\mathcal{L} = 163.21, \quad \chi^2 = 326.4, \quad \chi^2_{red} = 2.654$

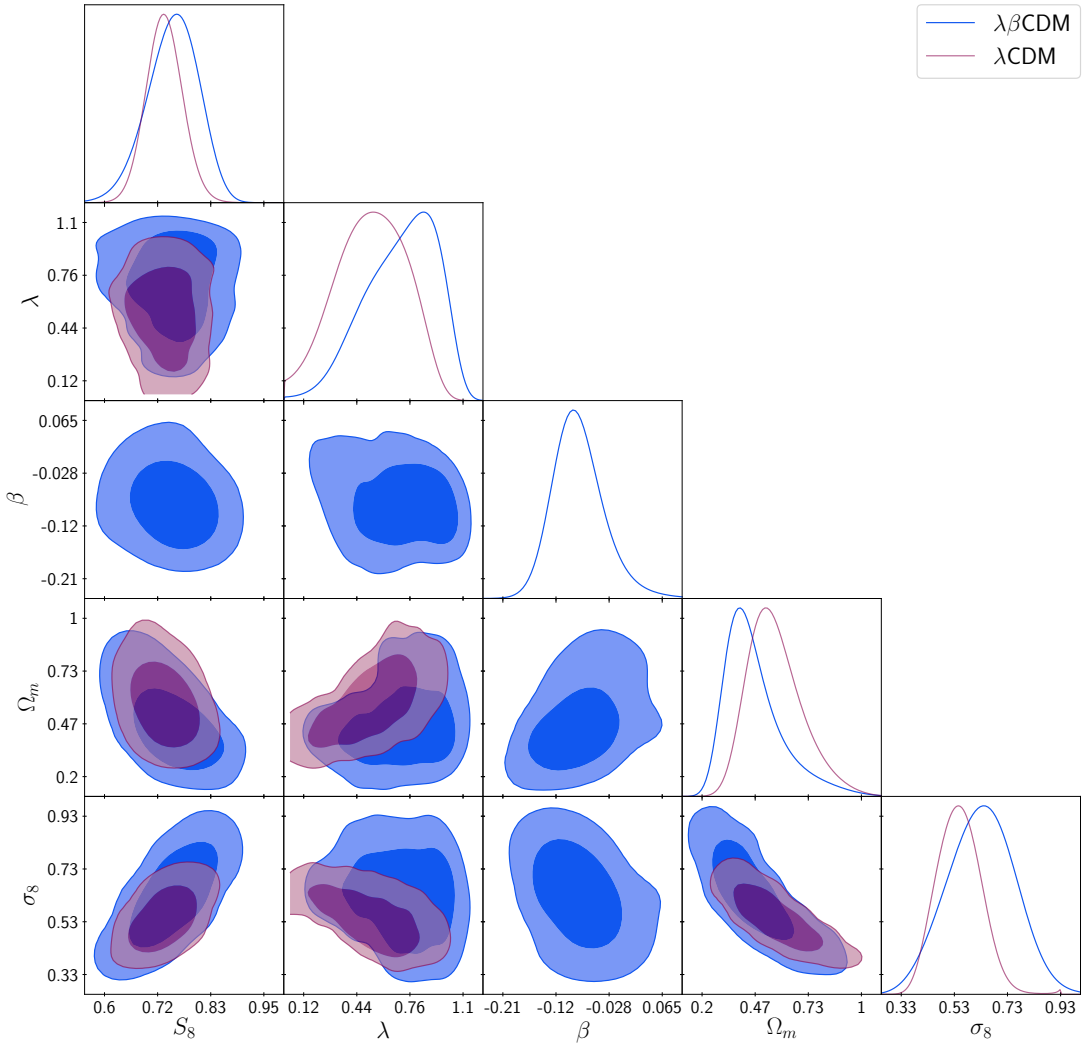

Figure 4.11: Constraints obtained with KiDS on $\lambda\beta$CDM. Probability distribution for marginalized parameter (plots at the top of the triangle) and contour plots showing the marginalized 2-dimensional constraints. Contours include 68% and 95% of the probability.

The model fitting is significantly in disagreement with Planck, as shown in Figure 4.12. The relatively larger interval found for the λ posterior allows for larger negative β values according to the cut off in Eq (4.29). Accordingly, the allowed β region in the parameter space is particularly wide with KiDS. Though, the value inferred for λ entails a quantity of early dark energy at the time of decoupling which appears to be incompatible with the CMB measurements.

It is to be recalled that additional chains should be run in the future, especially with the Nested-Sampling algorithm, to confirm these results. Furthermore, the HALOFIT model we are using was calibrated with N-body simulations for ΛCDM. They therefore may not be suitable in our case that speculates the existence of an extra force applied to dark matter, which is not foreseen by the standard model. These drawbacks jeopardize the confidence on the KiDS constraints that could be challenged with other cosmological probe at low redshift, such as redshift-space distortions observations.

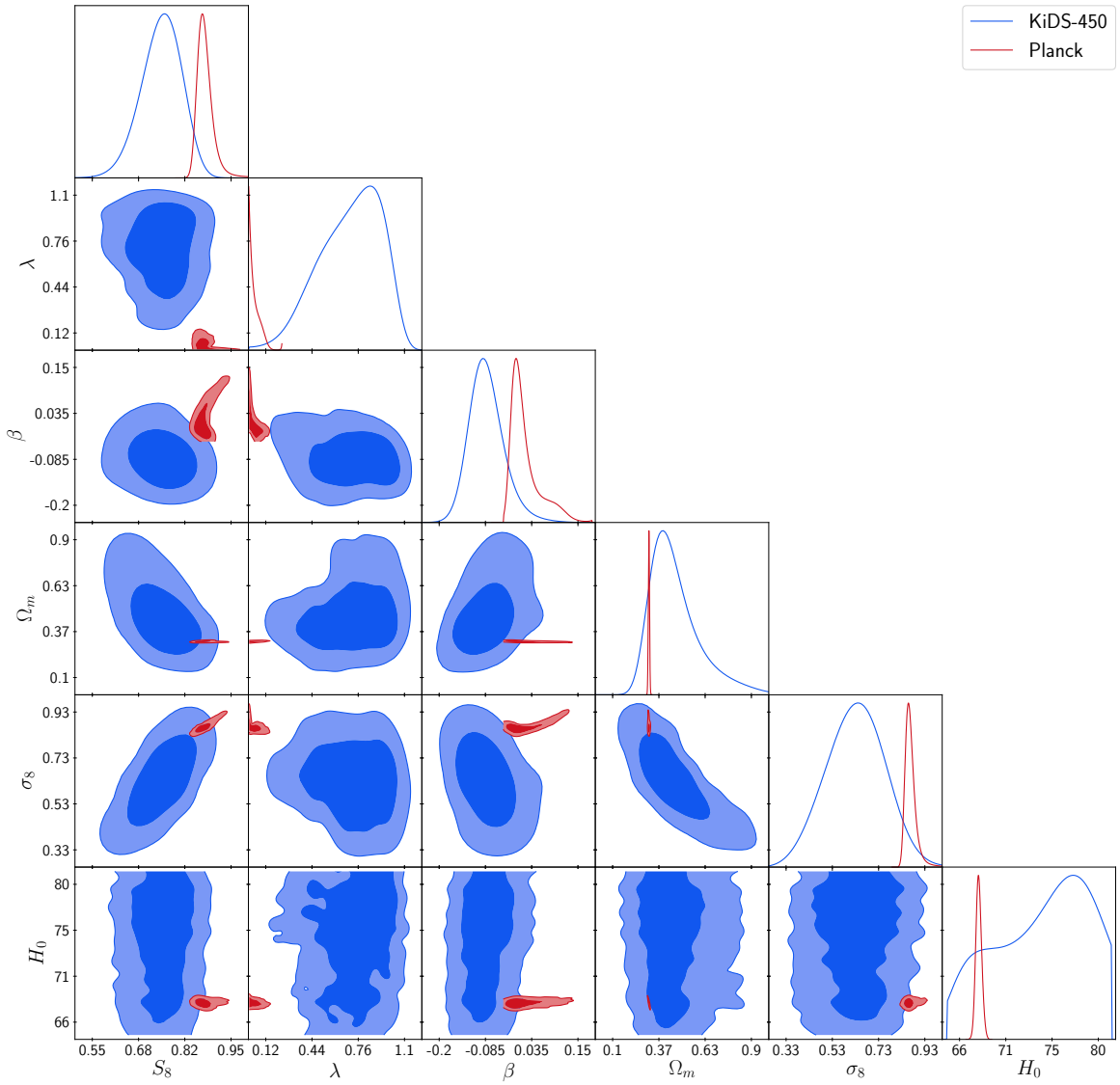

Figure 4.12: Constraints on $\lambda\beta$CDM. Probability distribution for marginalized parameter (plots at the top of the triangle) and contour plots showing the marginalized 2-dimensional constraints. Contours include 68% and 95% of the probability.

Chapter 5

Conclusions and prospects

We have been examining possible parametrisations of quintessence responsible for dark energy fuelling the observed late time cosmic acceleration. As it can reduce to a simpler linear form, we disregarded an exponential parametrisation of the canonical scalar field, $\phi = \phi_o e^{\epsilon N}$, generating a collapsed universe. It might be worth further investigating the cosmological behaviour of such model, perhaps in the primordial inflation context. We should add that we did not mention another parametrisation, $\phi^2 - \phi_0^2 = \epsilon N$, that also enables to extract an analytic expression of the dark energy density and potential, which could also be of interest in future works.

Instead, we have been focusing our attention on testing the linear parametrisation, $\phi - \phi_0 = \lambda N$, putting forward its simplicity as main attractiveness. Given the multiple parameter degeneracies that increase in more complex models, only simple ones can be constrained with current and future observations. Despite its simplicity, the λCDM model gives rise to an evolution of the Universe that necessarily converges to the current acceleration, for a very wide range of initial conditions. It also covers a large variety of possible dynamics of dark energy at late times, while keeping its equation of state bound at high redshift, contrary to other simple parametrisations we reviewed. Moreover, it can reproduce the matter distribution at low redshift, as well as the anisotropies of the CMB at higher redshift. We have reached these conclusions by studying the analytic form of the model, confirmed by numerical results. We have realised that the model, being compatible with astrophysical observations, is a viable generalisation of the current ΛCDM paradigm, although we did construct it phenomenologically without anchoring it in existing particle physics theories. We have managed with Planck datasets to observationally constrain the principal parameter responsible for the variation of the scalar field, $|\lambda| < 0.052$ at 1σ CL, without being able to discard the cosmological constant. However, the observations in the late universe with KiDS-450 bring a very different constraint, $|\lambda| = 0.52^{+0.24}_{-0.18}$, yet with large error bars.

As a step further, we have introduced an additional parameter in the parametrisation by coupling the scalar field with cold dark matter through a constant coupling β. As a novelty, we have derived the

analytic expression of the quintessence potential, and modified an existing Boltzmann code to simulate the background and perturbations evolution in the $\lambda\beta$CDM model. Despite the existence of the additional degree of freedom, the Bayesian inference carried-out with Planck still continues to find a preference for vanishing values of the two parameters. The preliminary results we obtained with KiDS observations are significantly in disagreement, $\lambda = 0.70^{+0.28}_{-0.15}$ and $\beta = -0.080^{+0.041}_{-0.057}$, which can be interpreted as an energy injection from the dark matter fluid into the scalar field. Consequently, the level of clustering σ_8 increases relatively to the uncoupled parametrisation. However these results cannot be trusted at this stage as the HALOFIT model used is not tailored to cope with the existence of the fifth force applying to cold dark matter due to its coupling with the scalar field. We may envisage to recalibrate it on the basis of N-body simulations that would include the effective Newton constant specifically applying to dark matter.

As for the future, we would propose to complement the statistical analysis to better constrain the two models investigated. We have been confronted with Markov chains convergence difficulties that could be overcome with increased computational power and the choice of more appropriate sampling algorithms. The combination of the different data sets we used could also bring tighter constraints on the models. It would help break existent degeneracies between cosmological parameters. Another prospect of our present work could consist in testing the couplings of dark energy with a possible hot component of mixed dark matter. On top of pressureless cold dark matter, radiation, baryons and massless neutrinos, this model foresees a constituent of matter in a species of massive neutrinos. We could envisage to couple our parametrised scalar field with that component rather than with cold dark matter. Additionally, we could also consider an interaction term between quintessence and the electromagnetic field in the form of a gauge kinetic function $B_F(\phi)$ incorporated into the electromagnetic Lagrangian, $\mathcal{L}_{\phi F} = -\frac{1}{4}B_F(\phi)F_{\mu\nu}F^{\mu\nu}$ [29]. We could, as usually done, consider a linear dependence on the scalar field. Cosmological bounds on the variation of the fine structure constant α could further help constrain λ and β. Such measurements are performed by analysis of the spectrum of distant quasars and tight bounds are soon to be disclosed by the ESPRESSO consortium. Finally, we could envisage to provide forecast on the future constraints expected from the Euclid mission.

Bibliography

[1] Adam G. Riess et al. Observational evidence from supernovae for an accelerating universe and a cosmological constant. *Astron. J.*, 116:1009–1038, 1998.

[2] S. Perlmutter et al. Measurements of Omega and Lambda from 42 high redshift supernovae. *Astrophys. J.*, 517:565–586, 1999.

[3] Luca Amendola and Shinji Tsujikawa. *Dark Energy*. Cambridge University Press, 2015.

[4] Timothy Clifton, Pedro G. Ferreira, Antonio Padilla, and Constantinos Skordis. Modified Gravity and Cosmology. *Phys. Rept.*, 513:1–189, 2012.

[5] N. Aghanim et al. Planck 2018 results. VI. Cosmological parameters. 2018.

[6] Alan H. Guth. Inflationary universe: A possible solution to the horizon and flatness problems. *Phys. Rev. D*, 23:347–356, 1981.

[7] Jerome Martin. Everything You Always Wanted To Know About The Cosmological Constant Problem (But Were Afraid To Ask). *Comptes Rendus Physique*, 13:566–665, 2012.

[8] Svend Erik Rugh and Henrik Zinkernagel. The Quantum vacuum and the cosmological constant problem. *Stud. Hist. Phil. Sci.*, B33:663–705, 2002.

[9] P. J. E. Peebles and Bharat Ratra. The Cosmological constant and dark energy. *Rev. Mod. Phys.*, 75:559–606, 2003. [,592(2002)].

[10] S. Weinberg. The Cosmological constant problems. In *Sources and detection of dark matter and dark energy in the universe. Proceedings, 4th International Symposium, DM 2000, Marina del Rey, USA, February 23-25, 2000*, pages 18–26, 2000.

[11] Sebastian Bahamonde, Christian G. Böhmer, Sante Carloni, Edmund J. Copeland, Wei Fang, and Nicola Tamanini. Dynamical systems applied to cosmology: dark energy and modified gravity. 2017.

[12] Jochen Weller and Andreas Albrecht. Future supernovae observations as a probe of dark energy. *Physical Review D*, 65(10), May 2002.

[13] M. Chevallier and D. Polarski. Accelerating Universes with Scaling Dark Matter. *International Journal of Modern Physics D*, 10:213–224, 2001. (uses Latex, 12 pages, 6 Figures) Minor corrections, Figures 4, 6 revised. Conclusions unchanged.

[14] Eric Linder. Exploring the expansion history of the universe. *Physical review letters*, 90:091301, 04 2003.

[15] G. Efstathiou. Constraining the equation of state of the universe from distant type ia supernovae and cosmic microwave background anisotropies. *Monthly Notices of the Royal Astronomical Society*, 310(3):842–850, Dec 1999.

[16] P. S. Corasaniti and E. J. Copeland. Model independent approach to the dark energy equation of state. *Physical Review D*, 67(6), Mar 2003.

[17] Serguei Chatrchyan et al. Observation of a new boson at a mass of 125 GeV with the CMS experiment at the LHC. *Phys. Lett.*, B716:30–61, 2012.

[18] Andrei Linde. Inflationary Cosmology after Planck 2013. In *Proceedings, 100th Les Houches Summer School: Post-Planck Cosmology: Les Houches, France, July 8 - August 2, 2013*, pages 231–316, 2015.

[19] C. Boehm and J. Lesgourgues. Dark matter and dark energy. 2008.

[20] R. R. Caldwell, Rahul Dave, and Paul J. Steinhardt. Cosmological imprint of an energy component with general equation of state. *Physical Review Letters*, 80(8):1582–1585, Feb 1998.

[21] Shinji Tsujikawa. Quintessence: A Review. *Class. Quant. Grav.*, 30:214003, 2013.

[22] Andreas Albrecht and Constantinos Skordis. Phenomenology of a realistic accelerating universe using only planck-scale physics. *Phys. Rev. Lett.*, 84:2076–2079, 2000.

[23] Scott Dodelson, Manoj Kaplinghat, and Ewan Stewart. Solving the coincidence problem: Tracking oscillating energy. *Phys. Rev. Lett.*, 85:5276–5279, Dec 2000.

[24] Varun Sahni and Limin Wang. New cosmological model of quintessence and dark matter. *Phys. Rev. D*, 62:103517, Oct 2000.

[25] Jerome Martin. Quintessence: a mini-review. *Mod. Phys. Lett. A*, 23:1252–1265, 2008.

[26] Bharat Ratra and P. J. E. Peebles. Cosmological consequences of a rolling homogeneous scalar field. *Phys. Rev. D*, 37:3406–3427, 1988.

[27] C. Wetterich. Cosmology and the fate of dilatation symmetry. *Nuclear Physics B*, 302(4):668 – 696, 1988.

[28] Ewan R. M. Tarrant, Carsten van de Bruck, Edmund J. Copeland, and Anne M. Green. Coupled quintessence and the halo mass function. *Phys. Rev. D*, 85:023503, 2012.

[29] Nelson J. Nunes and James E. Lidsey. Reconstructing the dark energy equation of state with varying alpha. *Phys. Rev.*, D69:123511, 2004.

[30] Renata Kallosh, Jan Kratochvil, Andrei Linde, Eric V Linder, and Marina Shmakova. Observational bounds on cosmic doomsday. *Journal of Cosmology and Astroparticle Physics*, 2003(10):015–015, Oct 2003.

[31] Edmund J. Copeland, Andrew R Liddle, and David Wands. Exponential potentials and cosmological scaling solutions. *Phys. Rev.*, D57:4686–4690, 1998.

[32] T. Barreiro, Edmund J. Copeland, and N. J. Nunes. Quintessence arising from exponential potentials. *Phys. Rev.*, D61:127301, 2000.

[33] Rachel Bean, Steen H. Hansen, and Alessandro Melchiorri. Early-universe constraints on dark energy. *Phys. Rev. D*, 64:103508, Oct 2001.

[34] P. J. E. Peebles and Bharat Ratra. Cosmology with a Time Variable Cosmological Constant. *Astrophys. J.*, 325:L17, 1988.

[35] E. Lifshitz. Republication of: On the gravitational stability of the expanding universe. *J. Phys. (USSR)*, 10(2):116, 1946.

[36] Patrick Peter and Jean-Philippe Uzan. *Primordial cosmology*. Oxford Graduate Texts. Oxford Univ. Press, Oxford, 2009.

[37] Chung-Pei Ma and Edmund Bertschinger. Cosmological perturbation theory in the synchronous and conformal newtonian gauges. *The Astrophysical Journal*, 455:7, Dec 1995.

[38] Andrew R. Liddle and David H. Lyth. *Cosmological Inflation and Large-Scale Structure*. Cambridge University Press, 2000.

[39] D. Baumann. Cosmology, Part III Mathematical Tripos.

[40] Pedro G. Ferreira and Michael Joyce. Cosmology with a primordial scaling field. *Phys. Rev. D*, 58:023503, 1998.

[41] Luca Amendola and Domenico Tocchini-Valentini. Baryon bias and structure formation in an accelerating universe. *Physical Review D*, 66(4), Aug 2002.

[42] D. M. Scolnic, D. O. Jones, A. Rest, Y. C. Pan, R. Chornock, R. J. Foley, M. E. Huber, R. Kessler, G. Narayan, A. G. Riess, and et al. The complete light-curve sample of spectroscopically confirmed sne ia from pan-starrs1 and cosmological constraints from the combined pantheon sample. *The Astrophysical Journal*, 859(2):101, May 2018.

[43] J. Lesgourgues. Cosmology, Bern University, Master of Physics. 2015.

[44] C. Alcock and B. Paczynski. An evolution free test for non-zero cosmological constant. *Nature*, 281:358, October 1979.

[45] Julien Lesgourgues. The cosmic linear anisotropy solving system (class) i: Overview, 2011.

[46] Diego Blas, Julien Lesgourgues, and Thomas Tram. The cosmic linear anisotropy solving system (class). part ii: Approximation schemes. *Journal of Cosmology and Astroparticle Physics*, 2011(07):034–034, Jul 2011.

[47] Benjamin Audren, Julien Lesgourgues, Karim Benabed, and Simon Prunet. Conservative Constraints on Early Cosmology: an illustration of the Monte Python cosmological parameter inference code. *JCAP*, 1302:001, 2013.

[48] Thejs Brinckmann and Julien Lesgourgues. MontePython 3: boosted MCMC sampler and other features. 2018.

[49] Andreas Albrecht and Constantinos Skordis. Phenomenology of a realistic accelerating universe using only planck-scale physics. *Physical Review Letters*, 84(10):2076–2079, Mar 2000.

[50] Roberto Trotta. Bayes in the sky: Bayesian inference and model selection in cosmology. *Contemporary Physics*, 49(2):71–104, Mar 2008.

[51] B. Audren. Monte python's documentation. 2013.

[52] D. M. Scolnic, D. O. Jones, A. Rest, Y. C. Pan, R. Chornock, R. J. Foley, M. E. Huber, R. Kessler, G. Narayan, A. G. Riess, and et al. The complete light-curve sample of spectroscopically confirmed sne ia from pan-starrs1 and cosmological constraints from the combined pantheon sample. *The Astrophysical Journal*, 859(2):101, May 2018.

[53] M. Betoule et al. Improved cosmological constraints from a joint analysis of the SDSS-II and SNLS supernova samples. *Astron. Astrophys.*, 568:A22, 2014.

[54] Florian Beutler, Chris Blake, Matthew Colless, D. Heath Jones, Lister Staveley-Smith, Lachlan Campbell, Quentin Parker, Will Saunders, and Fred Watson. The 6df galaxy survey: baryon acoustic oscillations and the local hubble constant. *Monthly Notices of the Royal Astronomical Society*, 416(4):3017–3032, Jul 2011.

[55] Lauren Anderson, Éric Aubourg, Stephen Bailey, Florian Beutler, Vaishali Bhardwaj, Michael Blanton, Adam S. Bolton, J. Brinkmann, Joel R. Brownstein, Angela Burden, and et al. The clustering of galaxies in the sdss-iii baryon oscillation spectroscopic survey: baryon acoustic oscillations in the data releases 10 and 11 galaxy samples. *Monthly Notices of the Royal Astronomical Society*, 441(1):24–62, Apr 2014.

[56] Andreu Font-Ribera, David Kirkby, Nicolas Busca, Jordi Miralda-Escudé, Nicholas P. Ross, Anže Slosar, James Rich, Éric Aubourg, Stephen Bailey, Vaishali Bhardwaj, and et al. Quasar-lyman alpha forest cross-correlation from boss dr11: Baryon acoustic oscillations. *Journal of Cosmology and Astroparticle Physics*, 2014(05):027–027, May 2014.

[57] Ashley J. Ross, Lado Samushia, Cullan Howlett, Will J. Percival, Angela Burden, and Marc Manera. The clustering of the sdss dr7 main galaxy sample – i. a 4 per cent distance measure at z = 0.15. *Monthly Notices of the Royal Astronomical Society*, 449(1):835–847, Mar 2015.

[58] Planck Collaboration. Planck 2018 results. v. cmb power spectra and likelihoods, 2019.

[59] Ø. Rudjord, N. E. Groeneboom, H. K. Eriksen, Greg Huey, K. M. Górski, and J. B. Jewell. Cosmic microwave background likelihood approximation by a gaussianized blackwell-rao estimator. *The Astrophysical Journal*, 692(2):1669–1677, Feb 2009.

[60] Matthias Bartelmann and Peter Schneider. Weak gravitational lensing. *Physics Reports*, 340(4-5):291–472, Jan 2001.

[61] H. Hildebrandt, M. Viola, C. Heymans, S. Joudaki, K. Kuijken, C. Blake, T. Erben, B. Joachimi, D. Klaes, L. Miller, and et al. Kids-450: cosmological parameter constraints from tomographic weak gravitational lensing. *Monthly Notices of the Royal Astronomical Society*, 465(2):1454–1498, Nov 2016.

[62] Ryuichi Takahashi, Masanori Sato, Takahiro Nishimichi, Atsushi Taruya, and Masamune Oguri. Revising the halofit model for the nonlinear matter power spectrum. *The Astrophysical Journal*, 761(2):152, Dec 2012.

[63] F. Köhlinger, M. Viola, B. Joachimi, H. Hoekstra, E. van Uitert, H. Hildebrandt, A. Choi, T. Erben, C. Heymans, S. Joudaki, and et al. Kids-450: the tomographic weak lensing power spectrum and constraints on cosmological parameters. *Monthly Notices of the Royal Astronomical Society*, 471(4):4412–4435, Jul 2017.

[64] Thejs Brinckmann and Julien Lesgourgues. Montepython 3: boosted mcmc sampler and other features, 2018.

[65] F. Feroz and M. P. Hobson. Multimodal nested sampling: an efficient and robust alternative to markov chain monte carlo methods for astronomical data analyses. *Monthly Notices of the Royal Astronomical Society*, 384(2):449–463, Jan 2008.

[66] F. Feroz, M. P. Hobson, and M. Bridges. Multinest: an efficient and robust bayesian inference tool for cosmology and particle physics. *Monthly Notices of the Royal Astronomical Society*, 398(4):1601–1614, Oct 2009.

[67] Farhan Feroz, Michael P. Hobson, Ewan Cameron, and Anthony N. Pettitt. Importance nested sampling and the multinest algorithm. *The Open Journal of Astrophysics*, 2(1), Nov 2019.

[68] Luca Amendola. Coupled quintessence. *Phys. Rev. D*, 62:043511, 2000.

[69] Shinji Tsujikawa, Kotub Uddin, Shuntaro Mizuno, Reza Tavakol, and Jun'ichi Yokoyama. Constraints on scalar-tensor models of dark energy from observational and local gravity tests. *Physical Review D*, 77(10), May 2008.

[70] L. Amendola. Perturbations in a coupled scalar field cosmology. *Monthly Notices of the Royal Astronomical Society*, 312(3):521–530, Mar 2000.

[71] Pier Stefano Corasaniti. Slow-roll suppression of adiabatic instabilities in coupled scalar field-dark matter models. *Physical Review D*, 78(8), Oct 2008.

[72] Rachel Bean, Éanna É. Flanagan, Istvan Laszlo, and Mark Trodden. Constraining interactions in cosmology's dark sector. *Physical Review D*, 78(12), Dec 2008.

[73] Enea Di Dio, Francesco Montanari, Julien Lesgourgues, and Ruth Durrer. The classgal code for relativistic cosmological large scale structure. *Journal of Cosmology and Astroparticle Physics*, 2013(11):044–044, Nov 2013.

[74] Bruno J. Barros, Luca Amendola, Tiago Barreiro, and Nelson J. Nunes. Coupled quintessence with a ΛCDM background: removing the σ_8 tension. 2018.

[75] Jun-Qing Xia. New limits on coupled dark energy from planck. *Journal of Cosmology and Astroparticle Physics*, 2013(11):022–022, Nov 2013.

[76] A.R. Liddle. *An introduction to modern cosmology*. Wiley, 2003.

[77] S. Weinberg. *Cosmology*. OUP Oxford, 2008.

[78] A. Einstein. The Foundation of the General Theory of Relativity. *Annalen Phys.*, 49(7):769–822, 1916. [Annalen Phys.14,517(2005)].

[79] Ray D'Inverno. *Introducing Einstein's Relativity*. Clarendon Press, 1992.

[80] E. Asmodelle. *Tests of General Relativity: A Review*. PhD thesis, Central Lancashire U., 2017.

[81] B. P. Abbott et al. Observation of Gravitational Waves from a Binary Black Hole Merger. *Phys. Rev. Lett.*, 116(6):061102, 2016.

[82] Charles W. Misner, K. S. Thorne, and J. A. Wheeler. *Gravitation*. W. H. Freeman, 1973.

[83] Albert Einstein. Cosmological Considerations in the General Theory of Relativity. *Sitzungsber. Preuss. Akad. Wiss. Berlin (Math. Phys.)*, 1917:142–152, 1917.

[84] A. Friedman. Uber die krummung des raumes. *Zeitschrift fur Physik*, 10(1):377–386, 1922.

[85] G. Lemaître. A homogeneous universe of constant mass and increasing radius accounting for the radial velocity of extra-galactic nebulæ. *Monthly Notices of the Royal Astronomical Society*, 91(5):483–490, 1931.

[86] H. P. Robertson. Kinematics and World-Structure III. *apj*, 83:257, 1936.

[87] Lloyd Knox and Lyman Page. Characterizing the peak in the CMB angular power spectrum. *Phys. Rev. Lett.*, 85:1366–1369, 2000.

[88] Edward W Kolb and Michael Stanley Turner. *The early universe*. Frontiers in Physics. Westview Press, Boulder, CO, 1990.

[89] Barry F. Madore, Jane Rigby, Wendy L. Freedman, S. E. Persson, Laura Sturch, and Violet Mager. The cepheid period-luminosity relation (the leavitt law) at mid-infrared wavelengths. iii. cepheids in ngc 6822. *The Astrophysical Journal*, 693(1):936–939, Mar 2009.

[90] Edwin Hubble and Milton L. Humason. The Velocity-Distance Relation among Extra-Galactic Nebulae. *Astrophys. J.*, 74:43–80, 1931.

[91] Vesto M. Slipher. Nebulae. *Proc. Am. Phil. Soc.*, 56:403–409, 1917.

[92] P. A. R. Ade et al. Planck 2015 results. XIII. Cosmological parameters. *Astron. Astrophys.*, 594:A13, 2016.

[93] Annika H. G. Peter. Dark Matter: A Brief Review. 2012.

[94] Douglas Clowe, Marusa Bradac, Anthony H. Gonzalez, Maxim Markevitch, Scott W. Randall, Christine Jones, and Dennis Zaritsky. A direct empirical proof of the existence of dark matter. *Astrophys. J.*, 648:L109–L113, 2006.

Appendix A

The homogeneous and isotropic universe

We aim to introduce in this Appendix the theoretical foundations of modern cosmology [36, 76, 77] that are built on General Relativity [78, 79], which is Albert Einstein's theory of gravitation [80, 81] generalising Special Relativity [82]. To begin with, we will recall that the background geometry of the universe is described by the Friedmann-Lemaître-Robertson-Walker (FLRW) spacetime metric that arises from the cosmological principle of homogeneity and isotropy.

From the four fundamental interactions, it is the long range gravitation that governs the cosmic evolution. The Universe being neutral, the electromagnetic interaction, which is the other long range force, does not impact it at large scales. Nor does the strong nor the weak force, those only produce effects at the subatomic level. It is natural to seek cosmological solutions to the Einstein field equations that characterize the dynamics of the universe as a whole [36, 76, 77]. Although matter gravitational attraction causes the Universe to be unstable, Einstein found a solution that prescribes a static universe akin to the paradigm at the time [83]. He incorporated a cosmological constant Λ into the geometrical side of his equations to counter balance the unthinkable contraction or expansion of the universe,

$$G_{\mu\nu} + \Lambda g_{\mu\nu} = \kappa^2 T_{\mu\nu}, \qquad \kappa^2 = \frac{8\pi G}{c^4}, \tag{A.1}$$

where $g_{\mu\nu}$ is the spacetime metric tensor, G the Newton's gravitational constant and c the light speed.

The Einstein field equations consist of 16 non-linear differential equations that reduce to 10 by assuming that the Einstein tensor $G_{\mu\nu}$ and stress-energy tensor $T_{\mu\nu}$ are symmetric. On the basis of the Bianchi identities, $\nabla_\mu G^\mu_\nu = 0$ [1], the number of independent equations is further reduced to 6. We can make simplifying assumptions to allow us to obtain exact analytical solutions. In modern cosmology, it is assumed that the universe is homogeneous and isotropic at large scales. The homogeneity assumption

[1]The covariant derivative for a given metric is defined as $\nabla_\mu G^\mu_\nu = G^\mu_{\nu;\mu} \equiv \partial_\mu G^\mu_\nu + \Gamma^\mu_{\alpha\mu} G^\alpha_\nu - \Gamma^\alpha_{\nu\mu} G^\mu_\alpha$, where Γ is the connection of the metric with components, $\Gamma^\alpha_{\beta\gamma} \equiv \frac{1}{2} g^{\alpha\delta} \left(g_{\delta\beta,\gamma} + g_{\delta\gamma,\beta} - g_{\beta\gamma,\delta} \right)$. We are using the Einstein summation convention that omits the summation sign whenever lower and upper indices are repeated. Moreover, Greek and Latin indices will respectively be denoting the four dimensional manifold and spatial coordinates.

means that the universe is exactly the same at any point in space. For instance, any background quantities such as energy densities are a function of time only. The isotropy is defined by the absence of a preferential direction, i.e. the universe is apparently the same in every direction. With pure geometrical arguments, it can be demonstrated that the FLRW metric [84–86] is the most generic spacetime that respects those principles. Its line element takes the following form in comoving spherical coordinates and metric signature $-+++$,

$$ds^2 = g_{\mu\nu}dx^\mu dx^\nu = -c^2dt^2 + a^2(t)\left[\frac{dr^2}{1-kr^2} + r^2\left(d\theta^2 + \sin^2\theta d\phi^2\right)\right], \tag{A.2}$$

where $a(t) > 0$ is the scale factor accounting for the relative and homogeneous expansion or contraction of the universe's three-dimensional space. The scale factor evolves with the cosmic (or cosmological) time t which is the proper time measured by a free-falling observer. It is spatially homogeneous and usually normalized by imposing $a_0 = 1$ today without loss of generality because the multiplication of a by a constant does not change the dynamics. k is a constant that depends on the geometrical curvature of the universe, which is respectively said to be spatially closed $k = 1$ or spatially open $k = -1$. Cosmological observations [87] suggest that the universe is nearly spatially flat with $k \simeq 0$. The extreme fine-tuning in k's value is called the flatness problem whose possible solution lies in the existence of an inflationary period at the very beginning of the Universe [6].

There is no unambiguous nor unique notion of distance in an expanding universe. All distances grow proportionally to the scale factor whereas observers at rest with the expansion have fixed comoving coordinates. As regards light, photons propagate along null geodesics over a distance, not observable, which is given by the line element in Eq. (A.2) by imposing $ds^2 = 0$. If one considers radial incoming photons emitted at t by a source located at r, the propagation of light is described by the comoving distance $\chi(r)$,

$$\chi(r) \equiv \int_0^r \frac{dr}{\sqrt{1-kr^2}} = c\int_t^{t_0} \frac{dt}{a(t)}, \tag{A.3}$$

travelled by those photons reaching, at t_0, the observer arbitrarily coinciding with the origin of the comoving reference frame. This allows us to define conformal time as $d\tau \equiv dt/a$, yielding a classical comoving distance $\chi = c\,\tau$. The FLRW line element can also be conveniently expressed with conformal time,

$$ds^2 = a^2(\tau)\left[-c^2d\tau^2 + \frac{dr^2}{1-kr^2} + r^2\left(d\theta^2 + \sin^2\theta d\phi^2\right)\right]. \tag{A.4}$$

The comoving distance coincides with the metric (or proper) distance d_M, not observable either, in a flat universe since d_M is defined as,

$$\chi = \int_0^{d_M} \frac{dr}{\sqrt{1-kr^2}}, \tag{A.5}$$

and for $k = 0 \Rightarrow \chi = d_M$.

In astrophysics, distances can be measured with the cosmological redshift z of light wavelength induced by the expansion. It can be determined by considering the path of photons propagating radially along null geodesics, as defined in (A.3). This redshift is related to the inverse of the scale factor: $1 + z = 1/a$. It is a useful look-back time quantity as well. The wavelength of light is stretched by the expansion like any physical distance when a increases, since the universe was smaller at the time when the photon was emitted [88]. The cosmological redshift is not limited, unlike in Newtonian physics where the redshift is interpreted as a Doppler effect $z = v/c$ and therefore limited to $z < 1$.

Its observation gave the indisputable evidence that the universe is expanding, through the discovery of the Hubble-Lemaître law. Based on the period–luminosity relationship, now known as Leavitt's law [89], Edwin Hubble combined his own observations of Cepheids in distant galaxies [90] with Slipher's velocities [91]. He discovered in 1929 that the recessional velocity of a galaxy was proportional to its distance, $v = H_0\, r$, where H_0 is the Hubble constant, usually written as $H_0 = 100\ h\ \mathrm{km\ s^{-1}\ Mpc^{-1}}$ (with nowadays $h \sim 0.67$ [5] embedding the observational uncertainty). The law is valid only at small redshift but can be generalized, $v = H\, r$, where $H = \dot{a}/a$ is called the Hubble parameter (or function) that represents the expansion rate of the scale factor. The Hubble radius r_H of an observer is the distance at which points have a recessional velocity equal to the speed of light,

$$r_H(t) = \frac{c}{H(t)}. \tag{A.6}$$

The Hubble radius can be considered as the proper distance that light travels during the characteristic expansion time scale H^{-1}.

There are other geometrical distances that are particularly useful in astrophysics because they can also be measured. One of them relates to the angular diameter of standard rulers, such as the sound horizon at decoupling that we discuss in 3.1.3. Knowing the physical size l of an object perpendicular to our line of sight, and noting θ its angular size in the sky, the angular diameter distance d_A is defined by,

$$d_A = \frac{l}{\theta} \quad \Rightarrow \quad d_A = \frac{d_M}{1+z}, \tag{A.7}$$

as $l = a\ r\ \theta$ and $r = d_M$. Distances can also be measured from the luminosity of standard candles, like supernovae type Ia (Cf. Section 2.3). It is possible to define the luminosity distance d_L, based on the knowledge of the intrinsic luminosity of a light source by,

$$d_L = (1+z)\, d_M = (1+z)^2\, d_A. \tag{A.8}$$

The expansion of the universe is governed by the scale factor a whose equations of motion are the Einstein field equations (A.1),

$$G_{\mu\nu} \equiv R_{\mu\nu} - \frac{1}{2} g_{\mu\nu} R, \tag{A.9}$$

where $R_{\mu\nu}$ and R are respectively the Ricci tensor [2] and Ricci scalar [3]. These equations fundamentally relate spacetime curvature to the matter content of the universe and can be obtained by applying the variational principle to an action $\mathcal{S}$ that includes one term relating to the Einstein-Hilbert gravitation Lagrangian L_G and another to the matter L_M,

$$\mathcal{S} = \int d^4x \left(L_G + L_M \right), \tag{A.10}$$

$$= \frac{1}{2\kappa^2} \int d^4x \, \sqrt{-g} \, R + \int d^4x \sqrt{-g} \, \mathcal{L}_M, \tag{A.11}$$

where $\mathcal{L}_M$ is the sum of Lagrangian densities for the fundamental fields of matter, g the metric determinant and $\sqrt{-g}$ the volume element. The stress-energy tensor $T_{\mu\nu}$, which describes the gravitational contributions from all forms of energy sources in the universe, is defined as,

$$T_{\mu\nu} = \frac{-2}{\sqrt{-g}} \frac{\delta(\sqrt{-g}\mathcal{L}_M)}{\delta g^{\mu\nu}}. \tag{A.12}$$

From the geometrical left hand side of the Einstein field equations, we have seen that the cosmological principle imposes a FLRW spacetime. For this metric, the non-vanishing connections are the following,

$$\Gamma^i_{j0} = \Gamma^i_{0j} = \frac{\dot{a}}{a} \delta^j_i, \qquad \Gamma^0_{ij} = a\dot{a}\delta_{ij}, \tag{A.13}$$

where δ_{ij} is the Kronecker symbol. Working in natural unites where $c = 1$, one can compute the non-vanishing components of the Einstein tensor G^ν_μ,

$$G^0_0 = -3 \left(H^2 + \frac{k}{a^2} \right), \qquad G^i_j = - \left(H^2 + 2\frac{\ddot{a}}{a} + \frac{k}{a^2} \right) \delta_{ij}. \tag{A.14}$$

From the right hand side, the matter content of the universe is supposedly well described by a mixture of radiation and pressureless dust, which is consistent with astrophysical observations. It is possible to include the cosmological constant too in a given model instead of considering it geometrically. At background level, matter is considered to be smoothly distributed and described by an idealized cosmological fluid that can be approximated by a perfect fluid consistent with the cosmological principle. Thus the form of the energy-momentum tensor $T_{\mu\nu}$ is fixed by,

$$T_{\mu\nu} = \rho \, u_\mu u_\nu + p \left(g_{\mu\nu} + u_\mu u_\nu \right), \tag{A.15}$$

[2] $R_{\mu\nu} \equiv \partial_\alpha \Gamma^\alpha_{\mu\nu} - \partial_\nu \Gamma^\alpha_{\mu\alpha} + \Gamma^\alpha_{\alpha\sigma} \Gamma^\sigma_{\mu\nu} - \Gamma^\sigma_{\mu\alpha} \Gamma^\alpha_{\nu\sigma}$

[3] $R \equiv R^\nu_\mu = g^{\mu\nu} R_{\mu\nu}$

where the fluid's energy density $\rho = \rho(t)$ and isotropic pressure $p = p(t)$ depend on time only. The remaining degree of freedom of the energy-momentum tensor is the equation of state of the barotropic fluid $p = p(\rho)$ that can be considered to be of the linear form $p = w\rho$, where w is the dimensionless equation of state parameter satisfying $-1 \leq w \leq +1$. For a relativistic fluid $w = 1/3$ while for non-relativistic $w = 0$. Moreover, the four-velocity of the fluid is defined by,

$$u^{\mu} = \frac{dx^{\mu}}{\sqrt{-ds^2}}, \tag{A.16}$$

which satisfies $u^{\nu}u_{\nu} = -1$, in the local rest frame of the fluid corresponding to a comoving observer, $u^{\nu} = (1, 0, 0, 0)$. T^{μ}_{ν} is diagonal: $T^{\mu}_{\nu} = \mathrm{diag}\,(-\rho, \mathrm{p}, \mathrm{p}, \mathrm{p})$.

Solving the Einstein field equations, the 0-0 component yields the so-called Friedmann equation that relates the expansion rate of the universe to its energy content and geometry,

$$H^2 = \frac{\kappa^2}{3}\rho - \frac{k}{a^2}, \tag{A.17}$$

while the i-i components give,

$$2\frac{\ddot{a}}{a} + \frac{\dot{a}^2}{a^2} + \frac{k}{a^2} = -\kappa^2 p. \tag{A.18}$$

The combination of the two last equations leads to the Raychaudhuri equation for the acceleration rate of the universe as a function of energy and pressure content,

$$\frac{\ddot{a}}{a} = -\frac{\kappa^2}{6}\left(\rho + 3p\right). \tag{A.19}$$

The time component $\nu = 0$ of the Bianchi identities $\nabla_{\mu}T^{\mu}_{\nu} = 0$ reduces to a single equation expressing matter conservation,

$$\begin{aligned} \nabla_{\mu}T^{\mu}_{0} &= 0, \\ \partial_{\mu}T^{\mu}_{0} + \Gamma^{\mu}_{\mu\sigma}T^{\sigma}_{0} - \Gamma^{\sigma}_{\mu 0}T^{\mu}_{\sigma} &= 0, \\ -\dot{\rho} - 3H\rho - 3Hp &= 0, \end{aligned} \tag{A.20}$$

the continuity equation,

$$\dot{\rho} + 3H\left(\rho + p\right) = 0. \tag{A.21}$$

When the fluid components do not interact with each other, each cosmological species satisfies a distinct equation. The total energy density and pressure can be written as the sum of the contributions of the individual components, $\rho = \sum \rho_i$ and $p = \sum p_i$. When the equation of state parameter w_i of any specie

i is constant, the continuity equation (A.21) can be solved to find the dependence of the energy density ρ_i on the scale factor: $\rho_i \propto a^{-3(1+w_i)}$.

The critical energy density $\rho_{\rm crit}$ corresponds to the value of the total energy density of a flat universe: $\rho_{\rm crit} \equiv 3H^2/\kappa^2$. Its present value is $\rho_0 = 1.878\ h^2 \times 10^{-29}\ g\ cm^{-3} \sim 4 \times 10^{-47}$ GeV^4 [92] and is very close to the present value of the total energy density. The Friedmann equations can also be rewritten with the help of the density parameter (also called fractional energy density or abundance) Ω_i of each component i, defined as,

$$\Omega_i \equiv \frac{\rho_i}{\rho_{\rm crit}} = \frac{\kappa^2 \rho_i}{3H^2}, \tag{A.22}$$

and therefore the Friedmann equation (A.17) reads,

$$1 = \sum \Omega_i(a) + \Omega_k(a), \tag{A.23}$$

where $\Omega_k(a) \equiv -\frac{k}{a^2H^2} \sim 0$. The present-time value of the density parameter is denoted $\Omega_i\,(a_0 = 1) = \Omega_{i_0}$. The Friedmann equation can also be expressed with the evolution of each component of the cosmological fluid,

$$H^2(a) = H_0^2 \left[\sum_i \Omega_{i_0} a^{-3(1+w_i)} + \Omega_{k_0} a^{-2} \right]. \tag{A.24}$$

The total matter content of the universe Ω_M is usually considered to be composed of relativistic (radiation) matter Ω_r with $w = 1/3$, which includes photons Ω_γ and massless neutrinos Ω_ν, along with non-relativistic matter Ω_m with $w = 0$, which includes baryons Ω_b and cold dark matter Ω_c. Cold dark matter is an unknown and non-relativistic component which solves several puzzling observations, such as the anomalous behaviour of the galaxies rotation curve [5, 92–94]. Also, without it, the baryonic content alone could not give rise to galaxies. It is a key ingredient enabling the formation of structures at large scales in the universe.

The continuity equation (A.21) governs the dilution of the energy density as the universe expands. The way it is diluted depends on the fluid pressure and thus on its equation of state. Considering a flat universe singly dominated by radiation or matter, the Friedman equation can be solved to find that the expansion of the universe depends on the nature of its content,

$$\rho_r \propto a^{-4} \quad \Rightarrow \quad a \propto t^{1/2} \quad \Rightarrow \quad a \propto \tau, \tag{A.25}$$

$$\rho_m \propto a^{-3} \quad \Rightarrow \quad a \propto t^{2/3} \quad \Rightarrow \quad a \propto \tau^2. \tag{A.26}$$

Consequently, since the radiation energy density is proportional to T^4 according to Stefan-Boltzmann law, one can conclude that the temperature of the universe is proportional to the cosmological redshift $\rho_r \propto T^4 \Rightarrow T \propto a^{-1} \Rightarrow T \propto (1+z)$.

Appendix B

1-D probability distributions and 2-D marginalized iso-likelihood contours

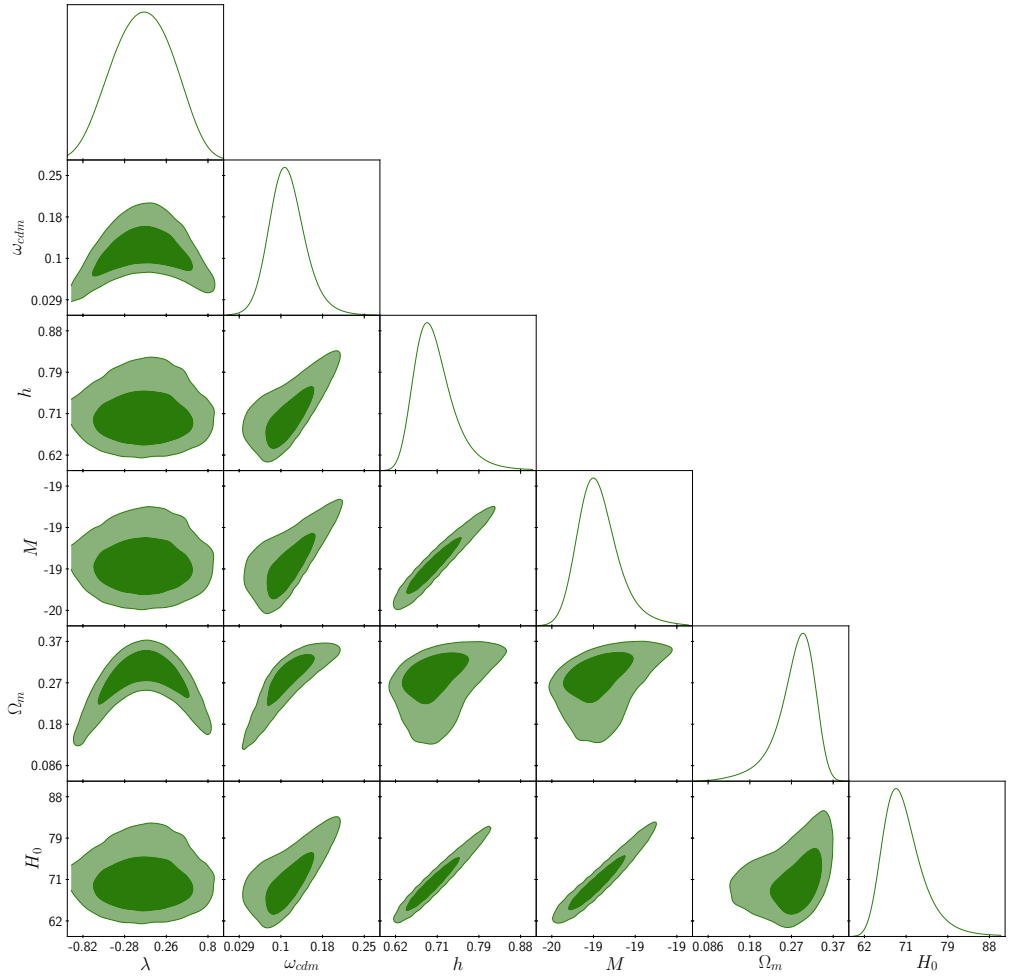

Figure B.1: Observational Constraints on λCDM with Pantheon+BOSS.
R-1 $= 0.0019$
Acceptance rate: 27%
Number of steps: 1,200,000

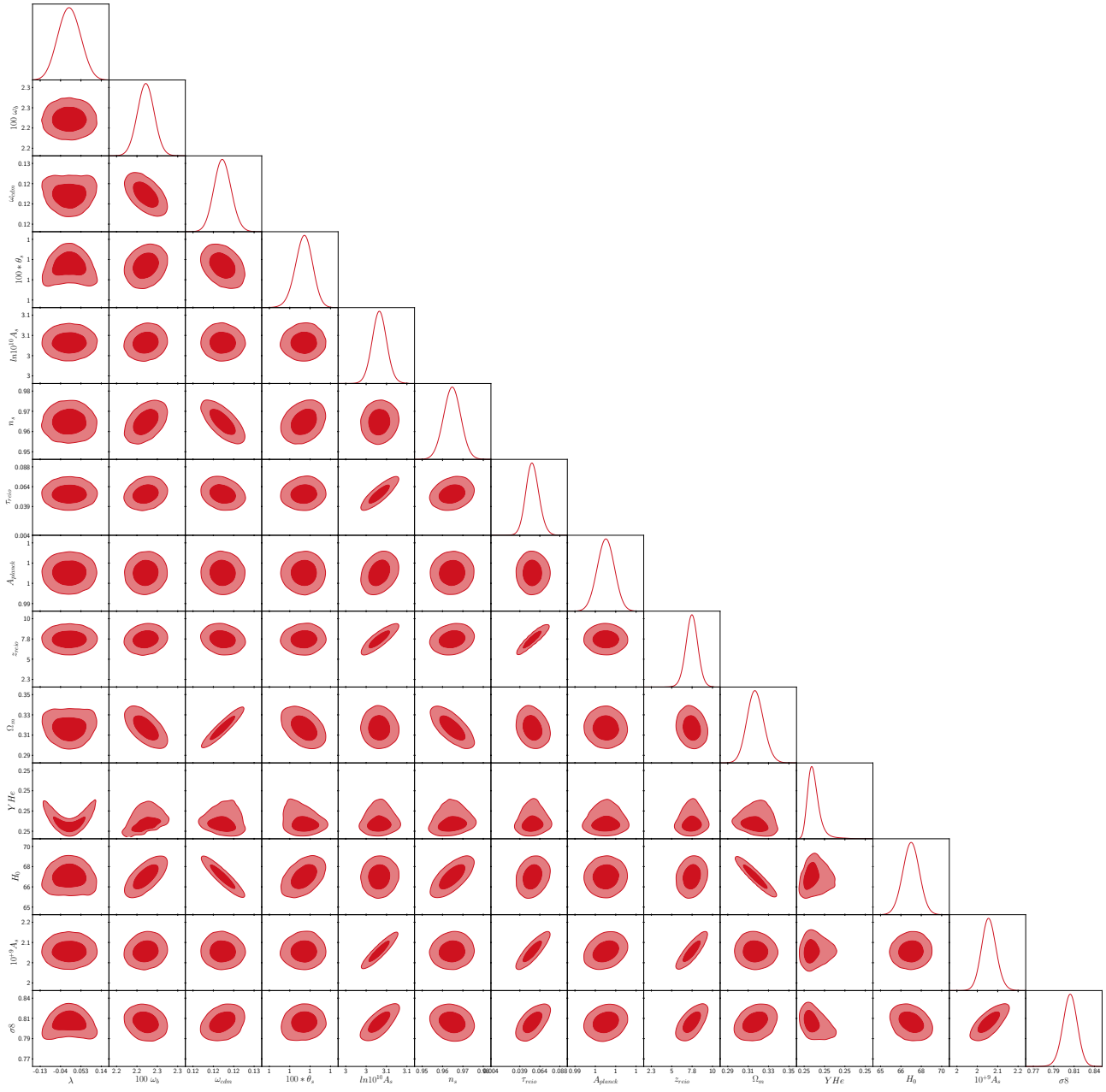

Figure B.2: Observational Constraints on λCDM with Planck.
R-1 = 0.0001
Acceptance rate: 29%
Number of steps: 1,365,428

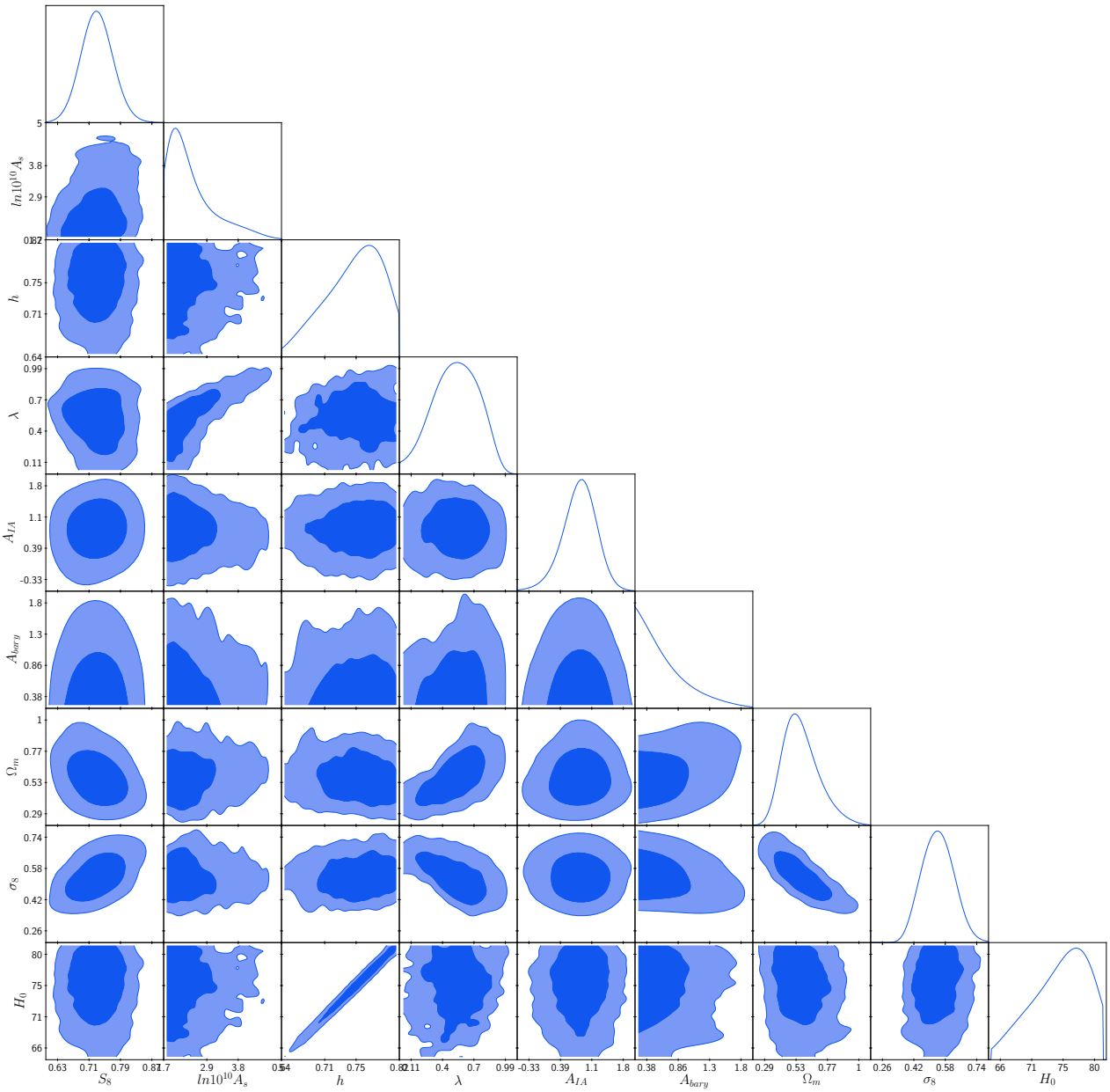

Figure B.3: Observational Constraints on λCDM with KiDS-450.

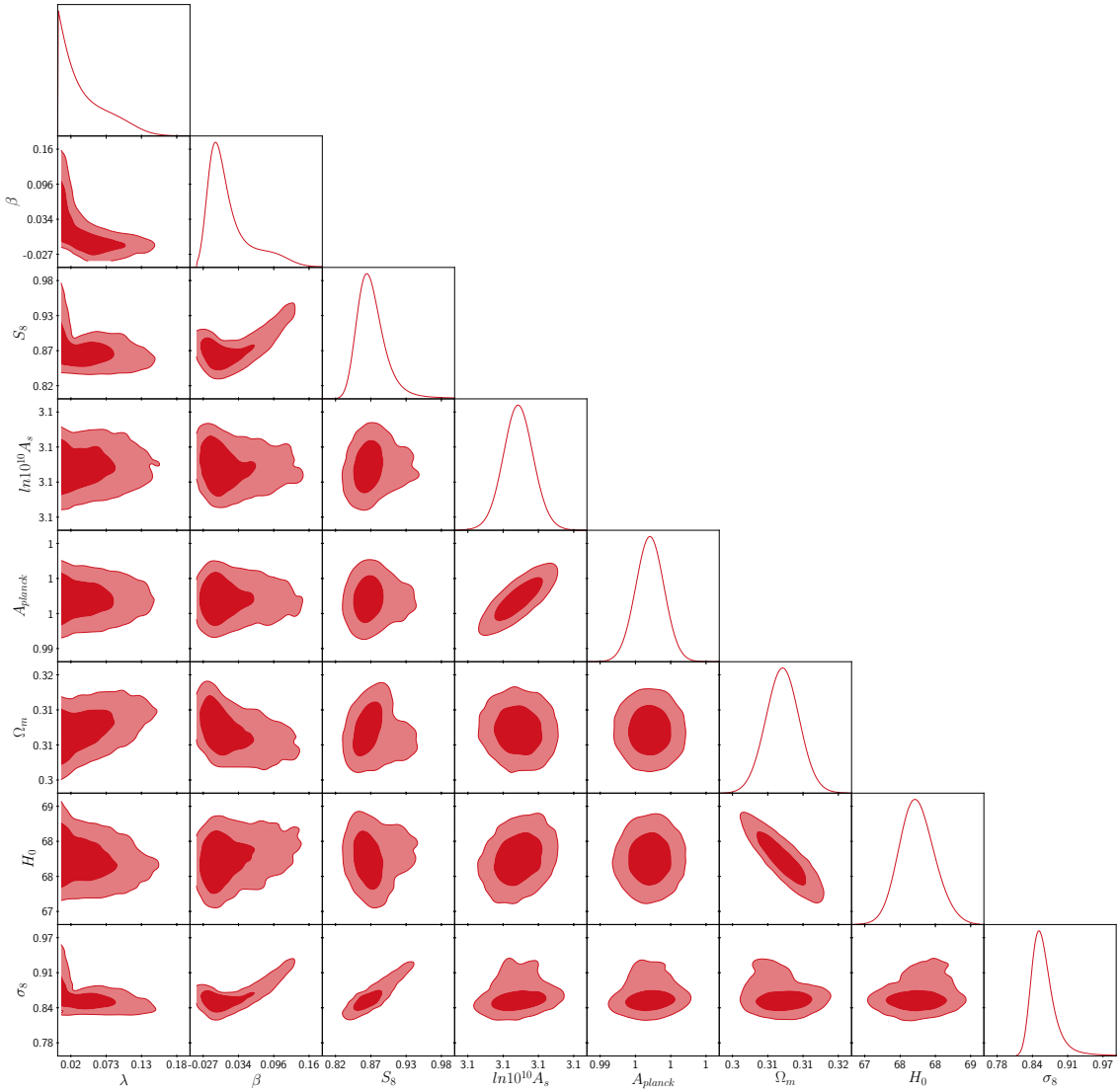

Figure B.4: Observational Constraints on $\lambda\beta$CDM with Planck.
R-1 $= 0.1278$
Acceptance rate: 24%
Number of steps: 985,793

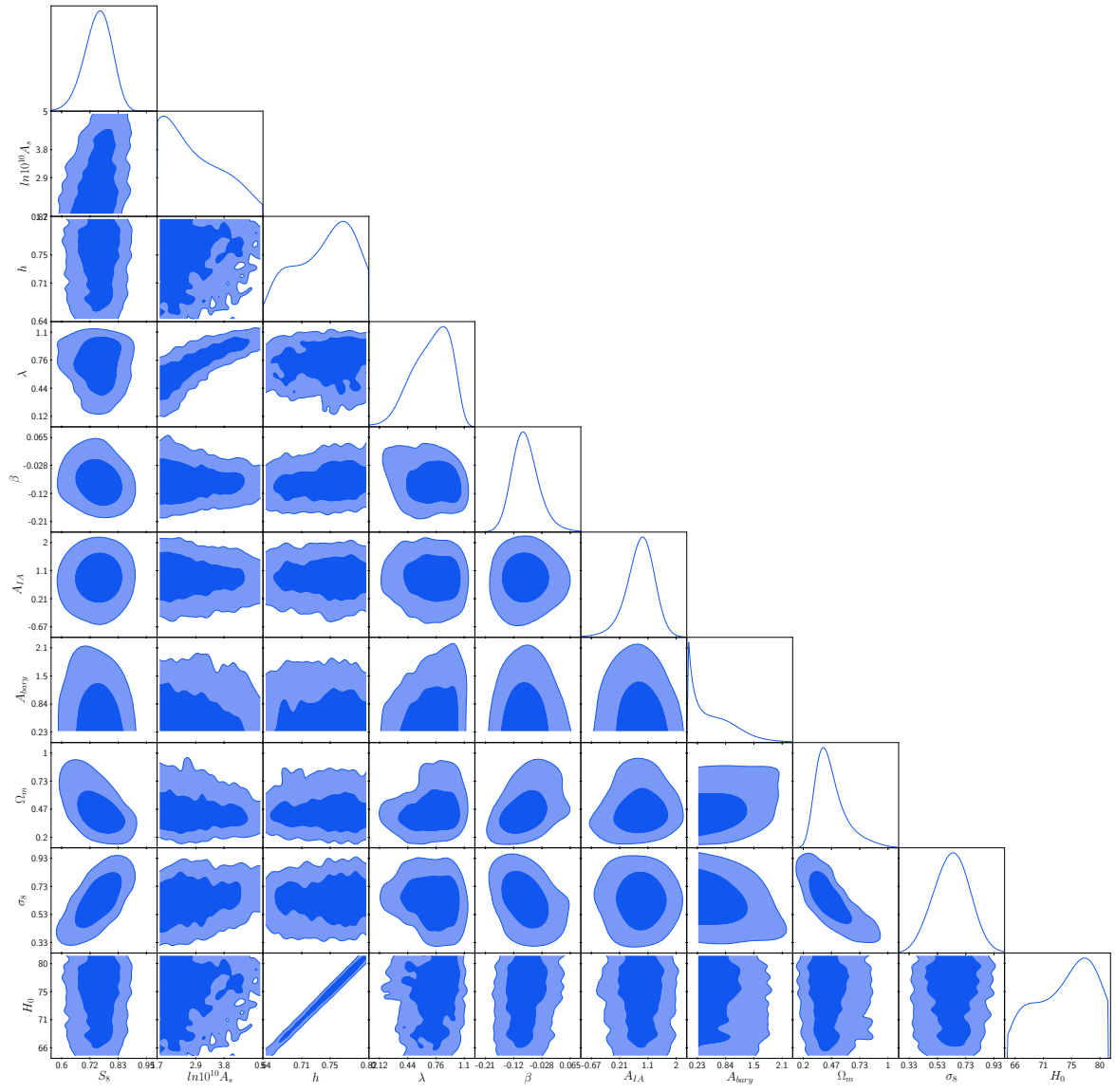

Figure B.5: Observational Constraints on $\lambda\beta$CDM with KiDS-450.